

# **Cross-Shore Transport on Gravel Beaches**

BY

BETSY HICKS, NOBUHISA KOBAYASHI, JENS FIGLUS,  
JACK A. PULEO, AND ALI FARHADZADEH

RESEARCH REPORT NO. CACR-10-01  
JULY 2010



**CENTER FOR APPLIED COASTAL RESEARCH**

Ocean Engineering Laboratory  
University of Delaware  
Newark, Delaware 19716



## **ACKNOWLEDGEMENTS**

This study was supported by the U.S. Army Corps of Engineers, Coastal and Hydraulic Laboratory under Contract No. W912HZ-10-P-0234 and W912BU-09-C-0023.



# TABLE OF CONTENTS

LIST OF FIGURES . . . . .	v
LIST OF TABLES . . . . .	vi
ABSTRACT . . . . .	vii

## Chapter

<b>1 INTRODUCTION . . . . .</b>	<b>1</b>
<b>2 EXPERIMENTAL PROCEDURES . . . . .</b>	<b>4</b>
2.1 Profile Construction . . . . .	4
2.1.1 Steep Slope Tests . . . . .	5
2.1.2 Mild Slope Tests . . . . .	6
2.2 Gravel Characteristics . . . . .	7
2.3 Profile Measurements . . . . .	8
2.4 Wave Generation and Gauges . . . . .	11
2.4.1 Irregular Wave Generation . . . . .	11
2.4.2 Location of Wave Gauges . . . . .	12
2.4.3 Calibration of Wave Gauges . . . . .	12
2.4.4 Validation of Wall Mounted Gauges . . . . .	14
2.5 Electromagnetic Current Meters . . . . .	16
2.6 Data Collection . . . . .	18
<b>3 EXPERIMENTAL RESULTS . . . . .</b>	<b>20</b>
3.1 Profile Data . . . . .	20
3.1.1 Test SL . . . . .	21

3.1.2	Test SH . . . . .	25
3.1.3	Test MH . . . . .	28
3.1.4	Test MB . . . . .	31
3.1.5	Final Profile Comparision . . . . .	33
3.2	Free Surface Data . . . . .	35
3.2.1	Offshore Incident Wave Statistics . . . . .	36
3.2.2	Nearshore Free Surface Statistics . . . . .	37
3.3	Velocity Data . . . . .	42
<b>4</b>	<b>NUMERICAL MODEL CSHORE . . . . .</b>	<b>45</b>
4.1	Combined Wave and Current Model . . . . .	45
4.2	Probabilistic Model for Wet and Dry Zone . . . . .	47
4.3	Sediment Transport Model . . . . .	56
<b>5</b>	<b>COMPARISON OF NUMERICAL MODEL WITH EXPERIMENT RESULTS . . . . .</b>	<b>62</b>
5.1	Input Parameters . . . . .	62
5.2	Test SL . . . . .	64
5.3	Test SH . . . . .	67
5.4	Test MH . . . . .	70
5.5	Test MB . . . . .	73
5.6	Gravel Edge Migration . . . . .	82
<b>6</b>	<b>CONCLUSIONS . . . . .</b>	<b>83</b>
	<b>REFERENCES . . . . .</b>	<b>85</b>
 <b>Appendix</b>		
<b>A</b>	<b>WAVE GAUGE AND VELOCITY DATA . . . . .</b>	<b>88</b>
A.1	Offshore Incident Wave Conditions . . . . .	88
A.2	Free Surface Data . . . . .	92
A.3	Velocity Data . . . . .	100
<b>B</b>	<b>NUMERICAL PREDICTIONS OF CROSS-SHORE SEDIMENT TRANSPORT . . . . .</b>	<b>104</b>

## LIST OF FIGURES

<b>2.1</b>	Initial beach geometry for the steep slope tests . . . . .	5
<b>2.2</b>	Initial beach geometry for the mild slope tests . . . . .	6
<b>2.3</b>	Sediment grain size distribution for sieve test 2. . . . .	7
<b>2.4</b>	Three measured profiles before averaging . . . . .	9
<b>2.5</b>	Measured profiles from the laser accuracy test . . . . .	10
<b>2.6</b>	Example of unsmoothed offshore wave frequency spectrum from burst SH06 . . . . .	11
<b>2.7</b>	Wave gauge locations . . . . .	12
<b>2.8</b>	Sample wave gauge calibration curve . . . . .	14
<b>2.9</b>	Picture of wall mounted wave gauges G6 and G7 and the furthest onshore current meters EMCM5-6. . . . .	15
<b>2.10</b>	Comparison of wall mounted with carriage mounted wave gauges .	16
<b>2.11</b>	Current meter locations . . . . .	18
<b>2.12</b>	Sample of data collected from a wave burst during test SH. . . . .	19
<b>3.1</b>	Profile evolution for test SL . . . . .	22
<b>3.2</b>	Grain sorting patterns observed in quasi-equilibrium final profiles. .	25
<b>3.3</b>	Profile evolution for test SH . . . . .	27
<b>3.4</b>	Profile evolution for test MH . . . . .	29

<b>3.5</b>	Profile evolution for test MB . . . . .	32
<b>3.6</b>	Comparison of the final profiles . . . . .	34
<b>4.1</b>	Schematic of CSHORE coordinate system . . . . .	46
<b>4.2</b>	Function $G_b(r)$ used in the wet and dry zone . . . . .	54
<b>5.1</b>	Computed profile evolution and measured and computed final profiles for the steep slope, low wave height test SL . . . . .	65
<b>5.2</b>	Comparison of measured free surface statistics with numerical model predictions for test SL . . . . .	66
<b>5.3</b>	Comparison of measured fluid velocity statistics with numerical model predictions for test SL . . . . .	67
<b>5.4</b>	Computed profile evolution and measured and computed final profiles for the steep slope, high wave height test SH . . . . .	68
<b>5.5</b>	Comparison of measured free surface statistics with numerical model predictions for test SH . . . . .	69
<b>5.6</b>	Comparison of measured fluid velocity statistics with numerical model predictions for test SH . . . . .	70
<b>5.7</b>	Computed profile evolution and measured and computed final profiles for the mild slope, high wave height test MH . . . . .	71
<b>5.8</b>	Comparison of measured free surface statistics with numerical model predictions for test MH . . . . .	72
<b>5.9</b>	Comparison of measured fluid velocity statistics with numerical model predictions for test MH . . . . .	73
<b>5.10</b>	Computed profile evolution and measured and computed final profiles for the mild slope with a nearshore bar test MB . . . . .	75
<b>5.11</b>	Comparison of measured and computed profiles after MB09 (top) and MB18 (bottom). . . . .	76

<b>5.12</b>	Comparison of measured free surface and fluid velocity statistics with numerical model predictions for test MB01-09 . . . . .	78
<b>5.13</b>	Comparison of measured free surface and fluid velocity statistics with numerical model predictions for test MB10-18 . . . . .	79
<b>5.14</b>	Comparison of measured free surface and fluid velocity statistics with numerical model predictions for test MB19-27 . . . . .	80
<b>5.15</b>	Comparison of measured free surface and fluid velocity statistics with numerical model predictions for test MB28-36 . . . . .	81
<b>B.1</b>	Numerical predictions of the probability of movement and suspension for test SL . . . . .	104
<b>B.2</b>	Numerical predictions of sediment transport rates for test SL . . . .	105
<b>B.3</b>	Numerical predictions of the probability of movement and suspension for test SH . . . . .	106
<b>B.4</b>	Numerical predictions of sediment transport rates for test SH . . . .	107
<b>B.5</b>	Numerical predictions of the probability of movement and suspension for test MH . . . . .	108
<b>B.6</b>	Numerical predictions of sediment transport rates for test MH . . . .	109
<b>B.7</b>	Numerical predictions of the probability of movement and suspension for test MB . . . . .	110
<b>B.8</b>	Numerical predictions of sediment transport rates for test MB . . . .	111



## LIST OF TABLES

<b>2.1</b>	Summary of sieve test 2 . . . . .	8
<b>2.2</b>	Wave Gauge Locations . . . . .	13
<b>2.3</b>	Current meter locations . . . . .	17
<b>3.1</b>	Conservation of gravel for test SL. . . . .	24
<b>3.2</b>	Onshore migration of the seaward edge of the gravel layer . . . . .	26
<b>3.3</b>	Conservation of gravel for test SH . . . . .	28
<b>3.4</b>	Conservation of gravel for test MH . . . . .	30
<b>3.5</b>	Conservation of gravel for test MB . . . . .	33
<b>3.6</b>	Average incident wave conditions and reflection coefficient R obtained from gauges G1-G3 . . . . .	37
<b>3.7</b>	Burst averaged free surface statistics for gauges G1-G5 . . . . .	38
<b>3.8</b>	Burst averaged free surface statistics for gauges G6-G8 . . . . .	40
<b>3.9</b>	Velocity statistics averaged from each test . . . . .	43
<b>5.1</b>	Summary of CSHORE input parameters . . . . .	63
<b>5.2</b>	Comparison of onshore movement of the gravel edge . . . . .	82
<b>A.1</b>	Offshore wave conditions for test SL . . . . .	88
<b>A.2</b>	Offshore wave conditions for test SH . . . . .	89

<b>A.3</b>	Offshore wave conditions for test MH . . . . .	90
<b>A.4</b>	Offshore wave conditions for test MB . . . . .	91
<b>A.5</b>	Free surface statistics at Gauges G1-G5 for test SL. . . . .	92
<b>A.6</b>	Free surface statistics at Gauges G6-G8 for test SL. . . . .	93
<b>A.7</b>	Free surface statistics at Gauges G1-G5 for test SH. . . . .	94
<b>A.8</b>	Free surface statistics at Gauges G6-G8 for test SH. . . . .	95
<b>A.9</b>	Free surface statistics at Gauges G1-G5 for test MH. . . . .	96
<b>A.10</b>	Free surface statistics at Gauges G6-G8 for test MH. . . . .	97
<b>A.11</b>	Free surface statistics at Gauges G1-G5 for test MB. . . . .	98
<b>A.12</b>	Free surface statistics at Gauges G6-G8 for test MB. . . . .	99
<b>A.13</b>	Velocity statistics for test SL. . . . .	100
<b>A.14</b>	Velocity statistics for test SH. . . . .	101
<b>A.15</b>	Velocity statistics for test MH. . . . .	102
<b>A.16</b>	Velocity statistics for test MB. . . . .	103

## ABSTRACT

Coastal gravel can be found in both natural beach settings and in man-made protective structures like revetments. The experiment presented in this report was conducted in a wave flume to investigate the cross-shore evolution of gravel beaches under irregular laboratory wave conditions. A total of four tests were performed with varying initial beach profiles and incident significant wave heights. The first two tests were on an initially steep slope of  $1/2$  with two different significant wave heights, both of which created erosional conditions. The third test had an initially milder  $1/5$  slope resulting in beach accretion and the final test measured the onshore migration of a gravel bar. Each test consisted of either 18 or 36 wave bursts of 400 seconds, after which the profiles appeared to be quasi-equilibrium. Free surface and velocity data was collected and time-averaged for each 400 second wave burst and profile measurements were recorded for the initial, final and at least three intermediate profiles. The quasi-equilibrium profiles observed were similar in shape, but were affected by the differences in wave height and the initial profile conditions.

Recorded hydrodynamic and profile evolution data was used for validation of a numerical model. The tests were designed to investigate the applicability of a numerical model developed for damage progression of stone armor layers to finer gravel material and to test the accuracy of the bed load formulation originally developed for a sand sediment transport model. The critical stability parameter used to determine movement for stone armors was found to predict profile change for the two erosion tests. The bed load formula required adjustment to better predict the amount and extent of onshore transport for the mild slope and bar migration test.



## Chapter 1

### INTRODUCTION

Gravel beaches can be found in several parts of the world including the west coast of the United States, parts of England's coastline, and in many other countries. Gravel has been traditionally used as a buffer at the toe of permanent protective structures like sea walls, groins, jetties, and breakwaters (Pilarczyk and den Boer 1983). However, interest in gravel as a more prominent part of shoreline protection has increased through design of gravel nourishment projects and dynamic revetments which are constructed of gravel or cobbles that can be mobilized by large wave action rather than large quarry stones used in traditionally static revetments (Ahrens 1990 and van Wellen et al. 2000). Advantages of using gravel in comparison to larger stones include reduction in cost, easier construction, and closer resemblance to natural beach conditions, especially in regions where gravel beaches naturally exist.

As with finer grained sand beaches, a gravel beach or protective structure is expected to evolve under wave action. Accurate prediction of this sediment transport and profile evolution is crucial in prediction of beach erosion during storm events and in the design of beach nourishment projects. However, the mechanisms of cross-shore transport are currently not well understood necessitating experimental studies of a wide range of beach conditions. Unfortunately, research on gravel beaches is limited when compared to similar work for sand beaches; however, there have been a few studies including work done by van Hyum and Pilarczyk (1982), van der Meer

and Pilarczyk (1986), Ahrens (1990), and Pedrozo-Acuña et al. (2006) as well as field studies by Allan and Komar (2002) and Austin and Masselink (2006). Similarly, research focused on gravel beach hydrodynamics has been historically limited with the exception of a study by Blewett, et al. (2000) which investigated differences in swash characteristics between sand and gravel beaches.

The hydrodynamics and morphology of gravel beaches have a few characteristic differences from sandy beaches. For a gravel beach, it is expected that the permeability and bottom slope are important for prediction of the magnitude and direction of transport. Work done by Blewett et al. (2000) suggested infiltration on gravel beaches is approximately two orders of magnitude greater than on sand beaches. Additionally, the larger grains on gravel beaches can sustain a significantly steeper slope than finer grained beaches. Having a steeper beach face allows waves to break much farther landward than they would on a mild slope, concentrating breaking in a narrow zone usually parallel to the shoreline (Baldock and Holmes, 1999). Finally, the concentration of wave breaking near the beach face creates swash dominated beach features including a berm, a beach step or terrace, and often beach cusps (Austin and Masselink, 2006).

The research presented in this study involves a series of test conditions on a fine gravel beach with variable initial beach geometry and incident wave conditions to further investigate cross-shore gravel transport both experimentally and numerically. The experiment included a total of four tests on laboratory gravel beaches with different initial beach geometries and incident wave heights. The first two created erosional conditions with an initially steep slope and two different incident wave heights. The second two tests created accretional conditions, one with a mild planar sloping beach and one with an offshore gravel bar. Each of the four tests were continued until a quasi-equilibrium profile was established.

Measured results from the four tests were compared with the time-averaged numerical model CSHORE. Previously, the model has been validated for a number of data sets in both laboratory and field settings. Much of the data was collected through flume experiments on sandy beaches (Schmied et al. 2006, Buck et. al 2007, and Figlus et al. 2009) where suspended sediment transport was believed to be dominant. By using coarser grains for the gravel beach tests, sediment transport was almost entirely restricted to bedload movement, with occasional suspension events under large wave breaking. This allowed for a more rigorous investigation of the bedload transport formulations used within the surf and swash zones.

The following chapters describe the experiments performed, the results obtained, and comparisons with model predictions. Chapter 2 explains the experimental set-up, including the wave and beach conditions used as well as the locations and types of equipment used for data collection. Chapter 3 compiles and discusses the results collected throughout the course of the experiment. Chapter 4 discusses the methods and equations used by the numerical model CSHORE to predict the hydrodynamic forcing conditions and profile evolution. Chapter 5 compares the experimental results with the quantities predicted in CSHORE. Finally, Chapter 6 gives a summary and conclusions from this study. Additional results from each of the experimental tests and CSHORE predictions are provided in Appendices A and B for those who are interested in the details of the experimental and numerical results.



## Chapter 2

### EXPERIMENTAL PROCEDURES

This chapter describes the experimental setup and procedure used to construct the beach profiles, run time series of waves, and collect data. A total of four tests were run to study cross-shore transport of gravel beaches under laboratory wave conditions. The first two tests investigated typically erosional conditions on an initially steep beach under two different sets of wave conditions, first under a lower wave height (test SL) and then under larger waves (test SH). Both tests consisted of eighteen 400 second bursts of waves which yielded an approximately equilibrium profile. The final two tests attempted to create accretional conditions using a milder slope. The first test consisted of a planar sloping beach (test MH); the second test included an artificial bar (test MB). Both tests used the larger wave conditions; again with eighteen wave bursts for test MH and 36 wave bursts for test MB. The spectral peak period,  $T_p$  for all tests was approximately 2.0 seconds and the spectral significant wave height,  $H_{mo}$  was 5.6 *cm* for the low wave height test and approximately 12 *cm* for the high wave height tests.

#### 2.1 Profile Construction

The experiments were conducted in a wave flume in the Center for Applied Coastal Research at the University of Delaware. The flume is 33 meters long, 0.6 meters wide, and 1.5 meters high. It contains an impermeable, fixed slope of 1/34.2 which begins 9.0 meters and ends 20.2 meters from the wave paddle. A gravel beach was constructed near the end of the impermeable slope, beginning at a distance 18.2

meters and ending 22.2 meters from the wave paddle. The initial profiles for the steep and mild beaches are described in sections 2.1.1 and 2.1.2, respectively. At the landward end of the flume, a platform was constructed underneath the gravel to reduce the gravel in the tank and a vertical wall was placed at 22.2 meters to reduce the amount water and gravel needed. Profile templates were created along the outside of the glass walls of the tank using string taped to outline the desired slope. Gravel was then filled in and shaped to match the profile outlines on either side of the flume. To ensure a constant gravel volume after wave bursts, the gravel was compacted by weight as it was added to the flume.

### 2.1.1 Steep Slope Tests

The seaward limit of the steep profile was initiated with a  $1/20$  slope intersecting the impermeable slope at 18.2 meters from the wave paddle in order to avoid any boundary effects from the edge of the impermeable slope. The  $1/20$  slope continued for 2.7 meters where it transitioned to a steep,  $1/2$  slope for 0.6 meters in the cross-shore direction. At the landward limit of the  $1/2$  slope, a 0.7 meter wide berm was constructed. Figure 2.1 illustrates the steep slope experimental set-up.

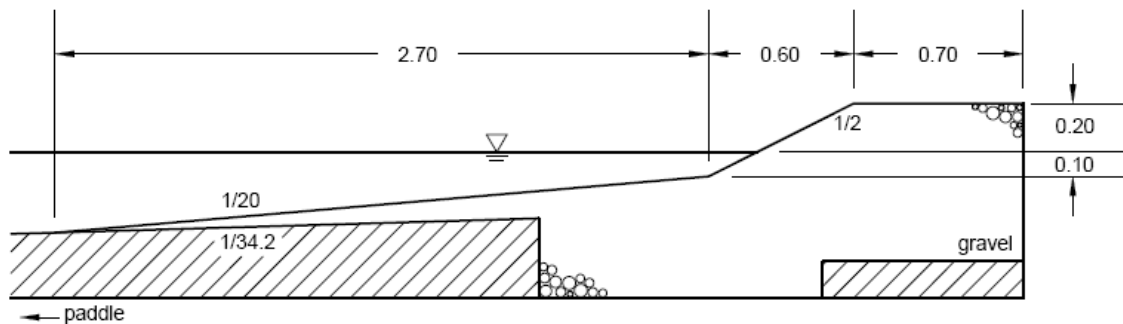


**Figure 2.1:** Illustration of the experimental set-up for the steep slope tests.

### 2.1.2 Mild Slope Tests

The initial mild slope profile used in test MH was also designed with a  $1/20$  slope from 18.2 to 20.9 meters from the wave paddle. At 20.9 meters, the profile shifted to a  $1/5$  slope to the end of the gravel profile at 22.2 meters. No berm was constructed in the mild slope profile. The initial slope for the mild slope with bar (MB) test used the equilibrium profile established at the end of test MH with the addition of a triangular bar with an approximate area of  $515 \text{ cm}^2$ . The bar began 0.9 meters from the seaward gravel edge with an approximately  $1/5$  slope for 50 cm. Then a decline of  $1/5$  was formed on the landward side until it intersected with the pre-existing equilibrium slope. Figure 2.2 illustrates the set-up used for both test MH and test MB.

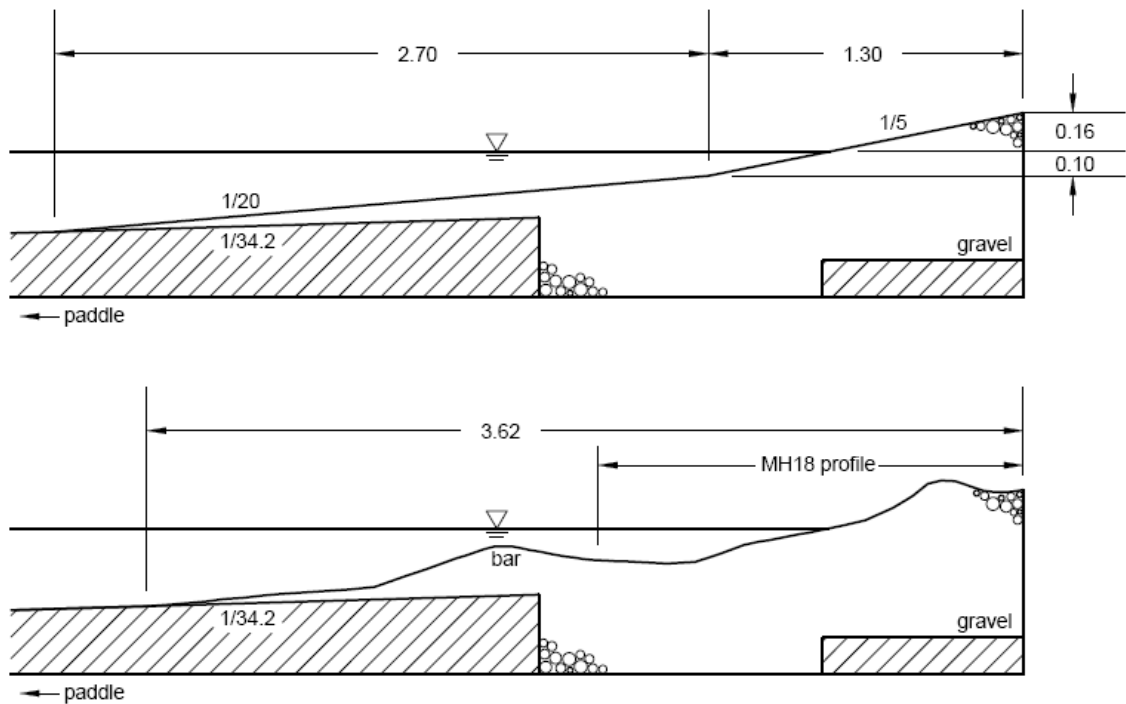


**Figure 2.2:** Illustration of the experimental set-up for the mild slope tests MH (top) and MB (bottom).

## 2.2 Gravel Characteristics

The gravel beach was constructed of approximately 700 kilograms of fine gravel. Two grain size distributions were obtained, the first with eight different sieve sizes according to ASTM standards. This analysis yielded poor resolution in the diameter range of interest and is not presented. The second distribution was obtained using ten sieves with openings ranging from 0.42 mm to 6.35 mm. The second gravel sample, weighing 400 grams was agitated for 20 minutes. Analysis was performed using the geometric mean of two adjacent sieves to obtain a more accurate representation of the grain diameter held in each sieve. The median diameter,  $d_{50}$  was found to be 2.0 mm. Figure 2.3 and Table 2.1 display the results from the second sediment analysis.

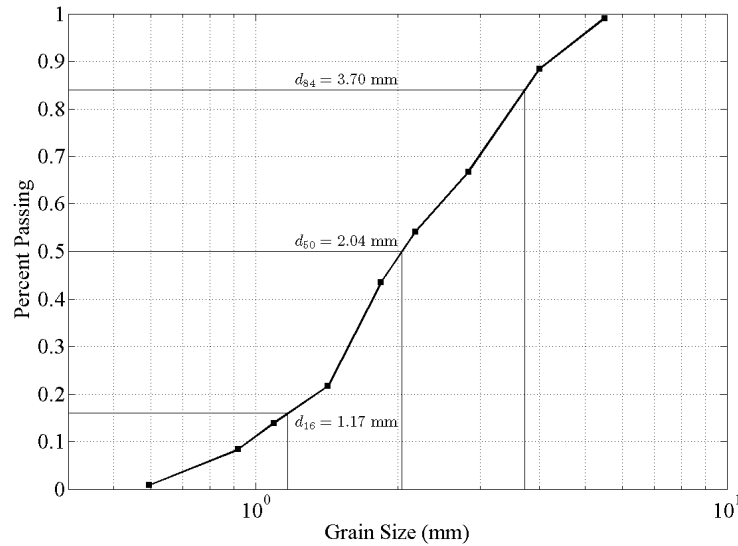


**Figure 2.3:** Sediment grain size distribution for sieve test 2.

The gravel density was estimated by determining the ratio between the gravel mass and the gravel volume. To obtain these measurements, a gravel sample with known mass was added to a graduated cylinder with a known volume of water. The displaced volume represents the volume of the gravel sample. From the measured

**Table 2.1:** Summary of sieve test 2

Sieve Size	Geometric Mean Diameter	Mass	Percent of $M_{total}$	Percent Passing
[mm]	[mm]	[g]	[%]	[%]
6.350	-	0.0	0.00	100.0
4.750	5.492	3.5	0.88	99.1
3.360	3.995	41.1	10.78	88.4
2.380	2.828	86.1	21.53	66.8
2.000	2.182	50.7	12.68	54.2
1.700	1.844	42.5	10.63	43.5
1.190	1.422	87.5	21.88	21.7
1.000	1.091	31.0	7.75	13.9
0.840	0.917	21.9	5.58	8.4
0.420	0.594	30.0	7.50	0.9
pan	-	3.7	0.92	0.0
Total		400.0	100.00	-

density, the specific gravity was estimated using the definition  $s = \rho_s/\rho_w$ , where  $\rho_s$  = gravel density and  $\rho_w$  = density of fresh water. Porosity was determined using the gravel sample volume divided by the total mixture volume including voids. Measurements yielded a density of  $2.7 \text{ g/cm}^3$ , specific gravity of 2.7, and porosity of 40%.

The fall velocity of the gravel was determined by dropping several grains of gravel from each of the nine size groups in the second sediment size distribution test into a clear container of fresh water. Ten fall times for each of the nine groups were recorded for a fall distance of 0.5 *meters*. The representative fall velocity was then calculated to be  $0.25 \text{ m/s}$  using a proportional weighting factor related to the percentage of the total mass,  $M_{total}$ .

### 2.3 Profile Measurements

The experiment beach profiles were measured using a Leica DISTO laser distance meter, which measures the vertical distance in air to the nearest millimeter.

To monitor accuracy of the laser profiler and evaluate alongshore variability, three transects were taken of each profile. The three profiles were spaced at equal increments across the wave flume, one along the centerline of the flume and two offset 15 cm on either side of the centerline. The profile elevation was measured and recorded manually at 2 *cm* increments in the cross-shore direction to obtain a sufficient resolution of bed elevation. Figure 2.4 displays all three measured transects from the initial profile of the steep slope test.

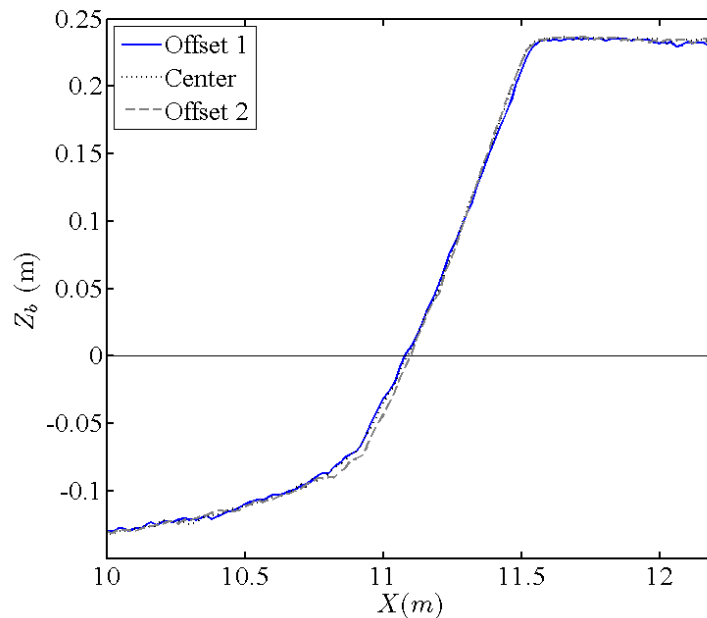


**Figure 2.4:** Three measured profiles before averaging. The similarity in the three cross-sections demonstrates the profile was longshore uniform.

An initial test of profile accuracy was performed before the actual experiment to evaluate how the laser would perform on the uneven gravel surface. The same profile transect was measured forwards and backwards to see if any large variations occurred due to the coarse grains, Figure 2.5 shows the results from this test of laser accuracy. The test yielded fairly consistent data, with small variations within the median gravel diameter equal to 2.0 *mm*.

The laser profile measurement required drainage of the tank. As a result, the profile was measured only after noticeable profile changes. The profile was measured with decreasing frequency as evolution slowed and the beach approached equilibrium. At least five profiles were measured in each test, these included the initial profile and final profile as well as three additional profiles after 1, 3, and 10 wave bursts for tests SL, SH, and MH. A total of seven profiles were recorded in test MB including the initial profile, after bursts 1, 3, 9, 18, 27, and after the 36th and final wave burst.

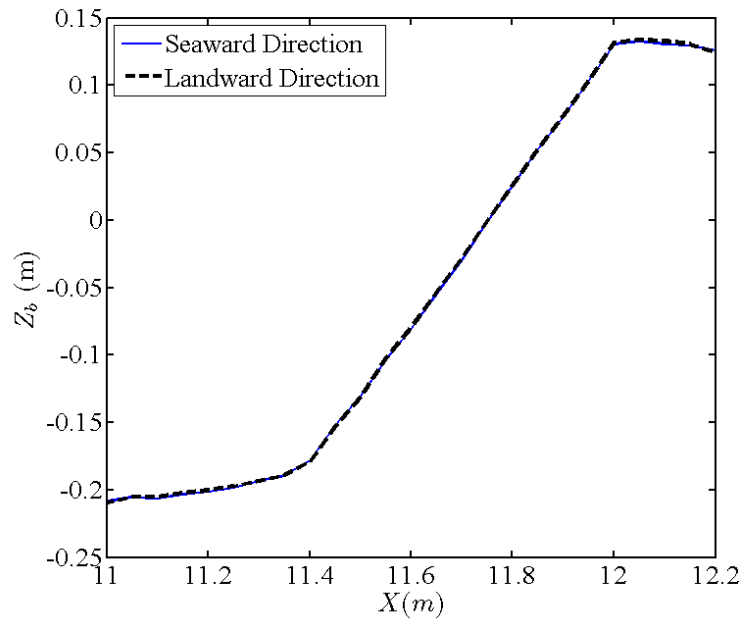


**Figure 2.5:** Measured profiles from the laser accuracy test in which a single transect of a profile was measured in opposing directions. The similarity in the two measurements demonstrates the uneven surface due to the gravel diameter does not have a large impact on accuracy of the laser measurements.

## 2.4 Wave Generation and Gauges

### 2.4.1 Irregular Wave Generation

Waves were generated using a piston-type wave paddle at the offshore end of the flume, 18.2 meters from the seaward edge of the gravel beach. The water depth at the wave paddle was kept constant at 57 cm, as shown in Figure 2.7. The wave paddle was perforated with an array of one inch diameter holes. The waves were generated using a 400 second time series of voltages read by the wave maker at a frequency of 50 Hz. Each voltage corresponds to a particular paddle displacement, generating wave motion. The irregular wave train was shaped to resemble the TMA spectrum with varying incident wave heights and periods as discussed in section 3.2. Figure 2.6 shows an example of the frequency spectra obtained from a wave burst. The figure shows the peak energy is at approximately 2 seconds or frequency,  $f = 0.5$  Hz, consistent with measurements of spectral peak period  $T_p$ , discussed further in Chapter 3.

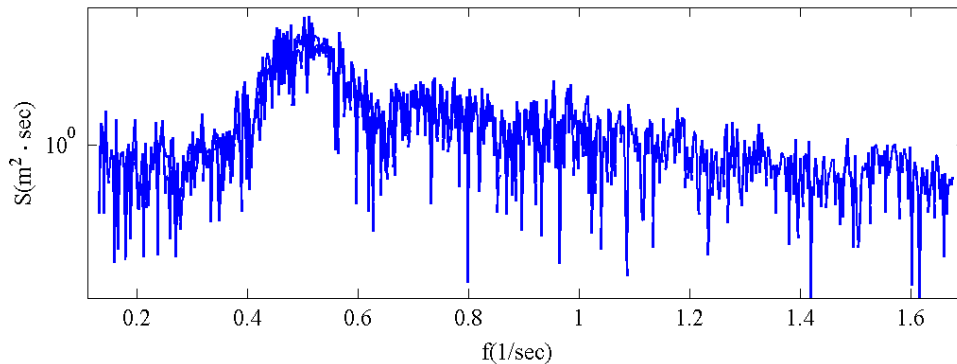


**Figure 2.6:** Example of unsmoothed offshore wave frequency spectrum from burst SH06. The peak at  $f = 0.5$  Hz shows the peak energy in the wave spectrum was approximately 2 seconds.

### 2.4.2 Location of Wave Gauges

Eight capacitance gauges, G1-G8 were placed as shown in Figure 2.7. The five offshore gauges, G1-G5 were mounted on mobile carriages along the centerline of the wave flume. G1-G3 were used to separate incident and reflective waves and to monitor the repeatability of wave conditions. Gauge G1 was considered the offshore boundary for the numerical model CSHORE input as explained in section 4.1 and was therefore defined as  $x = 0$  meters. Gauges G4 and G5 were used to track wave transformation over the 1/20 gravel slope. The remaining three wave gauges, G6-G8 were installed along the wall of the flume buried in the gravel beach so that part of the gauges would always be submerged. Gauges G6 and G7 were used to measure the free surface elevation in the surf zone of the gravel beach. Gauge G8 was used to obtain a point measurement of swash on the beach face. Table 2.2 details the cross-shore locations of these eight wave gauges where  $x$  is defined as the onshore coordinate with  $x = 0$  at G1 and  $z_b$ =bottom elevation of the initial steep and mild slope tests with  $z_b = 0$  at the still water level (SWL).

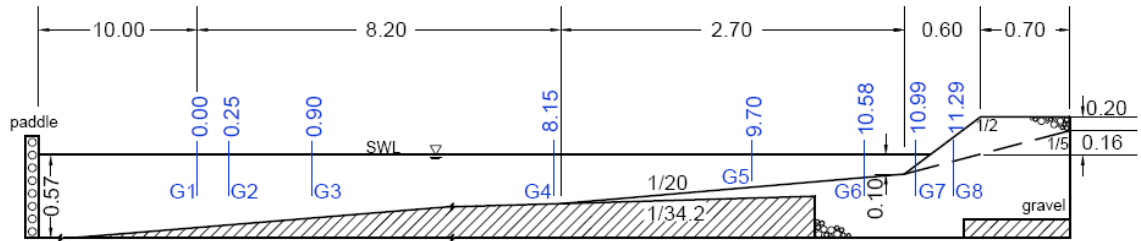


**Figure 2.7:** Wave gauge locations (not-to-scale). The eight wave gauges are shown in blue and the numbers above each gauge represent the cross-shore location in meters relative to the furthest offshore gauge G1.

### 2.4.3 Calibration of Wave Gauges

The five offshore wave gauges, G1-G5 were calibrated between each wave burst electronically using a computer program written in LABVIEW. The program

**Table 2.2:** Wave Gauge Locations

Wave Gauges	$x$	$z_b$	
[-]	[m]	[cm]	
G1	0.00	-51.1	
G2	0.25	-50.4	
G3	0.90	-48.5	
G4	8.15	-27.3	
G5	9.70	-17.3	
G6	10.58	-13.3	
G7	10.99	-7.7	-9.3
G8	11.29	+6.8	-3.1
slope:		steep	mild

controls the motors for all five gauges, raising and lowering the gauges in 1 *cm* increments in the range of -10 and +10 centimeters about the SWL. At every elevation, the voltage of each gauge was recorded by the LABVIEW program, creating a linear relationship between submerged gauge length and voltage. In the event of a non-linear or scattered relation, the calibration was run again to obtain a linear fit. The calibration relationship was imported into the computer program, automatically converting the recorded voltages to the free surface elevation.

The three wave gauges, G6-G8 were fixed on the wall and calibrated by changing the water level in the wave flume. At each water level, 15 seconds of voltage data was recorded by the DATAQ logger. The mean voltages were used to create a calibration curve for each of the three wall gauges. Due to the time required for manual calibration of gauges G6-G8, the calibration was performed only when the tank was drained for a profile measurement. The surface elevation of the gravel at each gauge location was measured simultaneously to interpret measured voltage. Figure 2.8 shows a sample calibration. For this calibration, the gravel level of gauge G8 was approximately midway along the length of the capacitance wires indicating the effect of moist gravel on the calibration curve. As can be seen in the right panel

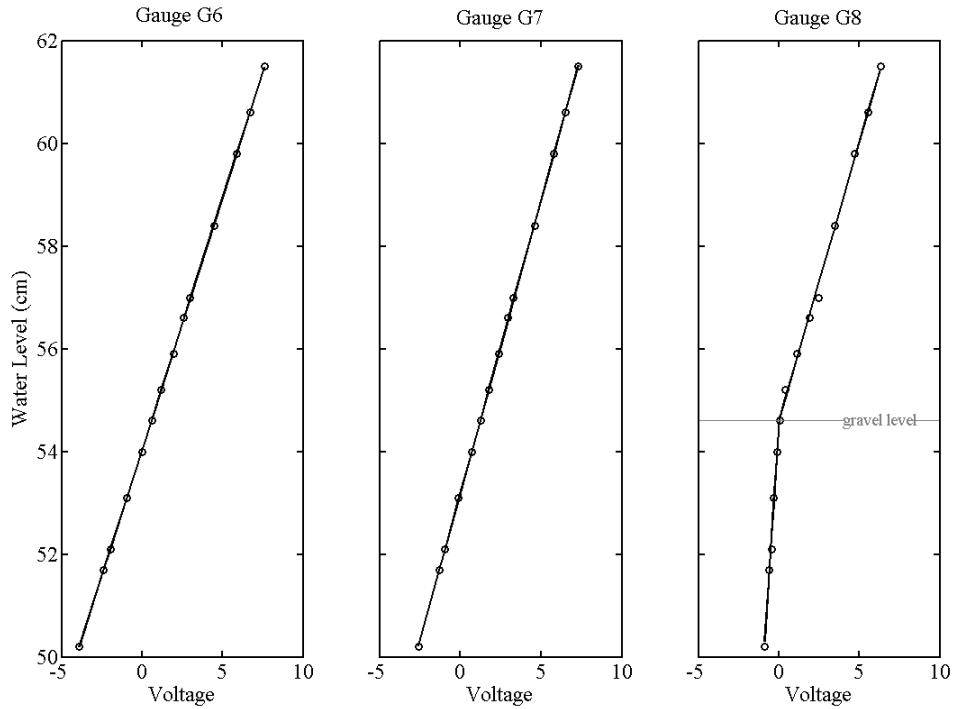


**Figure 2.8:** Calibration curve showing the different linear fits between the gravel covered and exposed portions of the wave gauge G8. The dashed line represents the elevation of the top of the gravel.

of Figure 2.8, there is a separate linear trend when the water level is below the gravel surface level. The linear relationship above the gravel level was used to obtain the water surface elevation above the gravel level only during the wet duration as will be explained in section 3.2.2.

#### 2.4.4 Validation of Wall Mounted Gauges

The three wall gauges operate using the same principle as the carriage mounted gauges. Because the three gauges were buried and fixed on the wall, the capacitance wires were positioned using suction cups at either end of the capacitance wire as showing in Figure 2.9. Each gauge had its own ground taped along the wall approximately 3 centimeters from the capacitance wires. The bottom of each gauge

was buried below the gravel surface as indicated in the calibration for gauge G8 in Figure 2.8. Water elevations below the gravel surface level were not analyzed due to the difficulty in interpreting the measured voltage.

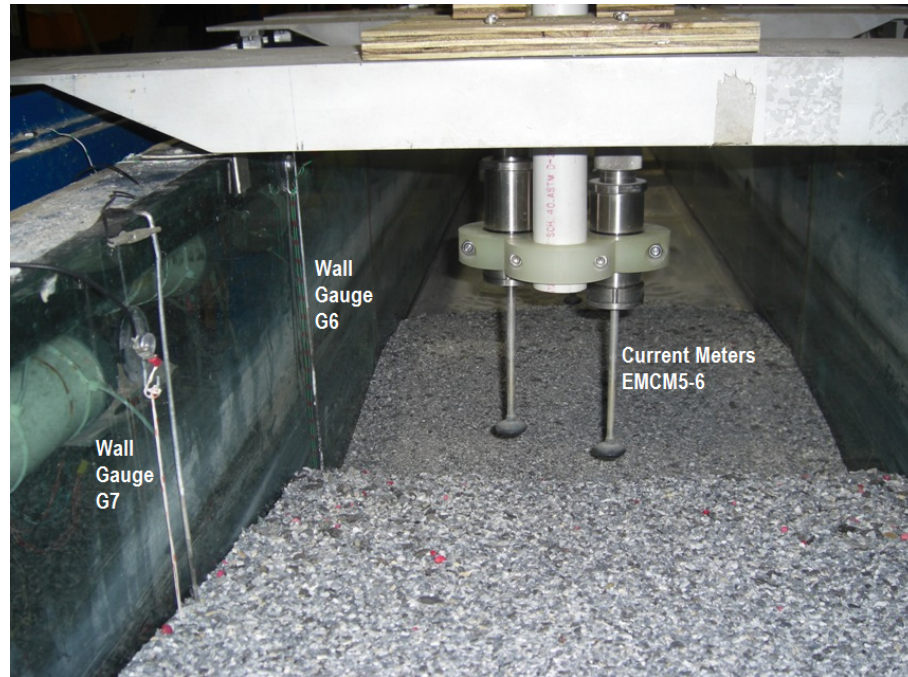


**Figure 2.9:** Picture of wall mounted wave gauges G6 and G7 and the furthest onshore current meters EMCM5-6.

Due to the close proximity to the wall, surface tension and wall effects were investigated prior to beginning the four tests. Using an equilibrium profile established by 22 wave bursts in a preliminary test, the carriage mounted gauge G5 was positioned at the same cross-shore location as wall gauge G6. After calibrating both gauges, several more wave bursts were run with the same conditions used when creating equilibrium. The free surface elevation data from both was recorded and compared. Figure 2.10 displays a 10 second segment of the 400 second wave burst. The average free surface elevation,  $\bar{\eta}$  was found to be  $-0.21\text{ cm}$  and  $-0.22\text{ cm}$  for gauge G5 and gauge G6, respectively. The two gauges produced very similar results yielding estimates of the wall effect on the order of  $1\text{ mm}$ .

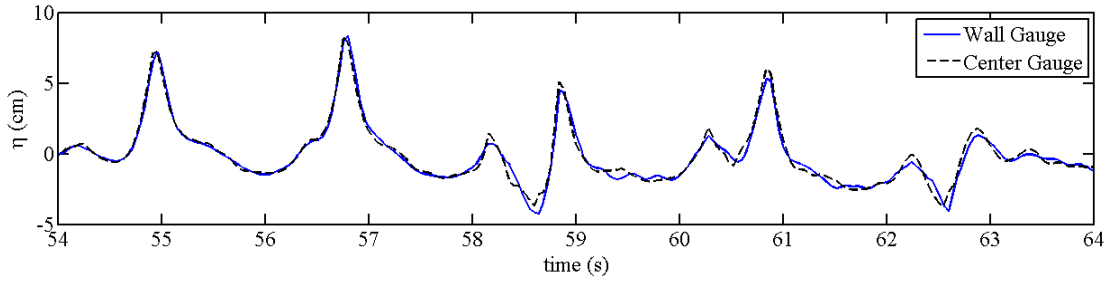


**Figure 2.10:** Comparison of the wall mounted gauges with the carriage mounted gauges, the 10 second segment of wave data demonstrates the strong correlation between the two gauges.

The erosion and accretion of gravel on the wall mounted gauges G6-G8 created another calibration concern. Gravel does not have the same conductance as water, as shown for gauge G8 in Figure 2.8. To account for the changing bed level, the surface elevation of gravel at the gauge was recorded together with the voltage corresponding to the SWL before and after each wave burst. The gravel level was used to determine the offset in the calibration curve caused by the change in gravel elevation as shown for gauge G8 in Figure 2.8. The SWL voltage measurement was used to define the free surface elevation relative to the SWL voltage for each burst.

## 2.5 Electromagnetic Current Meters

Three pairs of electromagnetic current meters were positioned along the gravel profile. The current meters operate using the Faraday principle, detecting how quickly water, acting as a conductor, moves past the sensors. The current meters measure velocity in both the cross-shore and long-shore directions; however only cross-shore data was used in this experiment. Each pair of current meters has a cross-shore separation of 10 *cm*, but each pair has a different vertical offset between the two current meters. EMCM1-2, EMCM3-4, and EMCM5-6 have a vertical separation of 2 *cm*, 3 *cm*, and 4 *cm*, respectively. Table 2.5 details the cross-shore locations and elevations of each of the 6 current meters.

Test	EMCM	$x$	$z_b$	$z_{EMCM}$	Nearest Wave Gauge
		[m]	[cm]	[cm]	
SL	1	8.30	-24.8	-10.8	G4
	2			-14.8	
	3	10.58	-14.1	-8.1	G6
	4			-11.1	
SH	1	8.30	-24.8	-10.8	G4
	2			-14.8	
MH	3	9.85	-16.7	-10.7	G5
	4			-13.7	
MB	5	10.58	-13.3	-8.8	G6
	6			-10.8	

**Table 2.3:** Current meter locations for tests SL, SH, MH, and MB where  $z_b$ =initial bottom elevation for each test. Note: EMCM3-4 and EMCM5-6 were moved to different cross shore locations after test SL due to the amount of air exposure of EMCM5-6 (placed in very shallow water) experienced during test SL. Consequently, no data from EMCM5-6 was used in the data analysis of test SL

Two different current meter arrangements were used during the four different test conditions. The first test SL paired the current meters EMCM1-2, EMCM3-4, and EMCM 5-6 with wave gauges G4, G6, and G7, respectively. However, frequency of air exposure during the test prompted a seaward relocation of current meters EMCM3-4 and EMCM5-6. For the remaining three tests, the furthest offshore pair of current meters EMCM1-2 were positioned at the seaward edge of the gravel in approximately the same cross-shore location as G4. Current meters EMCM3-4 were midway along the 1/20 slope of the gravel beach in approximately the same position as gauge G5. The furthest onshore pair of current meters were located in the same cross-shore position as gauge G6, near the landward edge of the 1/20 slope. Equipment size and mounting required a cross-shore separation of 15 *cm* between the wave gauge G4 and the pair of current meters EMCM1-2 and between G5 and

EMCM3-4. Figure 2.11 illustrates a planview and profile view of the nearshore current meter and wave gauge locations.

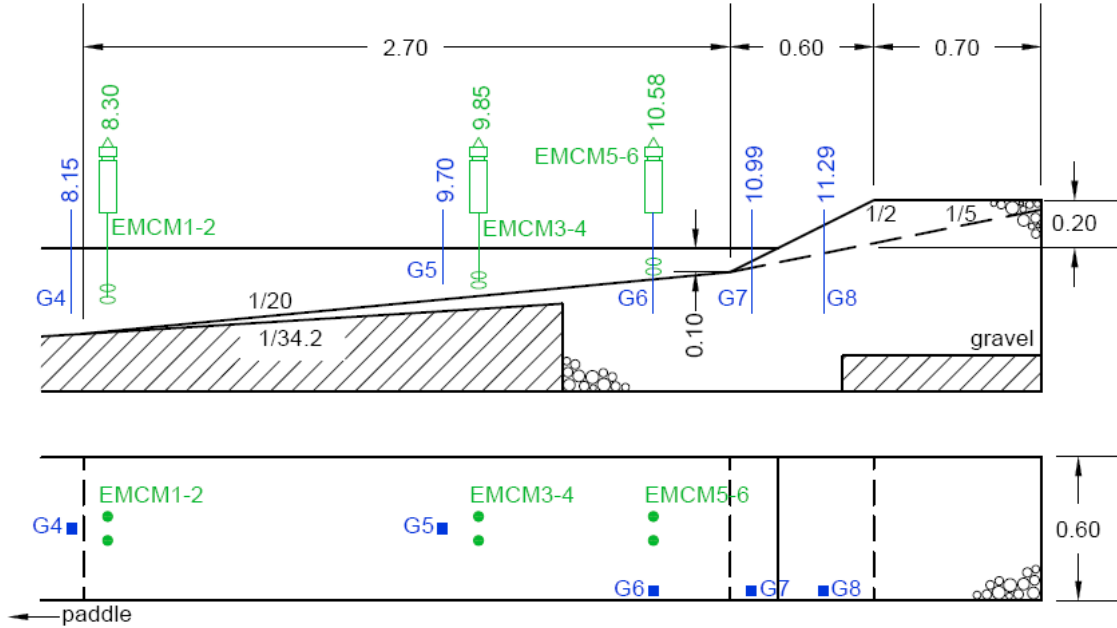


**Figure 2.11:** Locations of the three pairs of current meters, shown in green (all dimensions are in meters). The paired current meters are spaced 10 centimeters apart in the longshore direction. The nearshore wave gauges are also included in blue.

## 2.6 Data Collection

Data was collected by two different computers. The free surface elevation data for gauges G1-G5 was recorded by the same 16 channel National Instruments data acquisition board generating the time series of waves as explained in section 2.4.1. This data was collected at a frequency for 50  $Hz$ . Gauges G5-G8 and current meters EMCM1-6 were connected to a separate computer using a DATAQ system, collected at a frequency of 15  $Hz$ . The overlap at gauge G5 was used to synchronize the two sets of time series collected for 400 seconds. The first 40 seconds of the time series starting from no wave conditions were eliminated from the 400 second time

series when performing statistical and spectral analysis. Figure 2.12 shows sample wave gauge and current meter data collected from a burst in test SH.

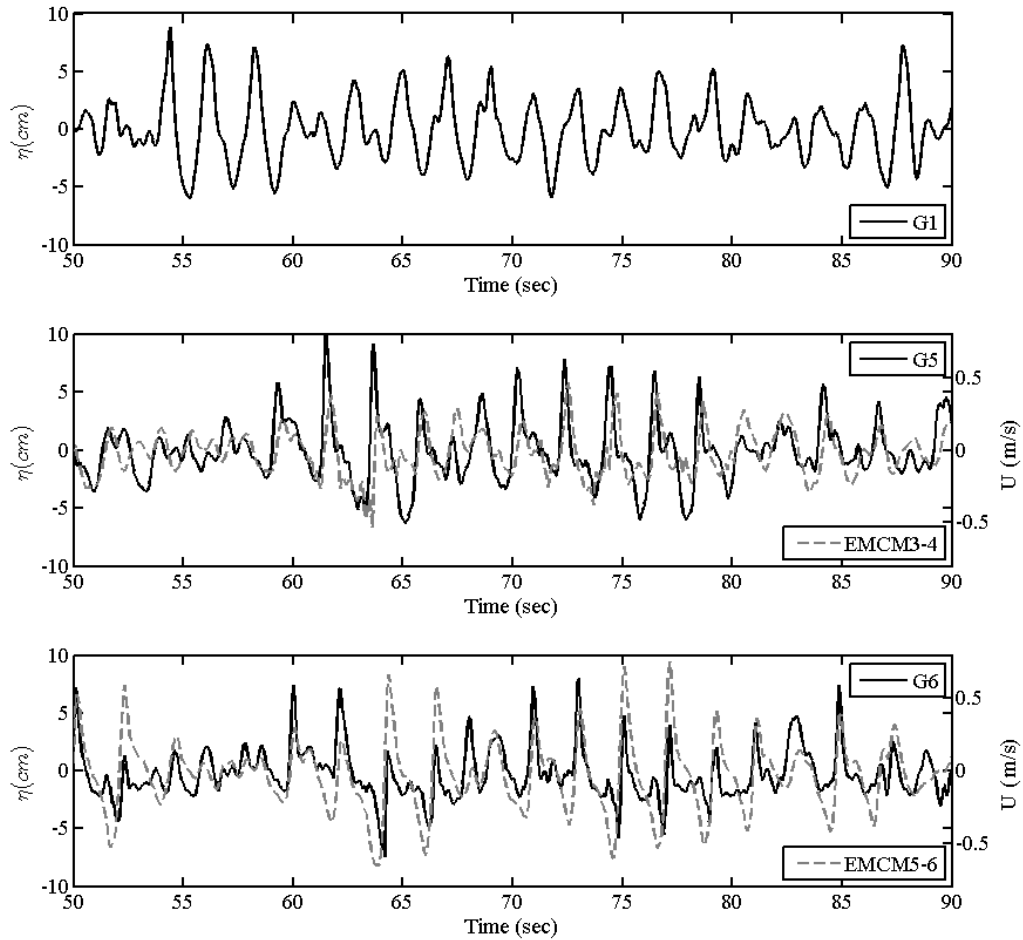


**Figure 2.12:** Sample of data collected from a wave burst during test SH. The solid black lines represent the free surface elevation from three wave gauges and the dashed gray lines represent the current meter data.

## Chapter 3

### EXPERIMENTAL RESULTS

As described in Chapter 2, a total of four tests were performed to investigate cross-shore transport of gravel under different initial beach profile and wave conditions. This chapter describes the methods taken to analyze data collected in the four tests and presents the results in a series of tables and figures. The first section focuses on the profile data collected and is further split into five subsections, the first four present measured profiles from each of the four tests and discuss trends in gravel transport observed during each test. The final subsection compares the quasi-equilibrium final profiles to examine the effects of the initial profile and wave height. The final two sections discuss analysis, trends, and variations in the collected free surface and velocity data.

#### 3.1 Profile Data

The beach profile was measured at least five times for each test, as discussed in Chapter 2. Using a tape measure secured along the edge of the wave flume for determination of the cross-shore position, a laser distance meter measured the distance from its constant vertical position on a mobile cart to the local bed level at 2 *cm* increments along the wave flume. The bottom of the flume at  $x = 8.2$  *m* on the impermeable slope of 1/34.2 was used as a baseline measurement to eliminate the offset between the cart and the beach. The still water level (SWL), measured using a tape measure on the side of the flume was considered the datum. Profiles were measured landward of  $x = 8.2$  *m* up to the vertical wall shown in Figures 2.1

and 2.2. The measured bottom elevation  $z_b$  is negative (positive) below (above) the SWL. As discussed in Chapter 2, three transects of each profile were measured to monitor cross-shore variation and reduce the effect of instrument error. The three profiles were averaged and are presented in subsequent sections. Each measured profile was compared to the corresponding initial profile to ensure that erosion and accretion values matched within an acceptable margin of error, this data examining the gravel volume conservation is also presented in the following sections.

### 3.1.1 Test SL

Test SL, with a steep initial slope of 1/2 and low significant wave height  $H_{mo} = 5.6 \text{ cm}$  had rapid initial profile change despite having very small waves, as shown in Figure 3.1 where the numeral after SL indicates the number of bursts after which the profile was measured. Profile change or gravel movement was primarily restricted to bedload over most of the active gravel profile. The maximum run-up during test SL was at the seaward edge of the wide berm. Periodically, wave action created a very steep scarp in the region of maximum run-up; however, the scarp rarely lasted for more than 1-2 bursts before it became too unstable and collapsed. This process created a new volume of gravel within the maximum wave run-up, allowing for more gravel to be eroded from above the SWL and deposited at the toe of the steep slope. The deposited material formed a beach terrace, visible in Figure 3.1 seaward of the still water level intersection from  $x = 10.8$  to  $x = 11.1 \text{ m}$ . The still water depth at the seaward edge of the terrace was approximately the same as  $H_{mo}$ .

Another interesting feature created in test SL and each of the following tests was the development of an erosional zone seaward of the beach terrace. The erosion was observed to develop due to the collision of incoming breaking waves with large backwash events. The eddies generated due to these hydrodynamic interactions lifted sediment and ultimately transported it onshore to the beach terrace. Once on

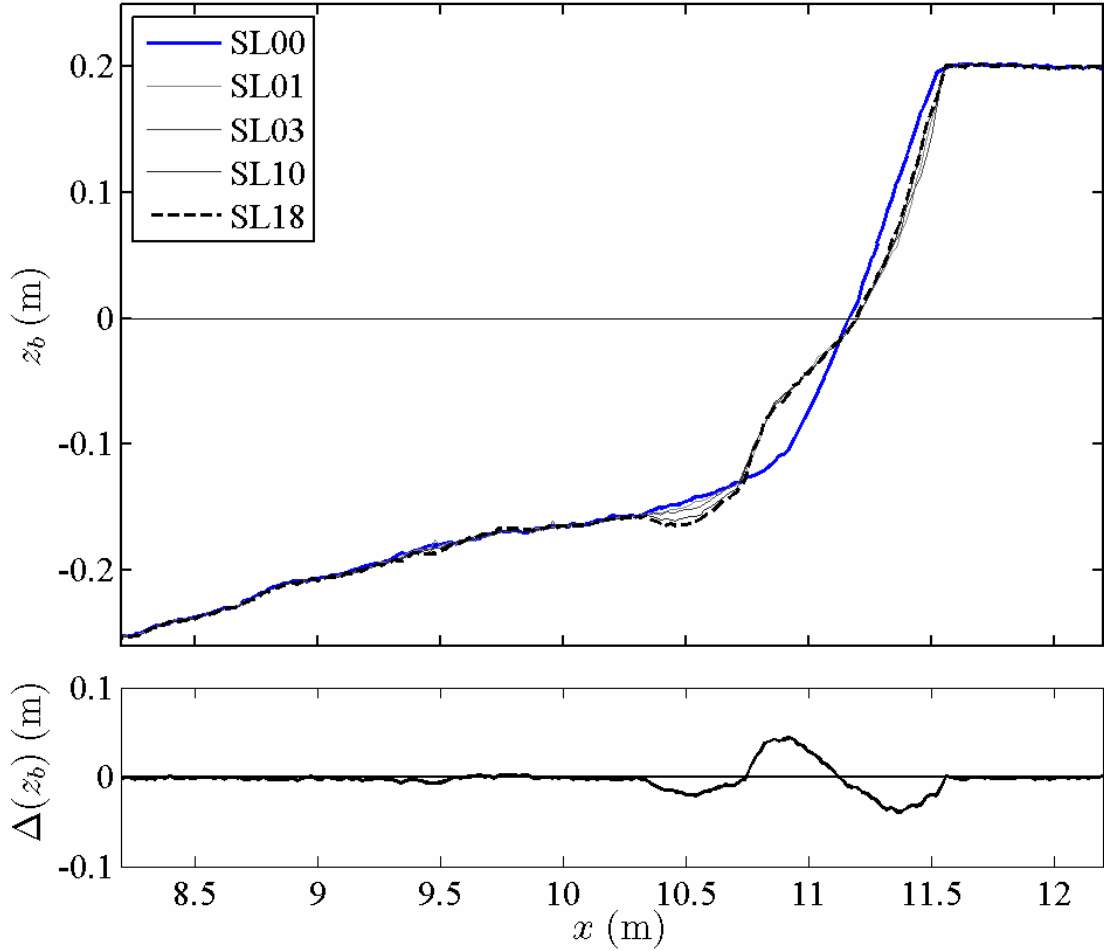


**Figure 3.1:** Profile evolution for test SL where  $\Delta(z_b)$ =bottom elevation change from SL00 to SL18.

the terrace, the net transport rate became negligible as reflected by the fairly constant terrace profile measurements after the first burst SL01. The profile evolution appeared to approach a quasi-equilibrium profile after three waves bursts with some minor fluctuations throughout the remainder of the test. The erosion zone seaward of the terrace continued to grow with continued bursts. The profile above the SWL was eroded but rebuilt after SL03 as shown in Figure 3.1. The proximity of the erosion zone to the edge of the impermeable slope and vertical wall might have created boundary effects, contributing to artificial profile changes. However, later tests (for

example, test MH) yielded similar erosion zones seaward of the terrace but further landward of the impermeable slope boundary.

Throughout the course of test SL (and also in the three subsequent tests), cusp-like features were observed at the berm of the beach face. The cause of these formations could likely be attributed to effects from the walls and current meters. Boundary effects from the wall and impedance from the current meters created small amounts of longshore non-uniformity of incoming waves which resulted in differences in the maximum run-up height of some of the larger waves as well as in the amount of berm erosion. Once irregularities were established, the cusps would further develop during subsequent waves due to the variability in beach slope. To minimize the effects of cusping, the features were smoothed in the longshore between bursts.

For the measured profiles, the volumetric change was evaluated between the initial profile  $z_{bi}(x)$  and each subsequent measured profile  $z_b(x)$ . A rectangular integration approximation method was used to compute the volumetric change for the entire gravel profile. The profile change  $\Delta z_b$  at each measured cross-shore location was multiplied by the 2 *cm* measuring interval in the gravel zone of  $x = 8.2 - 12.2$  *m* to obtain a volume change per unit width in the longshore direction. The volumes corresponding to locations with a decrease in bed elevation were summed to calculate the eroded volume  $V_e$  as follows

$$V_e(t) = \int_{8.2}^{12.2} [\Delta z(t, x)] \Delta x \begin{cases} \Delta z = z_{bi} - z_b & \text{if } z_{bi} > z_b \\ \Delta z = 0 & \text{if } z_{bi} \leq z_b \end{cases} \quad (3.1)$$

where the regions of deposition are excluded. The depositional volume  $V_d$  evaluates the regions where  $z_b > z_{bi}$  as shown in the following equation

$$V_d(t) = \int_{8.2}^{12.2} [\Delta z(t, x)] \Delta x \begin{cases} \Delta z = 0 & \text{if } z_{bi} \geq z_b \\ \Delta z = z_b - z_{bi} & \text{if } z_{bi} < z_b \end{cases} \quad (3.2)$$

computed for each measured profile. The sum of eroded and accreted volumes represented in equations (3.1) and (3.2) can be used to evaluate the net volume change  $V_c$  in the zone from  $x = 8.2 - 12.2 \text{ m}$

$$V_c(t) = V_d(t) - V_e(t) \quad (3.3)$$

The net volumetric change indicates the degree of porosity change and measurement error. In test SL,  $V_c$  values are negative and not negligible in comparison to the eroded and deposited volumes, suggesting compaction of the gravel occurred especially during the first wave burst. This compaction creates erosion values noticeably larger; however, an elevation measurement error of  $1 \text{ mm}$  over the entire 4 meter gravel profile would result in a similar volume error of  $40 \text{ cm}^2$ . As a result, the causes of these discrepancies in sediment volume are not clear.

**Table 3.1:** Conservation of gravel for test SL.

Test No.	$V_e$	$V_d$	$V_c$
	$[\text{cm}^2]$	$[\text{cm}^2]$	$[\text{cm}^2]$
SL01	140.5	111.2	-29.3
SL03	151.8	113.5	-38.3
SL10	143.9	112.9	-31.0
SL18	152.3	109.2	-43.1

A final important observation gained from test SL was the prevalence of grain sorting after wave bursts. Minor amounts of grain sorting were observed after the first wave burst and maintained throughout subsequent bursts in fairly constant patterns. Typically, the most coarse material tended to remain at the seaward edge of the berm where maximum run-up reached; the run-up deposited large grains while finer material was entrained in the backwash and carried offshore. A thick band of

slightly finer material accumulated around the SWL where swash oscillations were concentrated. Another band of coarse material developed at the seaward edge of the terrace, managing to fall quickly during suspension events while finer grains were transported onshore. Wave action seaward of the erosion zone was too weak to cause sorting and the gravel stayed well mixed throughout the test. Figure 3.2 illustrates the grain sorting observed in test SL as well as in the quasi-equilibrium final profiles of tests SH, MH, and MB. It should be stated that Figure 3.2 was based solely on the visual inspection of the surface gravel. The cross-shore variation of the grain size distribution was not measured.

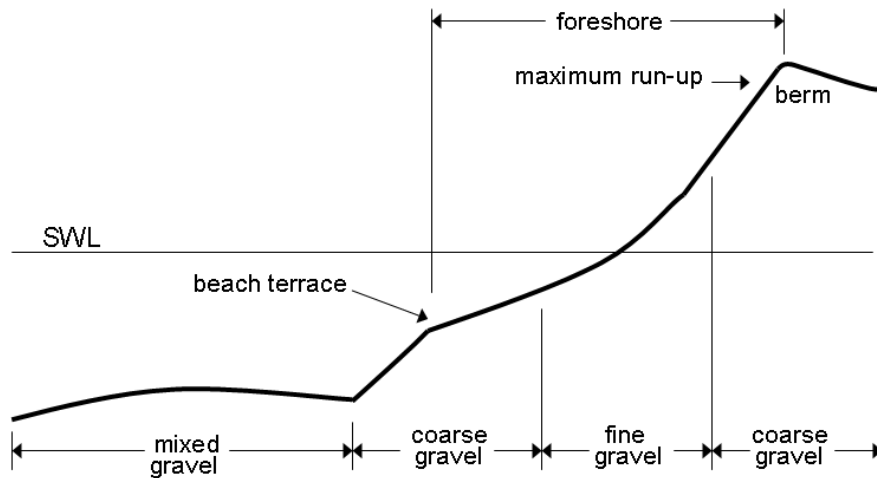


**Figure 3.2:** Grain sorting patterns observed in quasi-equilibrium final profiles.

### 3.1.2 Test SH

The second test performed, also with a steep initial slope of  $1/2$  but with double the significant wave height created profile evolution similar to test SL. The profile evolution again occurred very quickly reaching quasi-equilibrium conditions after 3 wave bursts. The wave action on the beach face created unstable beach scarps that collapsed and supplied sediment for offshore transport. Along the  $1/20$  slope, gravel consistently moved onshore as reflected in the onshore migration of the

seaward limit of gravel throughout the 18 bursts. The location of the gravel edge was noted during each profile measurement and is presented in Table 3.2 for test SH and the three other tests. The onshore transport on the 1/20 slope and the offshore transport on the 1/2 slope created a quasi-equilibrium profile with a concave beach face. As with the lower wave height, wave action created a large deposition or beach terrace at the intersection of the 1/2 and 1/20 slopes and a smaller erosion region landward of the SWL as shown in Figure 3.3. Also similar to test SL, was the hole of erosion which developed at the toe of the terrace. A noticeable difference between the two step tests was the gradual construction of a deposition region at the location of maximum run-up. In test SL, the maximum run-up did not exceed the berm; however, the larger waves in test SH overtopped the edge of the berm, creating a small region of deposition at the upper limit of the wave uprush. At this location, a significant portion of the uprush appeared to infiltrate into the gravel, leaving behind the formerly entrained sediment.

**Table 3.2:** Onshore migration of the seaward edge of the gravel layer on the impermeable slope of 1/34.2. Cross-shore locations are measured from offshore wave gauge G1.

Burst No.	Time	Edge of gravel location			
		SL	SH	MH	MB
[-]	[sec]	[m]	[m]	[m]	[m]
00	0.0	8.20	8.20	8.20	8.58
01	400.0	8.22	8.26	8.30	8.58
03	1200.0	8.23	8.30	8.34	8.58
09	3600.0	-	-	-	8.70
10	4000.0	8.26	8.40	8.44	-
18	7200.0	8.26	8.44	8.58	8.82
27	10,800.0	-	-	-	9.50
36	14,400.0	-	-	-	9.76

Unlike test SL, inconsistencies in the sediment budget for test SH can likely be accounted for by profile measurement error. Each of the measured profiles yielded a

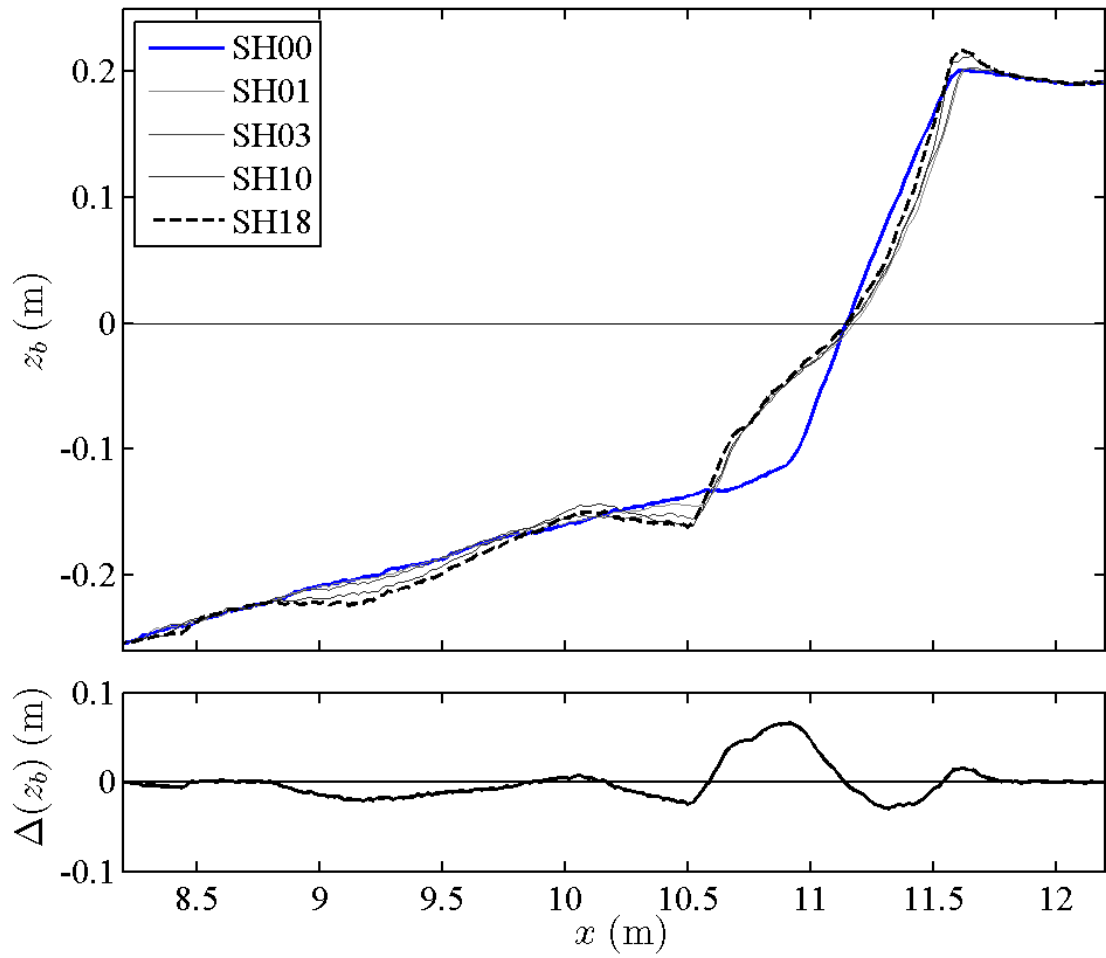


**Figure 3.3:** Profile evolution for test SH

surplus volume ( $V_d > V_e$ ) as detailed in Table 3.3. The difference between  $V_d$  and  $V_e$  needs to be interpreted in light of the 1 *mm* uncertainty of the laser distance meter and the irregularity of the surface of the gravel having a median diameter of 2 *mm*. The grain sorting patterns were consistent with observations described for test SL and illustrated in Figure 3.2.

**Table 3.3:** Conservation of gravel for test SH

Test No.	$V_e$	$V_d$	$V_c$
	[ <i>cm</i> <sup>2</sup> ]	[ <i>cm</i> <sup>2</sup> ]	[ <i>cm</i> <sup>2</sup> ]
SH01	193.6	217.1	23.5
SH03	208.4	238.0	29.6
SH10	247.8	261.5	13.7
SH18	261.3	285.6	24.3

### 3.1.3 Test MH

The goal of the third test was to reverse the profile evolution, creating accretional conditions with an initially milder slope and the larger significant wave height. The steepening of the beach face was a slower process than the destructive conditions witnessed in tests SL and SH. This is clearly illustrated in the progression of measured profiles shown in Figure 3.4 as well as in the sediment budget in Table 3.4, which show a gradual deposition well above the SWL even after 10 wave bursts. This contrasts significantly with the steep tests that established equilibrium after 3 wave bursts. Beach accretion occurred in the region of maximum run-up on the beach face, located around 11.8 to 12 meters. Deposition was initiated quickly, with noticeable deposition occurring after only 60 seconds of wave action during the first burst of waves. The depositional region appeared to have developed as a result of increased infiltration near the point of maximum run-up. The increased infiltration left the coarse material deposited near the upper limit of uprush. Finer materials were carried downslope with the remaining backwash. Once the depositional feature

had been established, it continued to grow upward and seaward because only very large waves could overtop the newly built berm and deposit sediment behind it. By the 11th burst, less than a dozen of the waves per burst were able to overtop the berm which further reduced to zero overtopping by the end 18 bursts.

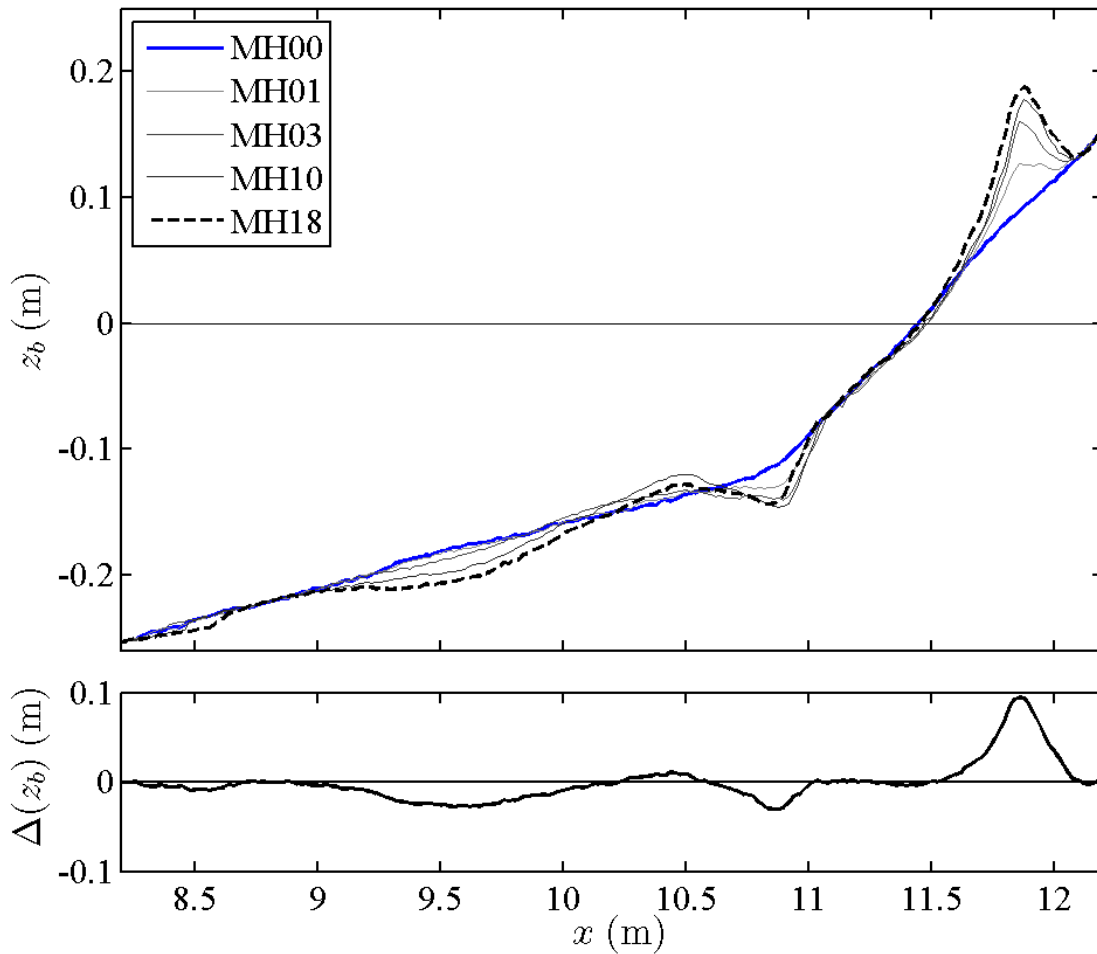


**Figure 3.4:** Profile evolution for test MH

The gravel supply for deposition came largely from a hole of erosion that developed at the toe of the 1/5 beach slope and recreated the beach terrace of coarse grains observed in the steep slope tests. However, by examining Figure 3.4 it is clear the erosion zone and beach terrace maintained fairly constant size throughout the

wave bursts, requiring an additional source of gravel to allow for continued growth of the deposition above the SWL. This supply came from further offshore gravel which was slowly transported onshore throughout the 18 wave bursts. The onshore transport along the 1/20 slope, which is not clearly discernable from the profile changes in the zone of  $x = 10.0 - 10.6$  m in Figure 3.4, is apparent in the migration of the edge of the gravel profile reported in Table 3.2 as well as in the erosion zone of  $x = 9.0 - 10.0$  m. Table 3.4 also indicates the sediment volume balance was within the measurement uncertainty.

Unlike the steep tests which yielded profile changes across the entire surf and swash zones, profile change was small near the still water shoreline. Figure 3.4 illustrates a constant 1/5 slope was maintained throughout the test with the majority of bed elevation changes occurring at the edges of the 1/5 slope. However, as with the steep tests, beach cusps were observed to develop on the berm. The cusps were not as prominent as in the steep tests, but were still smoothed to ensure longshore uniformity. The final profile very closely resembled the final quasi-equilibrium profile from test SH, an observation which will be further discussed in section 3.1.5. The same gravel sorting on the beach terrace and near the SWL described for test SL was witnessed throughout test MH.

**Table 3.4:** Conservation of gravel for test MH

Test No.	$V_e$	$V_d$	$V_c$
	[ $cm^2$ ]	[ $cm^2$ ]	[ $cm^2$ ]
MH01	90.4	83.9	-6.5
MH03	153.5	169.9	16.4
MH10	216.5	231.5	15.0
MH18	269.9	267.8	-2.1

### 3.1.4 Test MB

The final test shown in Figure 3.5 and Table 3.5 was by the far the most conspicuous due to the addition of a bar just offshore from the beach terrace established in the final profile from test MH. The bar migrated onshore under the same wave conditions as tests SH and MH and eventually created a profile very similar to those established in tests SH and MH. Initial wave action started to flatten out the artificial bar, spreading gravel in both onshore and offshore directions. However, net transport quickly transitioned onshore, steadily moving the bar onshore. By the end of the first burst, the bar appeared to be more natural for a bar migrating onshore with a gentler slope on the offshore side and a steeper gradient onshore. The bar continued to migrate onshore over the next several wave bursts until it connected with the beach terrace around burst 9. After the bar reached the beach terrace, the sediment was deposited across the beach face and essentially translated the profile seaward. By burst 18, the gravel contained in the bar was distributed across the beach. The deposition across the beach face continued until burst 27 at which point the profile became almost quasi-equilibrium. However, the additional 9 bursts caused measureable profile changes, reflected in slight difference between profiles MB27 and MB36 in Figure 3.5.

During initial wave bursts, the bar was still prominent and acted as a submerged breakwater to the beach face, creating a noticeable reduction in wave action through wave burst 9. The reduced wave action on the beach face explains minor profile changes on the beach face from MB01 to MB09 as shown in Figure 3.5. However at the end of burst 9, the bar had connected to the beach terrace, resulting in an increase in wave breaking on the beach face. The sediment budget in Table 3.5 indicates the increased profile changes for test MB in comparison to test MH in Table 3.4.

Test MB was observed to have significantly more sediment movement than

the other three tests. The sharp transition in bed elevation associated with the bar led to intense wave breaking and large events of sediment movement on the bar. The breaker zone moved further onshore with the bar migration. However, after the bar merged with the beach terrace, the beach terrace migrated onshore and an erosion zone started to form seaward of the terrace. The erosion hole observed in each of the other tests started to appear at the toe of the terrace by burst 21 and continued to grow as the beach slowly became quasi-equilibrium by burst 36.

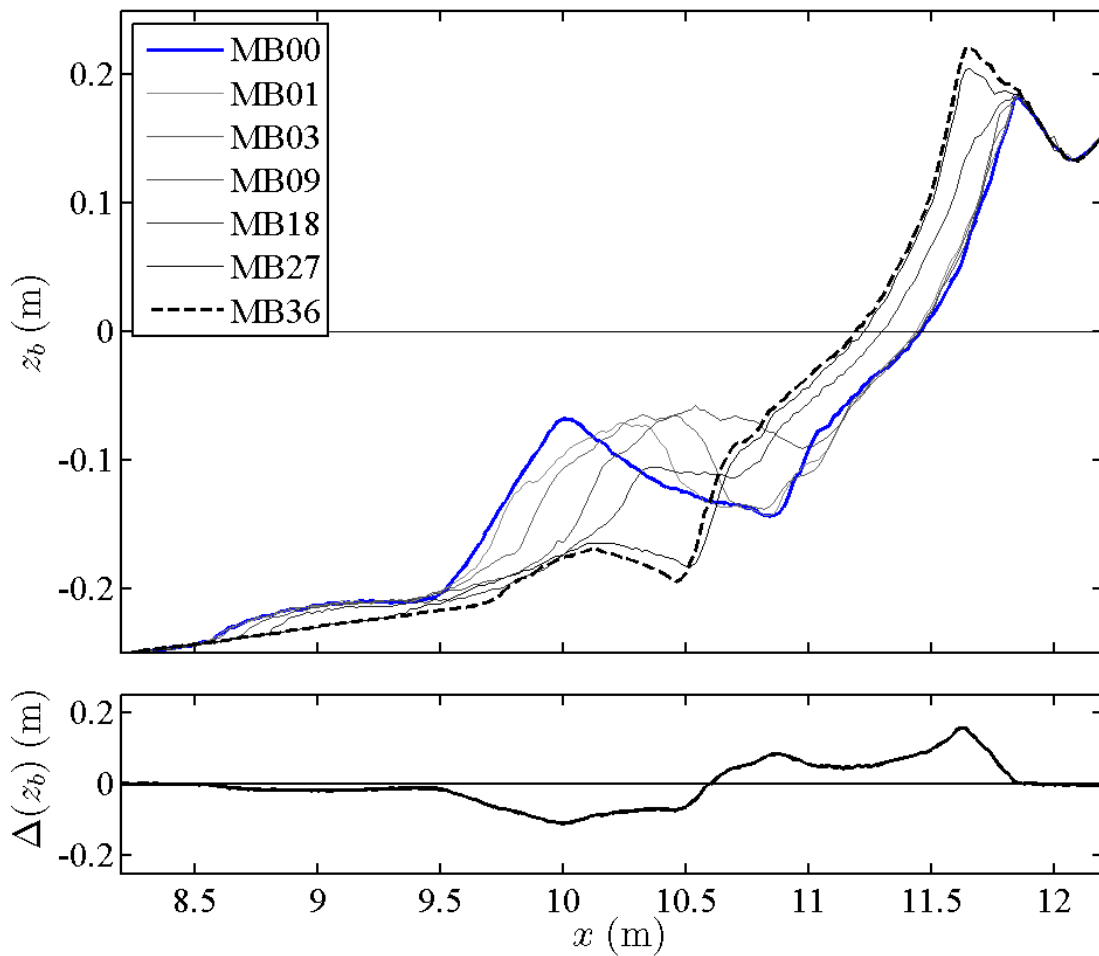


**Figure 3.5:** Profile evolution for test MB

Due to the longer duration of this test, it was easier to detect changes in the

offshore gravel. There was a clear onshore movement of the gravel on the impermeable 1/34.2 slope as the edge of gravel migrated onshore and the gravel layer was noticeably thinned by the end of the test with patches of the impermeable slope being exposed by the end. By the conclusion of test MB, the edge of the gravel profile had migrated nearly 1.2 meters. This significant migration is demonstrated in Table 3.2.

**Table 3.5:** Conservation of gravel for test MB

Test No.	$V_e$	$V_d$	$V_c$
	[ $cm^2$ ]	[ $cm^2$ ]	[ $cm^2$ ]
MB01	130.3	144.3	14.0
MB03	240.2	255.3	15.1
MB09	418.0	431.0	13.0
MB18	557.9	536.3	-21.6
MB27	807.5	783.9	-23.6
MB36	882.1	896.2	14.1

### 3.1.5 Final Profile Comparison

The first test SL used a significant wave height of about 6 *cm* and a peak period of 2.0 seconds. The last three tests all used the same set of wave conditions, again with a peak period of approximately 2.0 seconds and a significant wave height of approximately 12 *cm*. It was expected that each high wave test would create a similar final profile if enough bursts were run to reach a quasi-equilibrium state. To investigate the similarity between the measured profiles, each final measured profile was realigned to a new horizontal origin based on the cross-shore coordinate of the SWL intersection with the beach profile,  $x_{SWL}$ . The value  $x_{SWL}$  for each final profile is subtracted from each measured cross-shore coordinate  $x$  to give all four final profiles a common origin.

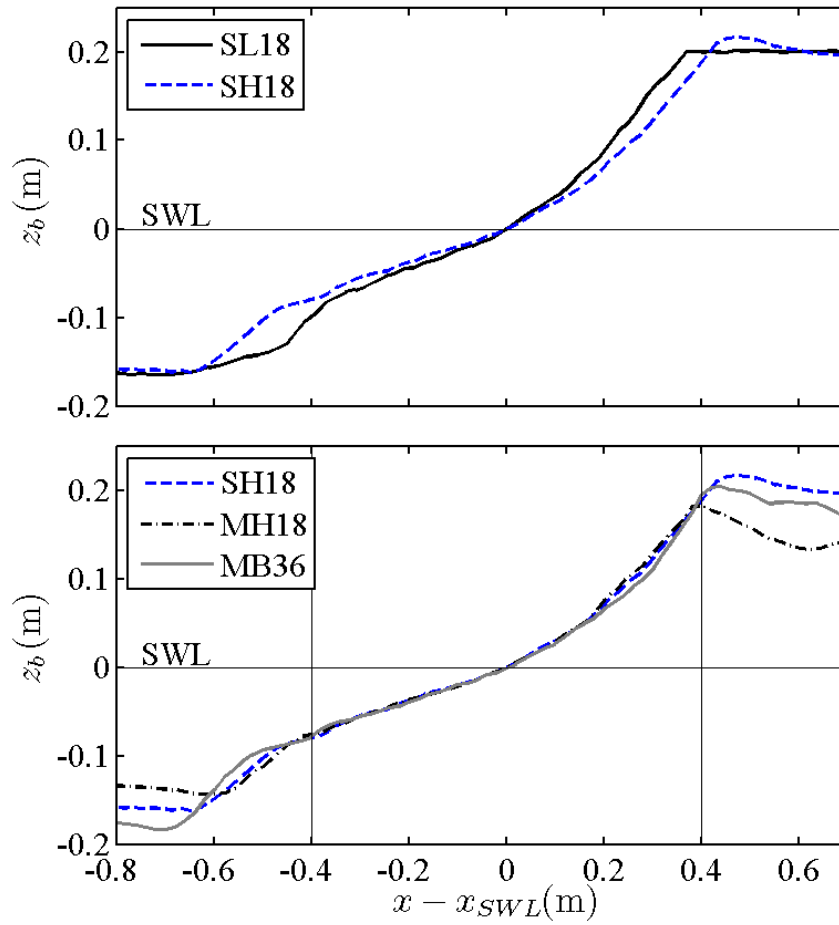


**Figure 3.6:** Comparison of the final profiles: SL18 vs. SH18 (top) for two different wave heights; SH18, MH18 and MB36 (bottom) for three different initial profiles

Figure 3.6 shows the final profiles  $z_b(x - x_{SWL})$  of tests SL and SH to examine the effect of the wave height as well as the three final profiles from tests SH, MH and MB to examine the effect of the initial profile differences. The two profiles  $z_b(x - x_{SWL})$  from tests SL and SH are similar but the smaller wave height of test SL resulted in a slightly steeper profile at the still water shoreline. The larger wave height in test SH, also created a deposition on the berm which was not observed for test SL. The bottom plot in Figure 3.6 shows the three higher wave height profiles match remarkably well in the zone of  $(x - x_{SWL}) = -0.4$  to  $0.4$  m, where  $0.4$  m approximately corresponds to  $3H_{mo}$  with  $H_{mo}$  = spectral significant wave height at  $x = 0$  for test SH, MH and MB. This zone with the similar profiles corresponded to the region where irregular wave uprush and downrush occurred. The slope of this quasi-equilibrium profile increases landward from about 0.2 to 0.6. The profiles outside the quasi-equilibrium zone have similar shapes but are affected by the initial profile differences and likely by the test duration.

### 3.2 Free Surface Data

As previously illustrated in Figure 2.7, a total of eight wave gauges were used during the four laboratory flume tests. Gauges G1-G5 collected data at  $50$  Hz throughout each of the 400 second bursts. The wall-mounted wave gauges G5-G8 collected data at a frequency of  $15$  Hz. Because the gauges were operated by different computers, gauge G5 was recorded by both data logging systems in order to synchronize the two sets of data. During analysis, the first 40 seconds of the free surface data was removed to allow for the establishment of wave set-down and eliminate the transitional waves due to starting in quiescent conditions before initiation of wave paddle movement. With the remaining 360 seconds of data, the mean free surface elevation  $\bar{\eta}$  and the standard deviation of the free surface  $\sigma_\eta$  were calculated from the times series collected by each of the eight gauges.

### 3.2.1 Offshore Incident Wave Statistics

In addition to the mean and standard deviation of the free surface elevation, several other important incident wave statistics were extracted from the data recorded by the wave gauges. The offshore gauge data (gauges G1-G3) was used to separate incident and reflected waves and to determine the offshore incident wave conditions, including spectral wave period  $T_p$ , spectral significant wave height  $H_{mo}$ , the root mean square wave height  $H_{rms}$ , and the reflection coefficient,  $R$ . The spectral significant wave height defined as  $H_{mo} = 4\sigma_\eta$  and the root-mean-square wave height defined as  $H_{rms} = \sqrt{8}\sigma_\eta$  were calculated using the separated incident wave standard deviation  $\sigma_\eta$ . The spectral peak period  $T_p$  is inverse of the peak frequency of the incident wave frequency spectrum. The reflection coefficient,  $R$  is defined as the ratio between the reflected and incident wave standard deviations.  $R^2$  is the ratio between the reflected and incident wave energy. An additional method of quantifying wave conditions is based on the zero upcrossing method applied to the incident wave time series. The largest third of individual waves are separated from the time series and their average height is defined as the significant wave height,  $H_s$ . The average period of these waves is the significant wave period,  $T_s$ . The described offshore wave parameters were calculated for each wave burst. The values obtained from each wave burst are available in Appendix A.1 in Tables A.1 to A.4.

Table 3.6 summarizes the incident wave statistics by averaging the values of a specified number of bursts. The offshore incident wave conditions remained almost constant throughout each of the tests. The significant wave height  $H_{mo}$  of test SL was 5.6 *cm* with a range of 0.2 *cm* where the range is defined as the difference between the largest and smallest values among the wave bursts. The high significant wave height tests, SH, MH, and MB all used the same time series of waves. The three tests had an average  $H_{mo}$  of approximately 12.2 *cm* and varied within a range of 0.5 *cm*. Similar estimates of significant wave height were found using the largest third of

**Table 3.6:** Average incident wave conditions and reflection coefficient  $R$  obtained from gauges G1-G3 where the bursts of test MB as separated into bursts 1-3, 4-9, 10-18, 19-27, and 28-36 due to the pronounced profile evolution.

Test No.	$H_{mo}$	$H_{rms}$	$H_s$	$T_p$	$T_s$	$R$
[-]	[cm]	[cm]	[cm]	[sec]	[sec]	[-]
SL01-18	5.64	3.99	5.37	1.94	1.81	0.35
SH01-18	12.01	8.49	12.41	1.97	1.90	0.28
MH01-18	12.35	8.74	12.61	1.98	1.91	0.26
MB01-03	12.42	8.78	12.98	1.97	1.90	0.24
MB04-09	12.37	8.75	12.89	1.98	1.89	0.25
MB10-18	12.34	8.73	12.86	2.00	1.90	0.26
MB19-27	12.13	8.58	12.58	1.99	1.89	0.30
MB28-36	12.04	8.51	12.50	1.98	1.90	0.28

incident waves. The average  $H_s$  for test SL was 5.37 *cm* and varied within a 0.4 *cm* range. For the large wave height tests, the average  $H_s$  was 12.6 *cm* and fluctuated within a range of 1.2 *cm*. Both the spectral peak period and the significant period remained consistent throughout the series of tests at 2.0 seconds and 1.9 seconds, respectively, with small fluctuations within a tenth of a second range. Finally, the reflection coefficient varied throughout the test, depending on the steepness of the beach face and the presence of a bar but stayed within 0.23 to 0.36.

### 3.2.2 Nearshore Free Surface Statistics

As mentioned previously, the mean and standard deviation of the free surface were determined for each wave gauge and for every wave burst. The data collected from each burst can be found in Appendix A.2 in Tables A.5 to A.12. To facilitate the data interpretation, the values from each burst were further averaged among the bursts and are presented in Tables 3.7 and 3.8 to represent burst-averaged conditions. For the three shorter tests SL, SH, MH, all 18 bursts were averaged because profile change was not significant enough to change the free surface elevation statistics

noticeably. Test MB was instead averaged in groups because of the large changes in bed elevation caused corresponding changes in free surface statistics as the bar migrated onshore. The groups were chosen based on the similarity in values which conveniently corresponded to the series of wave bursts between adjacent profile measurements. It should be stated that the values of individual wave bursts are used in the subsequent comparisons with the numerical model CSHORE in Chapter 5.

**Table 3.7:** Burst averaged free surface statistics for gauges G1-G5

Test No.	G1		G2		G3		G4		G5	
	$\bar{\eta}$	$\sigma_{\eta}$								
[-]	[cm]	[cm]								
SL01-18	-0.02	1.41	-0.04	1.40	-0.01	1.39	-0.03	1.40	-0.08	1.38
SH01-18	-0.15	3.00	-0.11	2.98	-0.11	3.05	-0.13	2.96	-0.15	2.94
MH01-18	-0.10	3.09	-0.10	2.99	-0.10	3.04	-0.11	2.84	-0.20	2.72
MB01-03	-0.09	3.10	-0.18	2.98	-0.10	3.03	-0.17	2.96	-0.07	2.83
MB04-09	-0.09	3.09	-0.04	3.00	-0.10	3.02	-0.15	2.84	-0.16	2.71
MB10-18	-0.10	3.09	-0.08	2.99	-0.10	3.06	-0.11	2.80	-0.10	2.69
MB19-27	-0.12	3.03	-0.14	2.96	-0.13	3.14	-0.11	2.91	-0.16	2.81
MB28-36	-0.12	3.01	-0.16	2.93	-0.12	3.11	-0.12	3.05	-0.14	2.87

Special attention was required for the two furthest onshore wave gauges, G7 and G8 due to their location in the swash zone resulting in an intermittently wet time series. Gauge G7 was submerged below the SWL for all test conditions; however the combination of a steep slope and high waves in test SH created instances where gauge G7 was exposed during events of large backwash. Gauge G8 was exposed to air during still water conditions for both of the steep slope tests and in later bursts of test MB once the bar had merged with the beach face. To handle the intermittent air exposure, the wet data was separated from the rest of the time series using a baseline gravel elevation recorded at the beginning and end of every wave burst. Data points of water surface elevations greater than the bed elevation

were considered submerged (wet) data, these data points were used in calculating the free surface statistics. The mean water depth  $\bar{h}$  above the bed and the free surface standard deviation  $\sigma_\eta$  of the wet data points were calculated for each burst. From the mean water depth, the mean free surface elevation was calculated using

$$\bar{\eta} = \bar{h} + z_b \quad (3.4)$$

where  $z_b$ =average gravel surface elevation during each burst. An additional parameter, the wet probability  $P_w$  was calculated for the intermittently submerged gauges by dividing the number of wet data points,  $J_{wet}$ , by the total number of data points,  $J$ , as follows

$$P_w = \frac{J_{wet}}{J} \quad (3.5)$$

Table 3.8 contains the free surface statistics for gauges G6-G8, including the wet probability and mean water depth for the intermittently submerged gauges. The mean water depth is listed only for the data points with  $P_w$  less than 100% for G7 and G8 except for MB01-03 and MB04-09 of G8 because  $P_w$  changed considerably during test MB. Burst data recorded by malfunctioning equipment and other unreliable measurements were removed from the burst averaging in Appendix A.2.

The data points for individual bursts tabulated in Appendix A.2 are plotted in comparisons with computed cross-shore variations of  $\bar{\eta}$  and  $\sigma_\eta$  in Chapter 5. The measured cross-shore and temporal variations of  $\bar{\eta}$  and  $\sigma_\eta$  are explained consisely using Tables 3.7 and 3.8. Test SL, with a low significant wave height was predominantly characterized by surging waves on the steep slope, with only the very largest waves resembling spilling breakers. However with the other three tests, wave height was more than doubled, creating a noticeable difference in wave breaking conditions

**Table 3.8:** Burst averaged free surface statistics for gauges G6-G8

Test No	G6		G7				G8			
	$\bar{\eta}$	$\sigma_{\eta}$	$P_w$	$h$	$\bar{\eta}$	$\sigma_{\eta}$	$P_w$	$h$	$\bar{\eta}$	$\sigma_{\eta}$
[-]	[cm]	[cm]	[-]	[cm]	[cm]	[cm]	[-]	[cm]	[cm]	[cm]
SL01-18	-0.06	1.33	100.0%	-	-0.17	1.62	12.1%	0.86	5.10	0.57
SH01-18	-0.39	2.46	97.5%	3.49	0.80	2.15	17.3%	1.68	6.72	1.28
MH01-18	-0.19	2.95	100.0%	-	-0.35	2.31	100.0%	-	0.49	2.10
MB01-03	0.61	2.46	100.0%	-	0.78	1.64	100.0%	3.93	0.71	2.34
MB04-09	-	-	100.0%	-	0.95	1.63	100.0%	4.29	0.77	2.31
MB10-18	-	-	100.0%	-	0.42	1.62	82.4%	2.86	1.32	1.76
MB19-27	-0.25	2.97	100.0%	-	0.21	2.56	45.4%	1.98	3.81	1.29
MB28-36	-0.34	2.92	100.0%	-	0.44	2.22	32.5%	1.82	4.74	1.19

within the surf zone. In tests SH and MH, the majority of waves resembled spilling breakers, breaking primarily along the 1/20 slope with a few large waves breaking further out along the impermeable slope (see Figure 2.7 for experimental setup). Occasionally, the largest waves in the time series could be classified as plunging breakers with collapsing bores creating brief sediment lifting events. The final test, MB had the highest frequency of plunging breakers, especially while the bar was still dominant in the profile. The abrupt change in bed elevation was observed to cause sudden wave plunging and consequently large sediment movement events across the bar. The frequency of plunging waves started to diminish as the bar merged with the beach face, creating conditions similar to those described for tests SH and MH.

The time-averaged mean free surface elevation,  $\bar{\eta}$  traces the wave setdown and setup of the mean water level as waves move onshore. The shift from setdown (negative  $\bar{\eta}$  values) to setup (positive  $\bar{\eta}$  values) serves as indication of where the most wave breaking occurs. Consequently, the location of the breaker zone can be estimated by evaluating the trends in  $\bar{\eta}$  recorded by all eight wave gauges. Test SL, having a low incident wave height, created offshore set-down values less than half those recorded during the other three tests with larger wave conditions. The

lower wave height also shifted wave breaking as far shoreward as the toe of the steep beach face reflected in the peak setdown value recorded at gauge G7 (see Figure 2.11 for the gauge locations). The large wave tests all generated much larger magnitudes of  $\bar{\eta}$ ; however, the shift from setdown to setup varied depending on the geometry of the beach. During test SH, the region of most concentrated wave breaking occurred near gauge G6. However, the milder slope of test MH created a slight onshore shift in the breaker zone which is reflected in the movement of peak setdown back toward gauge G7. This result is consistent with expectations of more gradual breaking on the milder slope. The added bar in test MB had a noticeable impact on the location of wave breaking, shifting it as far seaward as gauge G5 during the first 3 wave bursts. Unfortunately, gauge G6 malfunctioned for a large portion of test MB and was unable to track the movement of the breaker zone due to the onshore bar migration. However, G6 was fixed after burst 18 and recorded the maximum setdown values for the final 18 bursts, suggesting the breaker zone had indeed moved onshore. After wave breaking occurred, positive mean free surface elevations indicate wave setup increasing onshore. This trend was consistent in all four tests, with the largest setup values occurring in the swash zone recorded by the furthest onshore gauge G8. It should be stated that the wave setup value of G8 should be interpreted in view of the wet probability  $P_w$ .

The standard deviation of free surface elevation is proportional to wave height and can also be used to demonstrate where wave breaking occurs, indicated by a significant drop in  $\sigma_\eta$ . The reduction in  $\sigma_\eta$  occurs in the vicinity of the peak setdown  $\bar{\eta}$ . For test SL, the drop in  $\sigma_\eta$  occurred between gauges G7 and G8, reflecting limited wave breaking occurring right at the toe of the beach face. The larger wave height tests experienced breaking further offshore, with the sharp decrease in  $\sigma_\eta$  between gauges G6 and G7. During these tests, the breaker zone was wider, with some large waves breaking as far offshore as gauge G4. This is reflected in a smaller drop in  $\sigma_\eta$

between gauges G4 and G5.

The statistics recorded for gauges G1-G7 remained fairly consistent throughout each test as listed in Tables A.5 to A.12. The mean and standard deviation of the free surface elevation varied little among the bursts used for averaging for Tables 3.7 and 3.8. The small amounts of fluctuation between wave bursts are caused by the bottom elevation change especially for test MB and small instrument errors either in determination of the still water level or calibration of the capacitance wires. Larger ranges were observed for the onshore gauge G8; however the steady increase in  $\bar{\eta}$  for each test is associated with the increasing bed elevation at this gauge location and the formation of the terrace landward of G8. This increase was observed for all four tests in some degree.

### 3.3 Velocity Data

The velocity data was analyzed in a similar manner to the free surface data. As described in Chapter 2, the current meters were paired with three of the onshore wave gauges, G4-G6 (or G4, G6 and G7 during test SL). Their vertical elevations were chosen to capture an approximately depth-averaged fluid velocity, high enough to stay above the bottom boundary layer of the gravel bed and low enough to achieve minimal exposure to air. The current meter data was recorded at a frequency of 15  $Hz$ . Again, the first 40 seconds of the time series were eliminated for consistency. Time averaged statistics were utilized to reduce effects from turbulent fluctuations. Each current meter measured both cross-shore and longshore velocities; however, only the cross-shore values are presented because the measured longshore velocities contained turbulent velocities but were relatively small.

Like with the free surface data, the mean ( $\bar{U}$ ) and standard deviation ( $\sigma_U$ ) of each wave burst were computed and are presented in Tables A.13 to A.16 in Appendix A.3. Averaged values from each test are displayed in Table 3.9. As with the free surface data, test MB was divided into averaging groups based on similarity

**Table 3.9:** Velocity statistics averaged from each test. NOTE: Test SL used different current meter locations, see Table 2.3 for details.

Test No	EMCM1		EMCM2		EMCM3		EMCM4		EMCM5		EMCM6	
	$\bar{U}$	$\sigma_U$										
[-]	[cm/s]											
SL01-18	-0.03	8.57	-0.27	8.53	-1.50	10.50	-1.87	11.39	-	-	-	-
SH01-18	-1.97	17.63	-1.81	16.21	-3.60	17.02	-1.64	18.56	-6.31	27.05	-1.98	23.79
MH01-18	-1.87	17.81	-1.79	17.15	-3.19	18.01	-2.69	19.80	-7.25	18.28	-5.57	18.57
MB01-03	-2.19	17.51	-1.88	16.48	-	-	-6.15	31.87	-6.12	13.09	-6.94	11.75
MB04-09	-1.91	17.65	-1.64	16.89	-3.05	18.91	-2.42	20.01	-5.88	19.46	-8.45	22.96
MB10-18	-1.78	18.49	-1.61	17.29	-2.58	17.86	-2.14	18.80	-	-	-8.94	33.41
MB19-27	-1.66	17.19	-1.63	16.54	-2.94	16.96	-1.67	18.03	-5.27	24.85	-3.84	22.95
MB28-36	-1.74	17.10	-1.62	16.15	-2.87	16.96	-1.61	17.93	-5.43	27.94	-2.05	24.64

Note: If current meters were exposed to air during a burst, that data was unreliable and omitted.

in value and instances of profile measurement. Initially, in test SL the current meters were placed in the same cross-shore location as gauges G4, G6, and G7 as listed in Table 2.5; however, the frequency of air exposure at G7 required repositioning the current meters to align them with gauges G4, G5, and G6. Frequent air exposure also created an issue in portions of test MB when the peak of the bar migrated past current meter pair EMCM5-6. As the bar crest passed by, the current meters were raised to be at least 2 *cm* above the local bottom, causing the higher of the two current meters to be exposed to air for a significant portion of a wave burst. Consequently, this data has been omitted from Table A.16 and in MB10-18 in Table 3.9.

The mean fluid velocity  $\bar{U}$  is used to identify any currents generated by the wave motion. In each of the tests, all six current meters recorded negative time-averaged fluid velocities, indicating a return current or undertow. The magnitude of the undertow increased further onshore, as reflected in the increasing magnitudes of  $\bar{U}$ . The standard deviation of velocity  $\sigma_U$  is an indicator of the magnitude the wave-induced oscillatory velocity. This was also observed to increase onshore for each of

the four test conditions. The comparison of the values for each pair (EMCM1-2, 3-4, and 5-6) indicates the the vertical variation of  $\bar{U}$  and  $\sigma_U$ , which turned out to be relatively small above the bottom boundary layer and below the aerated zone.

Compared to the free surface statistics, the variation in the velocity statistics during each test were larger. The  $\bar{U}$  values for an individual current meter fluctuated within about 1 *cm/s* with the exception of the most landward current meters. The current meters EMCM5-6 experienced larger fluctuations for each of the tests and especially in test MB when the positive value ( $\bar{U}$ ) of current meter EMCM6 increased up to 9 *cm/s*. Even larger fluctuations in  $\sigma_U$  were observed during test MB. The variation was related to the evolving bed level and water depth. Care was taken to maintain a constant offset between the bed and the current meters at the beginning of each burst; however, the bottom elevation change during the burst carried over to fluctuations in fluid velocity statistics. This effect was amplified in test MB when the bar migrated onshore, creating appreciable changes in water depth during some wave bursts.



## Chapter 4

### NUMERICAL MODEL CSHORE

This chapter explains the time-averaged model CSHORE (Kobayashi, et al., 2010) and modifications made in this study. The subsequent sections describe the governing equations and probabilistic approach used to predict the hydrodynamics and sediment transport as used in CSHORE. The first section gives a general description of the combined wave and current model which is more rigorously explained in Kobayashi (2009). More focus will be given to the probabilistic model in the wet and dry zone which is used in the region that is intermittently wet. Finally, the sediment transport model will be presented along with modifications made to improve predictions of bedload transport for the present experiment.

#### 4.1 Combined Wave and Current Model

The model assumes the waves are normally incident to the longshore uniform gravel beach, creating a two dimensional model environment. As shown in Figure 4.1, the coordinate system is established at the furthest offshore gauge G1 where a datum of  $z = 0$  is the still water level (SWL),  $x$  is taken to be positive onshore and  $z$  is positive upward from the datum. The mean water level (MWL) is defined as  $z = \bar{\eta}$  where  $\bar{\eta}$  is defined as wave setup measured from the SWL. The still water level is allowed to change due to storm surge or tidal fluctuations, but the present experiment was limited to a constant still water level at  $z = 0$ . The input  $\bar{\eta}$  was generated using the measured values obtained from gauge G1 throughout the tests, listed in Tables A.5, A.7, A.9, and A.11. The mean water depth is defined as

$\bar{h} = (\bar{\eta} - z_b)$  where  $z_b$  represents the bed elevation and is negative below the SWL. In addition to establishing bed elevation, a lower boundary to the sediment layer is denoted by  $z_p$  and is assumed to be impermeable. With the exception of mean water depth, each of these parameters at  $x = 0$  (G1) are included in the input file along with sediment characteristics including median diameter,  $d_{50} = 2.0 \text{ mm}$ , fall velocity  $w_f = 0.25 \text{ m/s}$ , specific gravity  $S = 2.7$ , and porosity = 0.4. Also included as input are the wave forcing conditions, represented by the measured spectral peak period,  $T_p$  and the root-mean-square wave height  $H_{rms} = \sqrt{8}\sigma_\eta$  of the furthest offshore gauge G1 at  $x = 0$ . Figure 4.1 illustrates the input parameters defined above.

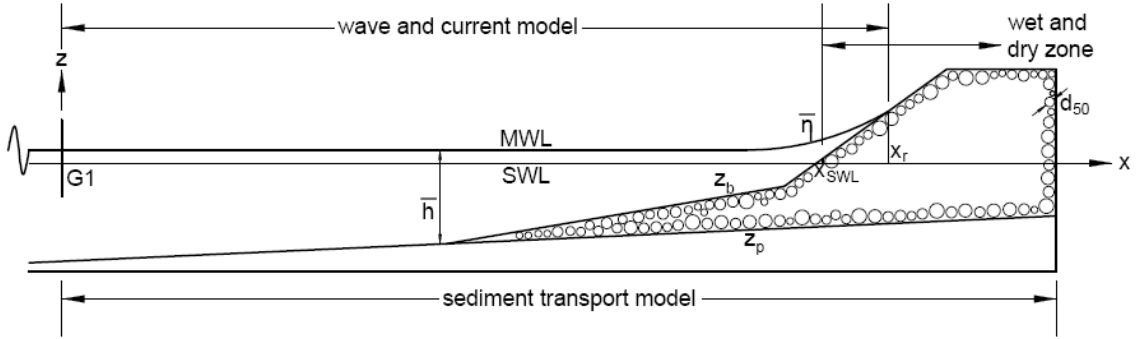


**Figure 4.1:** Schematic illustrating the coordinate system in CSHORE and the extent in which each model operates.

The intersection of the beach face and the mean water level,  $x_r$  indicates the landward limit of the time-averaged model in the wet zone. Everything seaward of this location is evaluated using the wet permeable slope model developed by Kobayashi et al. (2007) using linear wave and current theory (e.g. Mei 1989), where the current is generated if wave overtopping occurs. The time-averaged continuity, momentum, and wave action equations are used to predict the cross-shore variations of the mean  $\bar{U}$  of the depth-averaged cross-shore velocity  $U$ , the mean  $\bar{\eta}$  of the free surface elevation  $\eta$  above the SWL and the free surface standard deviation  $\sigma_\eta$ . Linear progressive wave theory in a finite depth is used to predict the local standard deviation of depth-averaged cross-shore velocity,  $\sigma_U$  which relates it to

the local  $\sigma_\eta$ ,  $\bar{h}$ , and the phase velocity  $C$ . The free surface  $\eta$  and the velocity  $U$  are expressed using a Gaussian probability distribution. The resulting probability-averaged hydrodynamic statistics are assumed to be equivalent to time-averaged values  $\bar{\eta}$ ,  $\sigma_\eta$ ,  $\bar{U}$ , and  $\sigma_U$ .

The equations used for the combined wave and current model in the wet zone are presented in the report by Kobayashi (2009). The landward marching computations predict the hydrodynamic statistics from the offshore gauge G1 at  $x = 0$  to the mean water level intersection with the beach face at  $x = x_r$  which the model evaluates as the location where  $\bar{h}$  or  $\sigma_\eta$  become less than 0.1 *cm*. The linear Gaussian wave theory equations used in the combined wave and current model are not valid in the region that is not always submerged, necessitating a separate model for prediction of fluid dynamics in the wet and dry zone.

## 4.2 Probabilistic Model for Wet and Dry Zone

The wet and dry zone model was developed to better represent swash conditions and wave overwash. The model extends from the SWL intersection with the beach face,  $x_{SWL}$  (as shown in Figure 4.1) to where the predicted water depth becomes less than 0.01 *cm*. In this region, the time-averaged cross-shore continuity and momentum equations are derived from nonlinear shallow-water wave equations (Wurjanto and Kobayashi 1993) as shown below

$$\frac{d}{dx} (\bar{h}U) = -\bar{w}_p \quad (4.1)$$

$$\frac{d}{dx} \left( \bar{h}U^2 + \frac{g}{2}\bar{h}^2 \right) = -gS_b\bar{h} - \frac{1}{2}f_b|\bar{U}|\bar{U} - \bar{u}_b\bar{w}_p \quad \text{with } S_b = \frac{dz_b}{dx} \quad (4.2)$$

where  $h$  is the instantaneous water depth,  $U$  is the cross-shore velocity,  $g$  is the gravitational acceleration, and  $w_p$  represents the the vertical seepage velocity which is considered positive downward. Equation (4.1) demonstrates the spatial

changes in water volume are balanced by the vertical seepage into the permeable bed. The bottom slope,  $S_b$  is defined as the spatial gradient of the permeable bed elevation measured from the datum  $z = 0$  as shown in Figure 4.1. The term  $f_b$  represents the bottom friction factor allowed to vary spatially across the profile,  $z_b$  and  $u_b$  is defined as the horizontal fluid velocity at  $z = z_b$ . The bottom friction factor is taken as  $f_b = 0.002$  on the smooth impermeable bottom and  $f_b = 0.01$  on the rough bottom in the same way as in Kobayashi et al. (2010) for stone slopes. The last term in equation (4.2) represents the time-averaged flux of the horizontal momentum into the permeable layer which is the region between the permeable bed elevation  $z_b$  and the impermeable bed elevation  $z_p$ . Also, it should be noted that the overbars in equations (4.1) and (4.2) indicate time-averaging during only the wet duration because there is no water during the dry duration.

Within the permeable layer, the equations for the continuity and approximate momentum equations are as follows

$$\frac{dq_p}{dx} = \overline{w_p} \quad (4.3)$$

$$(\alpha_p + \beta_1 |\overline{U_p}|) \overline{U_p} = -g \frac{d\bar{\eta}}{dx} \quad (4.4)$$

where  $\alpha_p$  and  $\beta_1$  are defined as

$$\alpha_p = 1000 \left( \frac{1 - n_p}{n_p} \right)^2 \frac{\nu}{d_{50}^2}; \quad \beta_1 = \frac{5(1 - n_p)}{d_{50} n_p^3} \quad (4.5)$$

In the equations above,  $q_p$  represents the time-averaged horizontal volume flux within the permeable layer and  $\overline{U_p}$  represents the time-averaged discharge velocity. The two coefficients,  $\alpha_p$  and  $\beta_1$  are related to flow resistance for laminar and turbulent flow conditions, respectively. The final three parameters are related to the gravel and fluid characteristics,  $n_p =$  the porosity of the permeable layer,  $d_{50} =$

median gravel diameter which is assumed to represent the nominal grain diameter used in Kobayashi et al. (2009), and  $\nu =$  the kinetic viscosity of the fluid taken as  $\nu = 0.01 \text{ cm}^2/\text{s}$ . The resistance coefficients in equation (4.5) are based on the formula developed by van Gent (1995) and calibrated by Kobayashi et al. (2007). The resistance component associated with the oscillatory flow is neglected in equation (4.4) which is solved analytically to obtain the discharge velocity  $\overline{U}_p$  driven by the horizontal pressure gradient. The horizontal pressure gradient is created due to cross-shore variation in the mean free surface  $\overline{\eta} = (\overline{h} + z_b)$  where  $\overline{h}$  and  $z_b$  vary with  $x$ . It is noted that equation (4.4) retains only the leading terms in the horizontal momentum equation given by Wurjanto and Kobayashi (1993).

Addition of the two equations (4.1) and (4.3) and integration with respect to  $x$  yields the following vertically integrated continuity equation

$$\overline{hU} + q_p = q_o \quad (4.6)$$

where the wave overtopping rate  $q_o$  includes the sum of the volume fluxes from both above and within the permeable layer. This volume flux within the permeable layer is estimated using

$$q_p = P_w \overline{U}_p (\overline{\eta}_p - z_p) \quad (4.7)$$

where  $P_w$  is the wet probability or the ratio between the wet duration and the entire test duration as described in section 3.2.2. The term  $\overline{\eta}_p$  is defined as the average water level inside the permeable layer in reference to the datum  $z = 0$ . The term  $(\overline{\eta}_p - z_p)$  represents the thickness of the saturated region inside the permeable layer. The estimation of volume flux in the permeable layer requires determination of  $\overline{U}_p$  and  $\overline{\eta}_p$ . The discharge velocity  $\overline{U}_p$  is found using equation (4.4) and the mean water level within the permeable layer  $\overline{\eta}_p$  is predicted using the following equations

$$\begin{aligned}\bar{\eta}_p &= P_w z_b + (1 - P_w) z_p \quad \text{for } z_p \geq 0 \\ \bar{\eta}_p &= P_w z_b \quad \text{for } z_p < 0\end{aligned}\tag{4.8}$$

The upper bound of  $\bar{\eta}_p$  occurs when  $P_w = 1$  and simplifies to  $\bar{\eta}_p = z_p$  or the upper boundary of the permeable layer. Similarly, the lower bound of  $\bar{\eta}_p$  is determined when  $P_w = 0$ , which simplifies equation (4.8) to the higher elevation of either the impermeable bed elevation  $z_p$  or the still water level. Inclusion of the wet probability in equation (4.7) ensures that  $q_p$  goes to zero when  $P_w$  goes to zero. Equations (4.7) to (4.8) are based largely on physical reasoning, but are used along with equations (4.4) and (4.5) to estimate the volume flux  $q_p$  for known  $\bar{h}$  and  $P_w$ .

The momentum flux into the permeable layer included as the last term in equation (4.2) is computed as

$$\overline{u_b w_p} = \alpha_m P_w (g\bar{h})^{0.5} w_m; \quad \alpha_m = 2 \left( \frac{z_b - z_p}{d_{50}} \right)^{0.3}\tag{4.9}$$

where  $w_m$  represents the maximum downward seepage velocity due to gravity which is determined analytically using the equation

$$(\alpha_p + \beta_1 w_m) w_m = g\tag{4.10}$$

To obtain equation (4.9), the seepage velocity  $w_p$  is assumed to be on the same order of  $w_m$  or less and the horizontal velocity  $u_b$  at the bed level  $z = z_b$  is assumed to be on the order of  $(g\bar{h})^{0.5}$ . Upward momentum flux from the permeable layer is assumed to be much smaller in magnitude than the downward flux of horizontal momentum and is therefore not included in equation (4.9). The empirical parameter  $\alpha_m$  calibrated by Kobayashi et al. (2010) for stone structures depends on the permeable layer thickness normalized by the median grain diameter.

The cross-shore variation of the mean water depth  $\bar{h}$  is determined by solving the momentum equation (4.2) in tandem with the continuity equation (4.6).

The instantaneous water depth  $h$  at a given cross-shore location,  $x$  is described probabilistically using an exponential probability distribution. This assumption is based on the work of Kobayashi et al. (1998) which analyzed free surface elevations measured within the shoaling, surf, and swash zones. The exponential probability distribution was found to best describe the free surface measurements within the swash zone and consequently was adopted in CSHORE formulations of water depth in the wet and dry zone. Use of this assumption simplifies CSHORE within the wet and dry zone. The exponential probability density function  $f(h)$  is defined as

$$f(h) = \frac{P_w^2}{\bar{h}} \exp\left(-P_w \frac{h}{\bar{h}}\right) \quad \text{for } h > 0 \quad (4.11)$$

with

$$P_w = \int_0^\infty f(h)dh; \quad \bar{h} = \int_0^\infty hf(h)dh \quad (4.12)$$

As discussed previously, the wet probability  $P_w$  equates to the probability of the instantaneous water depth  $h > 0$ . Therefore, the dry probability representing the likelihood of  $h = 0$  is equal to  $(1 - P_w)$ . The mean water depth for only the wet duration is evaluated as  $\bar{h}$ . However, the mean water depth for the entire duration is represented by  $P_w \bar{h}$ .

The free surface elevation  $\eta$  is measured from the still water level (SWL) and can be computed as  $\eta = (h + z_b)$  where  $z_b$  is assumed to be constant during the time-averaging duration. The standard deviations of  $\eta$  and  $h$  are equivalent and represented by

$$\frac{\sigma_\eta}{\bar{h}} = \left(\frac{2}{P_w} - 2 + P_w\right)^{0.5} \quad (4.13)$$

which simplifies to  $\sigma_\eta = \bar{h}$  when  $P_w = 1$ . Depth measurements in the lower swash zone done by Kobayashi et al. (1998) correspond to the simplification of equation (4.13) by assuming  $P_w = 1$  in equation (4.11) in the lower swash zone.

The cross shore velocity  $U$  is related to the water depth  $h$  in the wet and dry zone using the following equation

$$U = \alpha\sqrt{gh} + U_s \quad (4.14)$$

where  $\alpha$  equals a positive constant and  $U_s$  is defined as the steady velocity allowed to vary in the cross-shore direction. The steady velocity  $U_s$  accounts for the offshore return flow on the seaward slope and the downward velocity increase on the landward slope. An investigation by Holland et al. (1991) measured the bore speed and flow depth on a barrier island using video techniques. Analysis yielded  $\alpha \simeq 2$  where the celerity and fluid velocity of the bore are assumed to be approximately the same. Consequently,  $\alpha \simeq 2$  is used as a first approximation. According to equation (4.14), the cross-shore velocity in the wet and dry zone should increase with increasing water depth and approach the steady velocity  $U_s$  as the depth approaches zero. Using equations (4.11) and (4.14) yields the following equations for the mean  $\bar{U}$  and standard deviation  $\sigma_U$  of the cross-shore velocity  $U$

$$\bar{U} = \frac{\sqrt{\pi}}{2}\alpha(P_w g \bar{h})^{0.5} + P_w U_s \quad (4.15)$$

$$\sigma_U^2 = \alpha^2 g \bar{h} - 2(\bar{U} - U_s)(\bar{U} - P_w U_s) + P_w (\bar{U} - U_s)^2 \quad (4.16)$$

The resulting equations (4.13), (4.15) and (4.16) express  $\sigma_\eta$ ,  $\bar{U}$  and  $\sigma_U$  in terms of  $\bar{h}$ ,  $P_w$ , and  $U_s$ , each of which vary with  $x$ .

The cross-shore velocity equation (4.14) is substituted into the momentum and continuity equations, (4.2) and (4.6) which are then averaged for the wet duration using equation (4.11). The resulting continuity equation is

$$\frac{3\sqrt{\pi}\alpha}{4}\bar{h}\left(\frac{g\bar{h}}{P_w}\right)^{0.5} + U_s\bar{h} = q; \quad q = q_o - q_p \quad (4.17)$$

where  $q$  represents the volume flux above the permeable layer. The momentum equation (4.2) becomes

$$\frac{d}{dx}\left(B\frac{g\bar{h}^2}{P_w} + \frac{q_o^2}{\bar{h}}\right) = -gS_b\bar{h} - \frac{f_b}{2}\alpha^2g\bar{h}G_b(r) - \alpha_m P_w (g\bar{h})^{0.5}w_m \quad (4.18)$$

after lengthy algebra. The coefficients  $B$  and  $r$  are defined as

$$B = \left(2 - \frac{9\pi}{16}\right)\alpha^2 + 1; \quad r = \frac{3\sqrt{\pi}}{4}\frac{U_s\bar{h}}{q - U_s\bar{h}} \quad (4.19)$$

where the parameter  $B$  is related to the momentum flux term on the left hand side of equation (4.2). The function  $G_b(r)$  included in equation (4.18) is given by

$$\begin{aligned} G_b(r) &= 1 + \sqrt{\pi}r + r^2 && \text{for } r \geq 0 \\ G_b(r) &= 2exp(-r^2) - r^2 - 1 + \sqrt{\pi}r [2erf(r) + 1] && \text{for } r < 0 \end{aligned} \quad (4.20)$$

where  $erf$  is the error function. The function  $G_b$  increases monotonically with the increase of  $r$  as shown in Figure 4.2. The function  $G_b$  is equal to zero when  $r = -0.94$  and is equal to 1 when  $r = 0$ . Further,  $G_b$  can be approximated as  $G_b = -(1 + \sqrt{\pi}r + r^2)$  when  $r < -1.5$ .

Equations (4.17) and (4.18) are used to predict the cross-shore variation of mean water depth  $\bar{h}$  and steady velocity  $U_s$  for an assumed  $q_o$ . To simplify the integration of equation (4.18) it is necessary to estimate the wet probability  $P_w$  empirically as given by

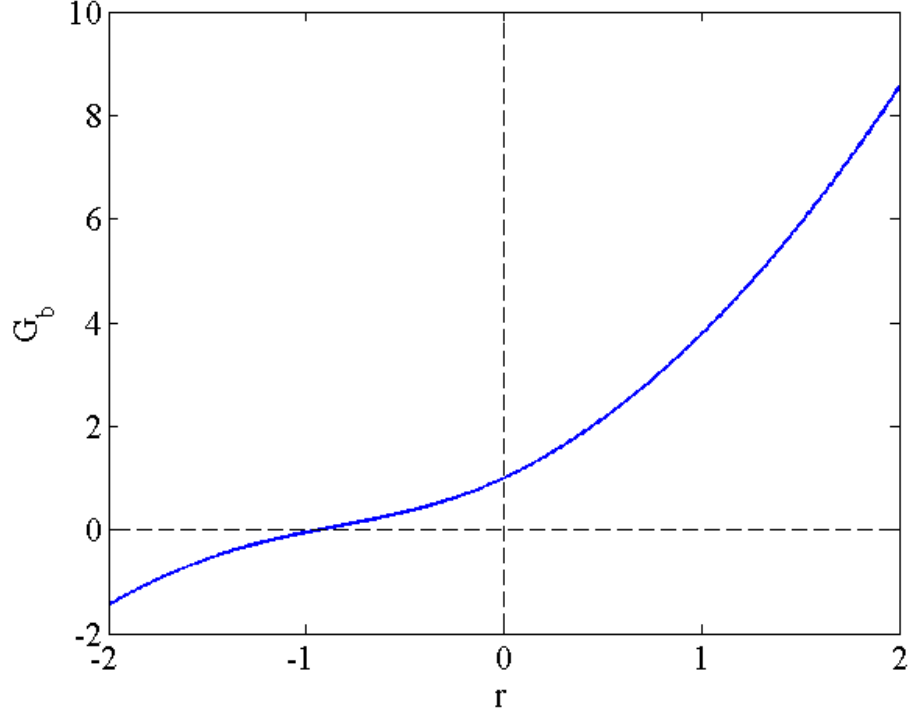


**Figure 4.2:** Function  $G_b(r)$  used in the wet and dry zone

$$P_w = \left[ (1 + A_1) \left( \frac{\bar{h}_1}{h} \right)^n - A \left( \frac{\bar{h}_1}{h} \right)^3 \right]^{-1}; \quad A = \frac{q^2}{Bg\bar{h}_1^3}; \quad A_1 = \frac{q_1^2}{Bg\bar{h}_1^3} \quad (4.21)$$

where  $\bar{h}_1$  and  $q_1$  represent the mean water depth and volume flux, respectively, at the location of  $x = x_1$  where  $P_w = 1$ . The exponent  $n$  is an empirical parameter for  $P_w$  and the coefficients  $A$  and  $A_1$  are dimensionless variables related to  $q$  and  $q_1$ , respectively. The transition from the wet ( $P_w = 1$  *always*) zone to the wet and dry ( $P_w < 1$ ) zone may be taken at  $x_1 = x_{SWL}$  where  $x_{SWL}$  is defined as the cross-shore location of the still water shoreline of an emerged crest as shown in Figure 4.1. The empirical equation for wet probability (4.21) is assumed to be valid on the upward slope and horizontal crest in the region where  $x_1 \leq x \leq x_c$  where  $x_c$  is the highest and most landward location of the bottom elevation  $z_b$ . In

the case of an impermeable structure, equation (4.21) reduces to that used by Kobayashi et al. (2010) for an impermeable beach with  $q = q_1 = q_o$ .

Integration of equation (4.18) for  $P_w$  defined by equation (4.21) from  $\bar{h} = \bar{h}_1$  at  $x = x_1$  yields

$$B_n(1 + A_1)\bar{h}_1 \left[ \left( \frac{\bar{h}_1}{\bar{h}} \right)^{n-1} - 1 \right] = z_b(x) - z_b(x_1) + \int_{x_1}^x \left[ \frac{f_b}{2} \alpha^2 G_b + \alpha_m \frac{P_w w_m}{(g\bar{h})^{0.5}} \right] dx \quad (4.22)$$

where  $B_n = B(2 - n)/(n - 1)$  and  $z_b(x)$  equals the bottom elevation at a cross-shore location  $x$ . The mean water depth  $\bar{h}$  at a given  $x$  is computed by solving equation (4.22) iteratively. The empirical parameter  $n$  is taken to be in the range of  $1 < n < 2$  so that  $B_n > 0$ . The formula for  $n$  calibrated by Kobayashi et al. (2010) using 207 for wave overtopping of smooth impermeable structures is expressed as  $n = 1.01 + 0.98[\tanh(A_o)]^{0.3}$  where  $A_o = q_o^2/(Bg\bar{h}_1^3)$  in the range  $1.01 \leq n \leq 1.99$ .

On the downward slope landward of the crest, located at  $x = x_c$ , the wet probability is given by

$$P_w^{-1} = P_c^{-1} + \frac{q_c^2 - q^2}{Bg\bar{h}^3} \quad (4.23)$$

substitution of equation (4.23) into equation (4.18) yields

$$\frac{\bar{h}}{\bar{h}_c} - 1 + \frac{P_c q_c^2}{4gB\bar{h}_c^3} \left[ \left( \frac{\bar{h}_c}{\bar{h}} \right)^2 - 1 \right] = \frac{P_c}{2B\bar{h}_c} \left\{ z_b(x_c) - z_b(x) - \int_{x_1}^x \left[ \frac{f_b}{2} \alpha^2 G_b + \alpha_m \frac{P_w w_m}{(g\bar{h})^{0.5}} \right] dx \right\} \quad (4.24)$$

which is valid in the zone of  $x > x_c$  and  $\bar{h} = h_c$  at  $x = x_c$ .

The wave overtopping rate  $q_o$  is predicted by imposing  $U_s = 0$  in equation (4.17) at the crest location  $x_c$

$$q_o = \frac{3\sqrt{\pi}\alpha\bar{h}_c}{4} \left( \frac{g\bar{h}_c}{P_c} \right)^{0.5} + q_p \quad \text{at } x = x_c \quad (4.25)$$

The wave overtopping probability  $P_o$  may be related to the wet probability  $P_c$  at  $x = x_c$  where both  $P_o$  and  $P_c$  are in the range of 0.0 - 1.0. The empirical relation of  $P_o = [\tanh(5P_c)]^{0.8}$  was fitted by Kobayashi et al. (2010) using 207 tests for wave overtopping of smooth impermeable structures. The computed wave overtopping rates and probabilities for the present four tests are found to be negligible as observed during the experiment.

For an assumed  $q_o$  the landward marching computation of  $\bar{h}$ ,  $\sigma_\eta$ ,  $\bar{U}$ , and  $\sigma_U$  is initiated using the wet model from the seaward boundary  $x = 0$  to the landward limit located at  $x = x_r$ . The predicted mean depth at the location of  $x = x_{SWL}$  is taken as the boundary condition for the wet and dry model. The landward marching computation is continued using the wet and dry model from the location of  $x = x_{SWL}$  where  $\bar{h} = \bar{h}_1$  and  $P_w = 1$  to the landward end of the computation domain or until the mean depth  $\bar{h}$  becomes less than 0.01 *cm*. The rate  $q_o$  is computed using equation (4.25) together with the overtopping probability  $P_o$ . This landward computation starting from  $q_o = 0$  is repeated until the difference between the computed and assumed values of  $q_o$  become less than 1%, normally achieved after several iterations. The computed values of  $\bar{h}$ ,  $\sigma_\eta$ ,  $\bar{U}$ , and  $\sigma_U$  by the two different models in the overlapping zone of  $x_{SWL} < x < x_r$  are averaged to smooth the transition from the wet zone to the wet and dry zone.

### 4.3 Sediment Transport Model

The time-averaged probabilistic model may have its limitations, but it provides the necessary hydrodynamic predictions required for the sediment transport

model in CSHORE. Kobayashi et al. (2010) compared CSHORE with 207 tests for wave overtopping and overflow on impermeable structures as well as 8 data sets for dune profile evolution with no or minimal overwash. The agreement was mostly within a factor of 2. Work done by Figlus et al. (2009) compared CSHORE with sand dune tests designed to create major overwash. However, the previous calibrations of CSHORE were unable to examine the validity of the bedload transport equations because the computed suspended load transport rate  $q_s$  was found to be largely dominant in comparison with the bedload transport rate  $q_b$ . The comparison of measured and computed profile evolutions was used to evaluate the suspended sediment transport formula. In the following, the sediment transport formulas in CSHORE (Kobayashi et al. 2010) are summarized and modified for improvement of bedload transport predictions.

For finer grain beaches, the probability of sediment movement  $P_b$  is estimated using the criteria that movement will occur when the absolute value of the instantaneous bottom shear stress exceeds the shear stress corresponding to the critical Shields parameter  $\psi_c = 0.5$ . This criterion was found to underpredict sediment movement for the coarser and more permeable gravel material. Consequently, the probability of movement used for stone armor units is adopted for gravel which estimates the probability  $P_b$  of gravel movement under the Gaussian velocity  $U$  assuming gravel movement occurs when the absolute value of the instantaneous velocity  $U$  in the wet zone exceeds the critical velocity  $U_{cb}$  estimated as

$$U_{cb} = [N_c g (s - 1) d_{50}]^{0.5} \quad (4.26)$$

where  $s$  and  $d_{50}$  represent the specific gravity and median diameter of the gravel, respectively. The empirical parameter  $N_c$  represents the critical stability number which was calibrated as  $N_c = 0.7$  using the damage progression tests of a stone structure with  $s = 2.66$  and nominal diameter of 3.64 *cm* conducted by Melby and

Kobayashi (1998). The probability of sediment suspension is estimated using the criterion that suspension will occur when the turbulent velocity exceeds the sediment fall velocity, found experimentally. In instances where the estimated  $P_s$  exceeds  $P_b$ , the relation  $P_s = P_b$  is used to ensure that sediment suspension only occurs when sediment movement occurs.

The probability  $P_b$  of sediment movement is determined for the probability distribution of  $U$  based on equations (4.11) and (4.14) for the wet and dry zone. The movement of sediment represented by the median diameter  $d_{50}$  is assumed to occur when the instantaneous velocity  $U$  exceeds the critical velocity  $U_{cb}$  in equation (4.26). Therefore the probability  $P_b$  of sediment movement is the same as the probability of  $|U| > U_{cb}$  and is given by

$$P_b = P_w \quad \text{for } U_s > U_{cb} \quad (4.27)$$

$$P_b = P_w \exp \left[ -\frac{P_w(U_{cb} - U_s)^2}{\alpha^2 g \bar{h}} \right] \quad \text{for } |U_s| \leq U_{cb} \quad (4.28)$$

$$P_b = P_w \left\{ 1 - \exp \left[ -\frac{P_w(U_{cb} + U_s)^2}{\alpha^2 g \bar{h}} \right] + \exp \left[ -\frac{P_w(U_{cb} - U_s)^2}{\alpha^2 g \bar{h}} \right] \right\} \quad \text{for } -U_s > U_{cb} \quad (4.29)$$

where the upper limit of  $P_b$  is the wet probability  $P_w$  because no sediment movement will occur during dry durations.

The time-averaged bedload transport rate in both the wet zone and the wet and dry zone is estimated using

$$q_b = \frac{bP_b G_s B_r \sigma_U^3}{g(s-1)}; \quad B_r = \left( \frac{z_b - z_p}{d_{50}} \right) \leq 1 \quad (4.30)$$

where  $b$  is the empirical bedload parameter,  $G_s$  is a function of the bottom slope  $S_b$ , and  $B_r$  is a reduction factor based on limited gravel availability. The bedload parameter was calibrated to be  $b = 0.002$  for sands by Kobayashi et al. (2008). However, for permeable gravel beaches with gentle slopes ( $S_b \leq 0.3$ ), the bedload parameter is allowed to vary onshore of the breaking zone using the relationship  $b = 0.002(1 + 8Q)$ . The parameter  $Q$  as given by Battjes and Stive (1985) represents the ratio of breaking waves to all (breaking plus nonbreaking) waves at each cross-shore location to account for expected increases in sediment mobilization due to wave breaking. The bedload parameter reduces to the input value of  $b = 0.002$  offshore of wave breaking. The reduction factor  $B_r$  was added to account for the thickness ( $z_b - z_p$ ) of the gravel layer where  $B_r = 1$  if  $(z_b - z_p) > d_{50}$  and  $B_r = 0$  in the zone of  $z_b = z_p$  or no gravel layer. Additional modification to the bedload transport formulation occurs landward of the still water level, where the bedload transport rate is kept at a constant value,  $q_b(x) = q_b(x_{SWL})$  in the region  $x_{SWL} \leq x \leq (x_{SWL} + 3H_{mo})$  where  $H_{mo}$  equals the spectral significant wave height at  $x = 0$ . This modification is based on the observed equilibrium profiles shown in Figure 3.6.

The bottom slope function  $G_s$  was introduced by Kobayashi et al. (2008) to account for the effect of steep cross-shore slope  $S_b$  on the bedload transport rate as follows

$$G_s(S_b) = \frac{\tan \phi}{\tan \phi + S_b} \quad \text{for } -\tan \phi < S_b < 0 \quad (4.31)$$

$$G_s(S_b) = \frac{\tan \phi - 2S_b}{\tan \phi - S_b} \quad \text{for } 0 < S_b < \tan \phi \quad (4.32)$$

where  $\tan \phi$  is the limiting bottom slope taken to be 0.63 for sands, gravels, and stone. The modifications of the bedload formula discussed above are applied only if the value of  $G_s$  at  $x = x_{SWL}$  is positive, corresponding to tests MH and MB.

The time-averaged suspended sediment transport rate  $q_s$  in both the wet zone and the wet and dry zone is expressed as (Figlus et al. 2009)

$$q_s = (a\bar{U} + a_o U_o) V_s \quad (4.33)$$

with

$$U_o = \frac{q_o}{\bar{h}}; \quad V_s = P_s V_{Bf} (1 + S_b^2)^{0.5}; \quad V_{Bf} = \frac{e_B D_B + e_f D_f}{\rho g (s - 1) w_f} \quad (4.34)$$

where  $a$  is the suspended load parameter on the order of 0.2 under the action of waves and wave-induced currents,  $a_o$  is an empirical parameter on the order of 1.0,  $U_o$  is the onshore current due to the wave overtopping rate  $q_o$  which becomes significant only in regions of very small water depth  $\bar{h}$ ,  $V_s$  is the suspended sediment volume per unit horizontal area,  $V_{Bf}$  is the potential suspended sediment volume on a horizontal bottom when the probability of suspension  $P_s = 1$ ,  $e_B$  and  $e_f$  are the suspension efficiencies for the energy dissipation rates  $D_B$  and  $D_f$  which were previously calibrated as  $e_B = 0.005$  and  $e_f = 0.01$ , and  $w_f$  is defined as the sediment fall velocity. It is noted that the computed suspended sediment transport rate  $q_s$  is found to be at least one-order-of-magnitude smaller than the bedload transport rate  $q_b$  for the present four tests, mainly because of the gravel fall velocity,  $w_f = 25 \text{ cm/s}$ . Sediment suspension is expected to occur when the turbulent velocity estimated as  $(f_b/2)^{1/3}|U|$  exceeds the sediment fall velocity  $w_f$ . Therefore, the probability  $P_s$  of sediment suspension in equation (4.34) is the same as the probability of  $|U| > U_{cs}$  where  $U_{cs} = w_f(2/f_b)^{1/3}$ . Consequently, the probability  $P_s$  of suspension can be described by replacing  $U_{cb}$  with  $U_{cs}$  in equations (4.27) to (4.29) in the wet and dry zone.

The cross-shore transport rates  $q_b$  and  $q_s$  are computed in both the wet zone and the wet and dry zone. The values are averaged in the region of  $x_{SWL} \leq x \leq x_r$

where the two models overlap. The continuity equation of bottom sediment is solved numerically to obtain the bottom elevation at the next time level (Kobayashi et al., 2009). This computation procedure is repeated starting from the initial bottom profile. The computation time is on the order of  $10^{-3}$  of the profile evolution time.



## Chapter 5

# COMPARISON OF NUMERICAL MODEL WITH EXPERIMENT RESULTS

This chapter compares the measured experimental results with those predicted by the numerical model CSHORE. The first section discusses the input parameters used to describe the gravel and wave conditions in CSHORE. The next four sections focus on the profile evolution and hydrodynamic results for each of the four tests. A final section focuses on the onshore movement of the gravel edge during each of the four tests. For additional numerical results, including predicted probability of sediment movement and sediment transport rates see Appendix B.

### 5.1 Input Parameters

CSHORE requires a series of input parameters to specify the offshore wave conditions and define the gravel characteristics. Several of these parameters and coefficients are kept constant for each of the four tests and are included in Table 5.1. The empirical parameters included in Table 5.1 are the same as those used by Kobayashi et al. (2009), with the exception of the breaker parameter  $\gamma$  and the bedload parameter  $b$ . By comparing the measured and computed cross-shore variations of the free surface standard deviation  $\sigma_\eta$ , the breaker parameter is calibrated to be 0.7 for the four gravel experiments. However, the predicted results are not found to be very sensitive to the breaker parameter within the range of 0.6 to 0.8. The bedload parameter has been increased in the region where wave breaking occurred for

the mild slope tests, as described in Chapter 4. The cross-shore nodal spacing  $\Delta x$  represents the uniform spacing used in the landward marching computation domain.

Offshore wave forcing conditions including significant wave height  $H_{mo} = 4\sigma_\eta$ , spectral peak period  $T_p$ , and wave set-down  $\bar{\eta}$  measured at gauge G1 ( $x = 0$ ) are specific to each wave burst and can be found in Appendix A.2. The initial gravel profile coordinates are also included in the input file to describe the four initial profiles shown in Chapter 3. Obliquely incident waves and changes in the still water level (SWL) can also be included in the input files; however, neither are included in the four gravel tests in this experiment. The wave overtopping parameter  $a_o$  is specified as its typical value of  $a_o = 1$ ; however, wave overtopping is negligible in this experiment.

Parameter	Value	Description
$\Delta x$	2 cm	cross-shore nodal spacing
$\gamma$	0.7	breaker parameter
$d_{50}$	2.0 mm	median gravel diameter
$w_f$	25 cm/s	fall velocity
$s$	2.7	specific gravity
$e_B$	0.005	breaking wave efficiency
$e_f$	0.01	bottom friction efficiency
$a$	0.2	suspended load parameter
$a_o$	1.0	overtopping parameter
$\tan \phi$	0.63	limiting gravel slope
$b$	0.002*	bedload parameter*

**Table 5.1:** Summary of CSHORE input parameters kept constant for all four tests.

\*NOTE: The bedload parameter is increased inside the surf zone of the mild slope tests as explained in Chapter 4.

## 5.2 Test SL

The prediction of profile evolution for test SL (steep initial slope, low wave height) is shown in Figure 5.1. The figure includes the initial and final measured profiles as well as the predicted profile evolution corresponding to the profile measurements shown in Figure 3.1. The numerical model is successful in capturing the trend of sediment transport for the given test conditions, predicting erosion above the still water level (SWL) and deposition below. The erosion and deposition volumes are also fairly accurate. Some finer details of the profile evolution were not accurately predicted, including the erosion zone at the edge of the beach terrace and location of the inflection point between erosion and deposition. As discussed in Chapter 3, the scour hole region was highly dynamic due to the collision of incoming breaking waves with backwash events. The turbulent eddies created velocities large enough to lift sediment particles and ultimately transport them onshore. However, these eddies were not simulated by the time-averaged model. The discrepancy near the still water shoreline is possibly due to some numerical oscillations initiated at the transition from onshore transport (below the SWL) to offshore transport (above the SWL).

The hydrodynamic figures in this section and the following three sections display the measured free surface and velocity statistics along with the computed predictions from the numerical model. In each figure the circles represent measured values and the solid lines represent the computed predictions with the grayscale color map differentiating between each individual burst. The free surface figures show only data collected by the onshore gauges G4-G8. The numerical model uses the wave conditions at gauge G1 to represent the offshore wave forcing. Consequently, the data recorded by G1 and the two additional offshore gauges G2 and G3 (located less than a meter from G1) are very similar to the numerical predictions of free surface statistics. The five onshore gauges shown in the figures capture the wave shoaling

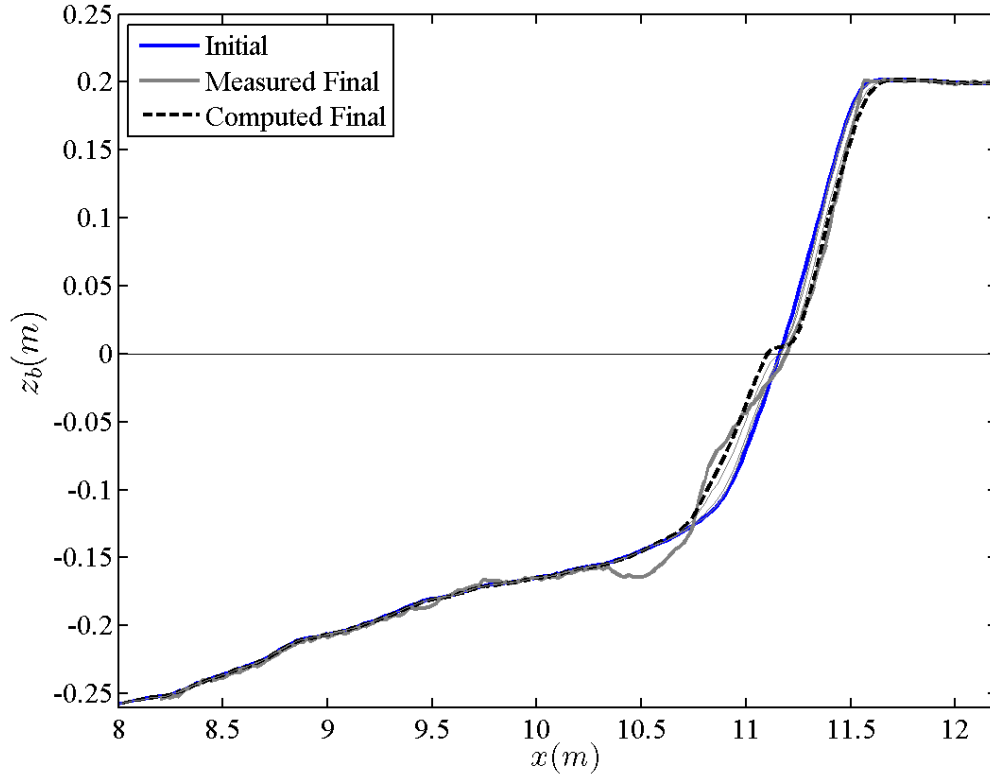


**Figure 5.1:** Computed profile evolution and measured and computed final profiles for the steep slope, low wave height test SL

and breaking as it progresses over the gravel profile. The measured velocity data is presented as the average value of  $\bar{U}$  and  $\sigma_U$  between each pair of current meters because the numerical model is based on the depth-averaged velocity  $U$ .

In test SL, both the measured and recorded hydrodynamic statistics remained fairly constant throughout the 18 wave bursts as can be see in Figures 5.2 and 5.3. This can be attributed to the limited profile change to reach quasi-equilibrium after just three bursts and the relatively small volume of net sediment transport on the gravel beach. Noticeable changes in the free surface predictions occur landward of the still water level, where much of the profile change was concentrated. The predicted mean free surface  $\bar{\eta}$  values are similar to the measured, with the largest

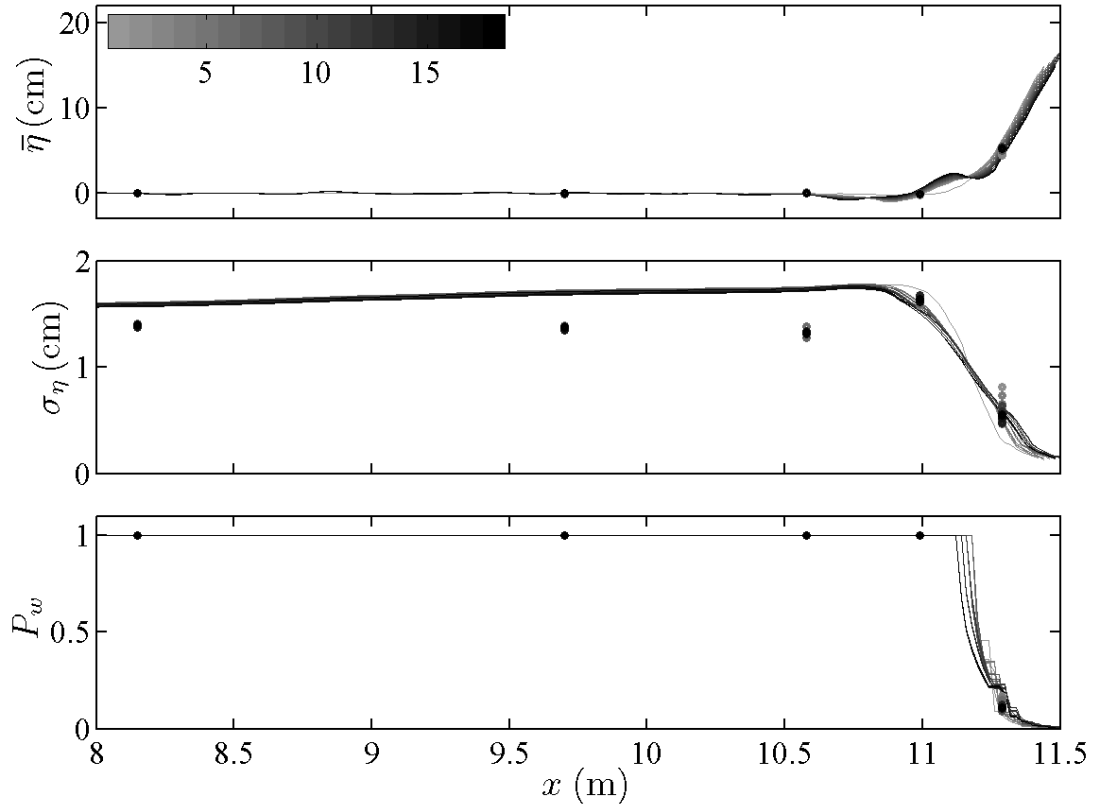


**Figure 5.2:** Comparison of measured free surface statistics with numerical model predictions for test SL. Shown are cross-shore variations in the mean water level (top), standard deviation of the free surface (middle), and the wet probability (bottom).

difference of approximately 1 *cm* occurring at the furthest landward gauge G8. Similar deviation from measured values are computed for the standard deviation of the free surface  $\sigma_\eta$ . CSHORE does not fully capture the wave shoaling and breaking for the low wave test, overpredicting  $\sigma_\eta$  for gauges G4-G6 by about 0.5 *cm*. A closer match between the measured and predicted values can be observed for the further onshore gauges G7 and G8. The final panel in Figure 5.2 shows the measured and predicted wet probability  $P_w$ , as described in Chapter 3. CSHORE predicts the transition of  $P_w$  from G7 to G8 well.

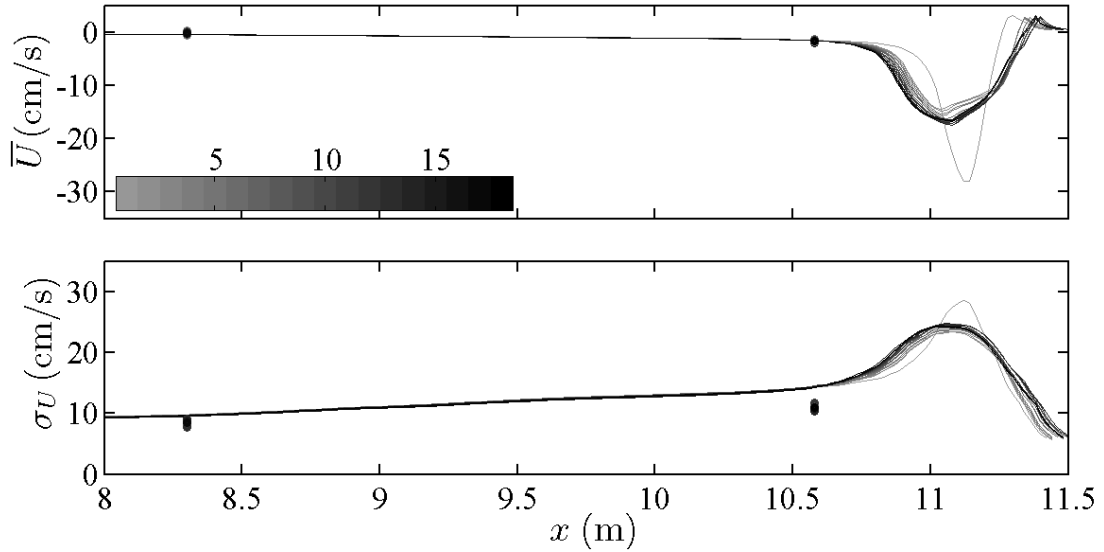


**Figure 5.3:** Comparison of measured fluid velocity statistics with numerical model predictions for test SL

The velocity predictions displayed in Figure 5.3 show CSHORE successfully predicted the velocity statistics. The mean velocity  $\bar{U}$  is accurately predicted with differences reaching only  $0.5 \text{ cm/s}$ . The velocity standard deviation  $\sigma_U$  is also predicted within about  $4 \text{ cm/s}$ . Overall, CSHORE predicts the hydrodynamic statistics for tests SL and each of the subsequent tests reasonably well, with results similar to those found by Figlus et al. (2009) and Kobayashi and Farhadzadeh (2008).

### 5.3 Test SH

Similar results are observed for test SH, again predicting erosion above the still water level and deposition below as shown in Figure 5.4 which corresponds to the measured profile evolution in Figure 3.3. However, the volumes of erosion and deposition are slightly underpredicted for this test. The inflection point between onshore and offshore transport is correctly determined by CSHORE for test SH, predicting its location at the still water shoreline. As in test SL, a few of the

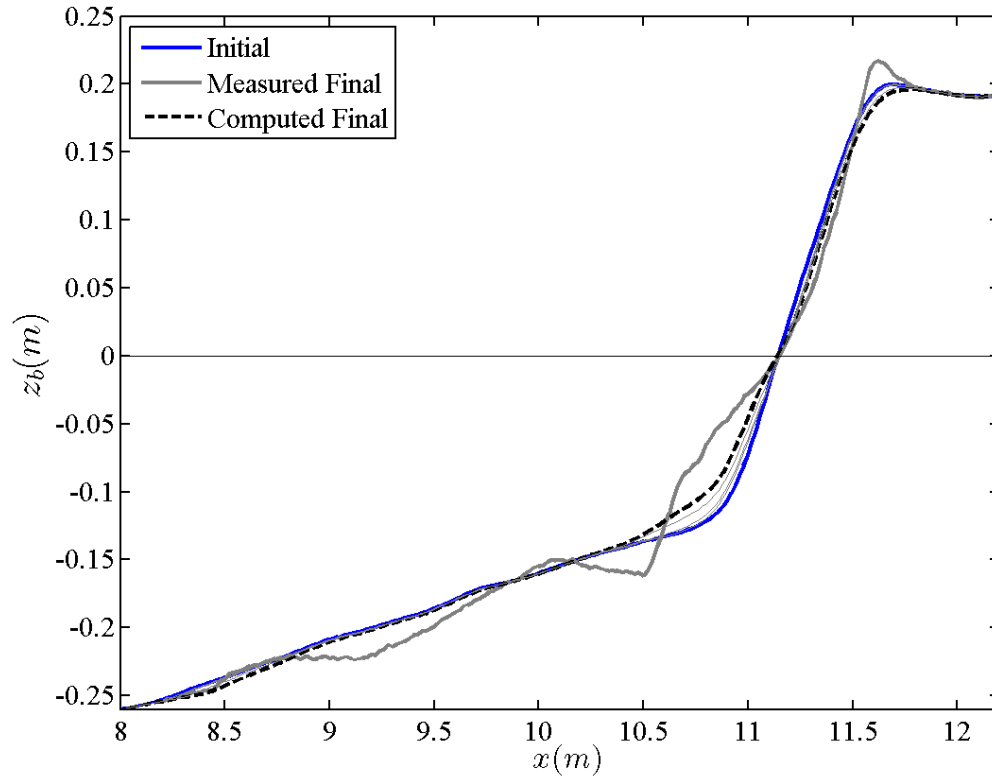


**Figure 5.4:** Computed profile evolution and measured and computed final profiles for the steep slope, high wave height test SH

finer details of the profile evolution are not predicted by CSHORE. The model is again unable to predict the scour hole that occurred seaward of the beach terrace. CSHORE also does not predict the small deposition occurring at the upper limit of wave uprush. This could be attributed to the present bedload formula which does not account for infiltration explicitly. The effect of bottom permeability is included in the hydrodynamic model but not in the sediment transport model directly. Overall, CSHORE is fairly successful in predicting profile evolution for the two steep slope tests. The same bedload transport equation was calibrated by Kobayashi et al. (2010) for the damage progression of stone armor layers also with a  $1/2$  slope. The good agreement for test SL and SH confirms the validity of the bedload formula for

both stone and gravel.

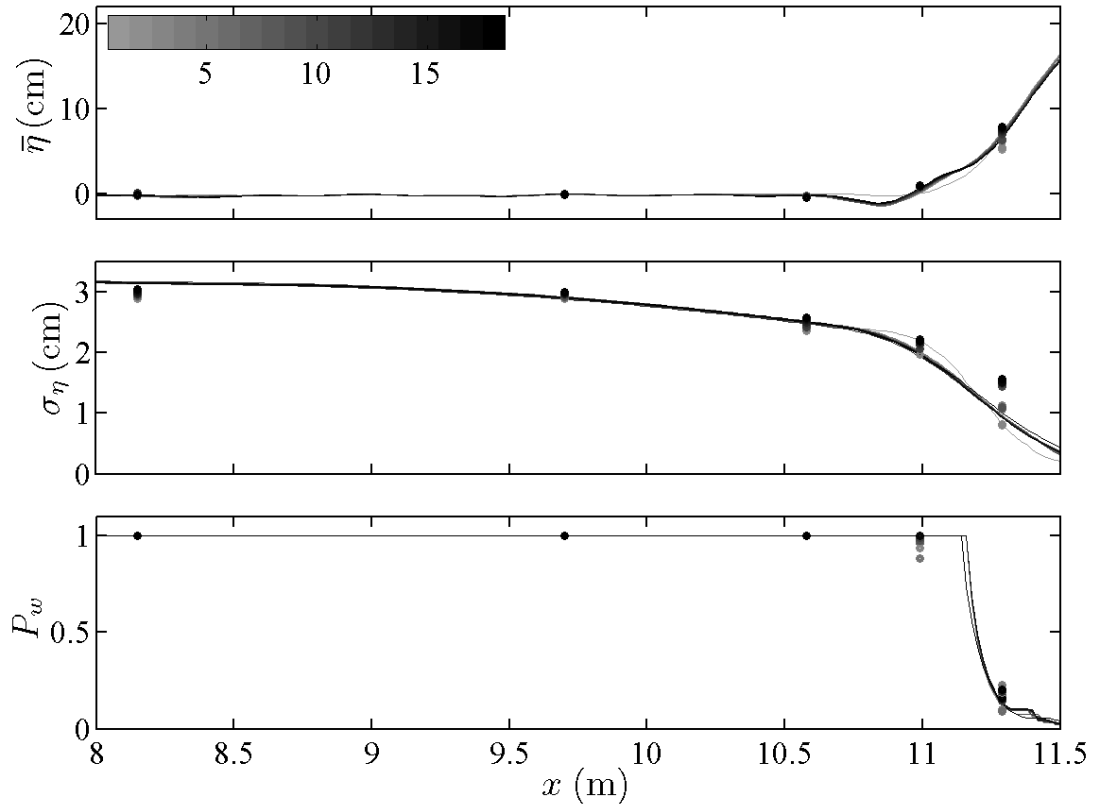


**Figure 5.5:** Comparison of measured free surface statistics with numerical model predictions for test SH

The hydrodynamic predictions for test SH are very close to measured statistics. The mean and standard deviation of the free surface predictions are within about  $0.6\text{ cm}$  with the exception of the furthest landward gauge G8. This gauge was most prone to the accuracy of the predicted bed elevation changes in Figure 5.4; consequently larger deviations of up to  $2\text{ cm}$  between measured and predicted values are not unreasonable. The final measured and predicted profiles for test SH have a  $2\text{ cm}$  difference in bed elevation at gauge G8, which could also account for the discrepancy. During test SH, gauge G7 was observed to be within the wet and dry zone, as demonstrated by measured  $P_w$  values less than 1 in Figure 5.5. However,

CSHORE does not predict similar results, showing only gauge G8 with  $P_w$  less than 1. Despite this shortcoming, CSHORE is still able to predict the wet probability within about 12% at gauge G7 and 8% at gauge G8.

The velocity predictions are not as accurate as with the free surface for test SH. The difference between the depth-averaged velocity and the average velocity of the measured velocities at two elevations is likely responsible for some of the disagreement. However, CSHORE is still able to predict the mean and standard deviation of the velocity within 3  $cm/s$  and 6  $cm/s$ , respectively.

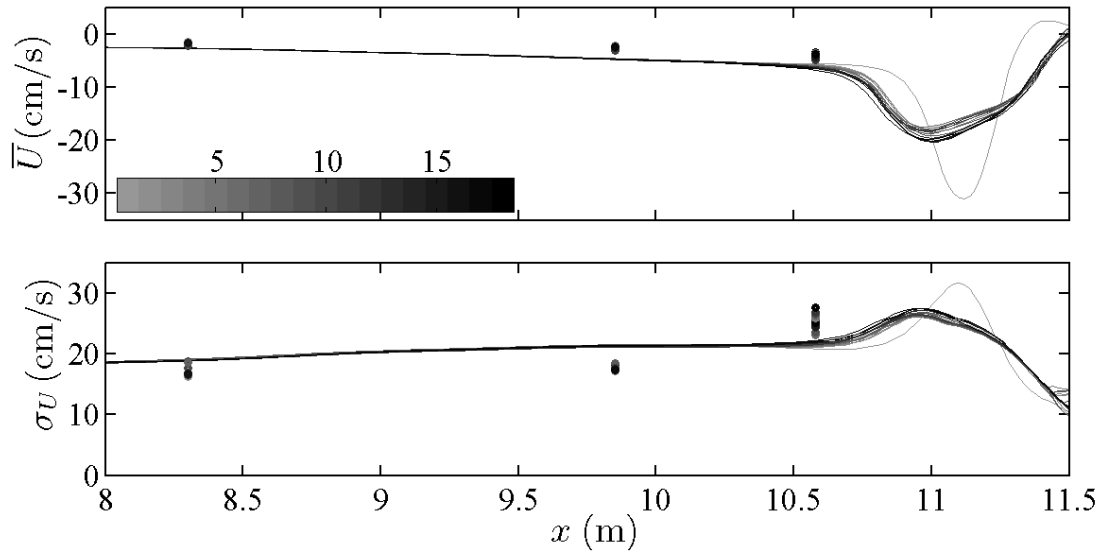


**Figure 5.6:** Comparison of measured fluid velocity statistics with numerical model predictions for test SH

#### 5.4 Test MH

The accretional evolution in test MH was noticeably slower, with the majority of profile change occurring in the vicinity of the upper limit of wave uprush. This observation is reflected in the CSHORE prediction of profile evolution shown in Figure 5.7. However, profile shape is not satisfactorily predicted for the milder initial

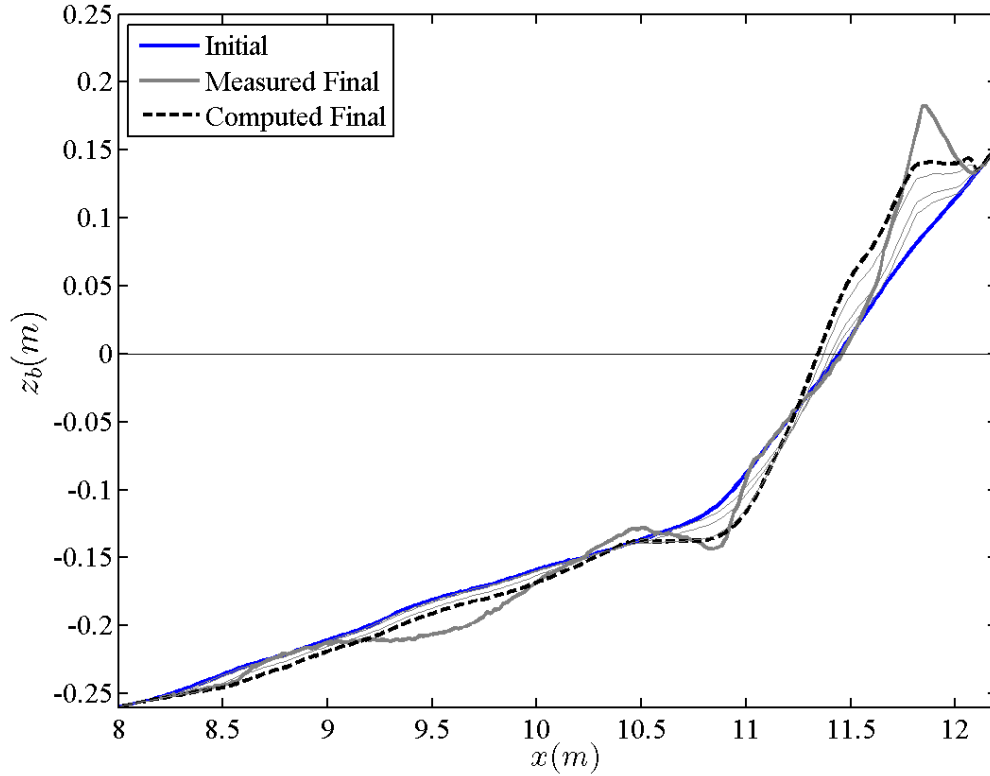


**Figure 5.7:** Computed profile evolution and measured and computed final profiles for the mild slope, high wave height test MH

slope test. CSHORE correctly predicts onshore transport above the still water level, but predicts a wider region of deposition. Efforts have been made to increase the onshore transport by increasing the bedload parameter,  $b$ , and increasing the bedload transport rate above the still water level. The bedload parameter is increased inside the surf zone using the relationship  $b = 0.002(1 + 8Q)$ , where  $Q$  equals the fraction of breaking waves as described by equation (4.30). A constant bedload transport rate  $q_b(x) = q_b(x_{SWL})$  is imposed landward of the still water shoreline in the region  $x_{SWL} \leq x \leq (x_{SWL} + 3H_{mo})$  where  $H_{mo}$  equals the spectral significant wave height at  $x = 0$ . Both of these adjustments significantly increase the volume of onshore sediment transport and the landward extent of the deposition zone. These

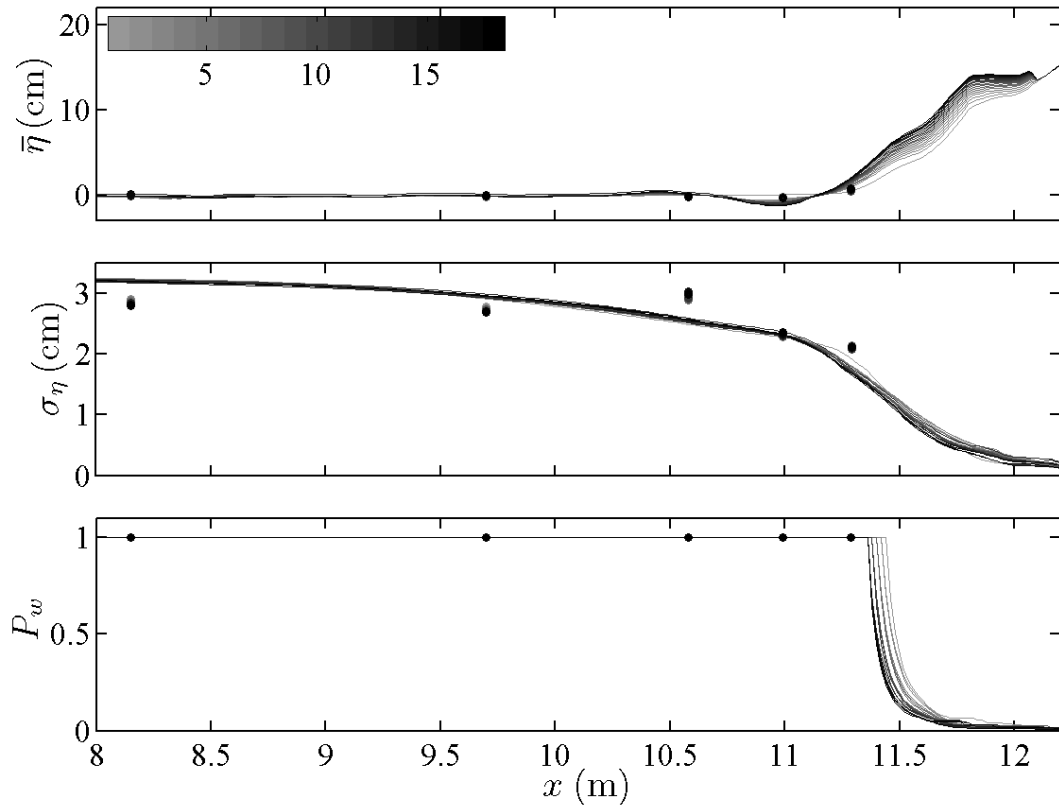


**Figure 5.8:** Comparison of measured free surface statistics with numerical model predictions for test MH

adjustments may be related to effects from infiltration or potential inequality in the friction factor between uprush and backwash as found by Pedrozo-Acuña et al. (2006). The time-averaged model represents the friction factor with a single value, which could contribute the reduced deposition at the maximum run-up. However, the quantitative understanding of these effects is very limited. Below the still water level, CSHORE adequately predicts the location and volume of erosion at the toe of the beach face. The shape of the beach terrace is not fully captured, but again this can likely be attributed to the inability of CSHORE to describe the dynamics of wave breaking in this region. A significant erosion zone was also formed further offshore along the 1/20 slope. This may be related to the steady onshore gravel

transport under partial standing waves along the 1/20 slope discussed further in section 5.6.

Despite shortcomings in the prediction of the profile evolution, the hydrodynamic statistics are accurately predicted. The current meters and wave gauges were all located seaward of the still water shoreline, in the region where the measured and predicted profiles were fairly consistent. Figure 5.8 shows the wave gauge statistics. The mean free surface  $\bar{\eta}$  is predicted within about 1 *cm* and the standard deviation  $\sigma_{\eta}$  is predicted within 0.5 *cm*. All eight gauges recorded a wet probability of 1.0, consistent with predictions by CSHORE. The mean velocity  $\bar{U}$  and the standard deviation  $\sigma_U$  are predicted within approximately 2 *cm/s* and 4 *cm/s*, respectively.

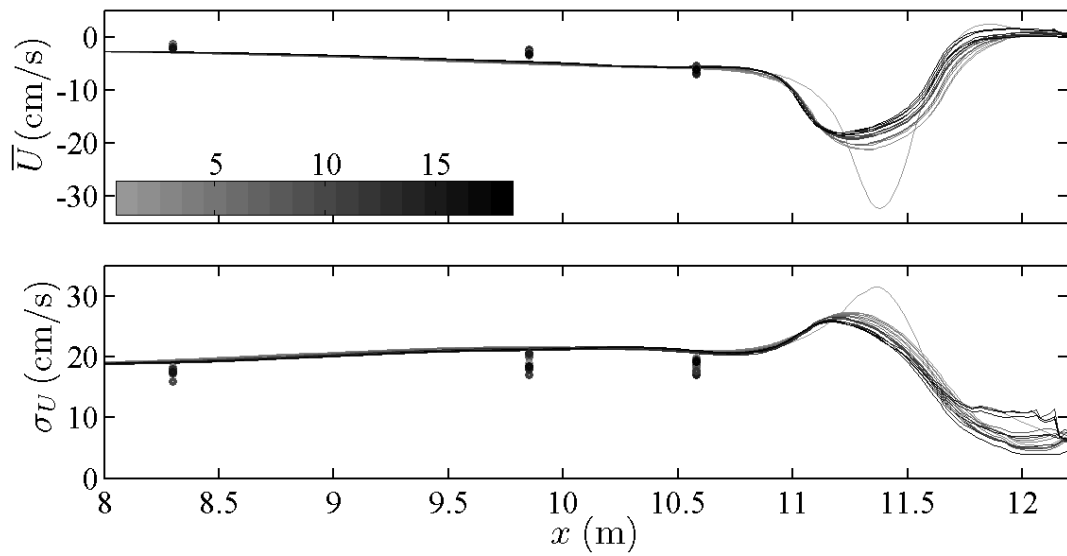


**Figure 5.9:** Comparison of measured fluid velocity statistics with numerical model predictions for test MH

### 5.5 Test MB

Test MB experienced the most profile change, requiring 27 bursts before quasi-equilibrium conditions were achieved. The addition of the bar allowed for

investigation of how well CSHORE could predict onshore bedload transport on the gravel beach. Figure 5.10 shows the entire profile progression predicted by CSHORE. CSHORE is successful in predicting the onshore bar migration and distribution of bar material across the beach face whose initial slope was  $1/5$  from test MH. Like with test MH, the increased bedload parameter  $b = 0.002(1 + 8Q)$  is used to increase bedload transport within the surf zone. The final computed profile has similarities to the measured final profile. However, a lens of gravel develops on the beach face from approximately 11.0 to 11.6 meters, that did not exist during test MB. Like in test MH, this feature is likely a result of the slope function given by equation (4.32) trending to zero at a critical slope of approximately 0.3. CSHORE does better capturing the shape of the depositional region at maximum run-up, but with a slight overprediction of the landward extent of the deposition. There are also apparent discrepancies below the still water level. CSHORE predicts enough erosion to expose the impermeable bottom at 10.2  $m$ , which did not occur during the experiment. CSHORE is also unable to predict the development of the beach terrace formed below the still water level.

Figure 5.11 highlights two critical stagess in the profile progression, when the bar reached the beach face after 9 bursts and when the bar material started to distribute across the beach face at burst 18. Both the measured and computed profiles are presented for comparison. CSHORE does an excellent job of predicting the speed and shape of the onshore migratory bar, as illustrated in the top panel. The agreement at burst 18 is not quite as good, but shows CSHORE is able to predict the transition from onshore bar migration to distribution of gravel across the beach face.

Due to the large number of bursts and large changes in the profile, the hydrodynamic data from test MB is best represented in groups. A single plot of hydrodynamic statistics would be difficult to interpret; consequently, the data is split

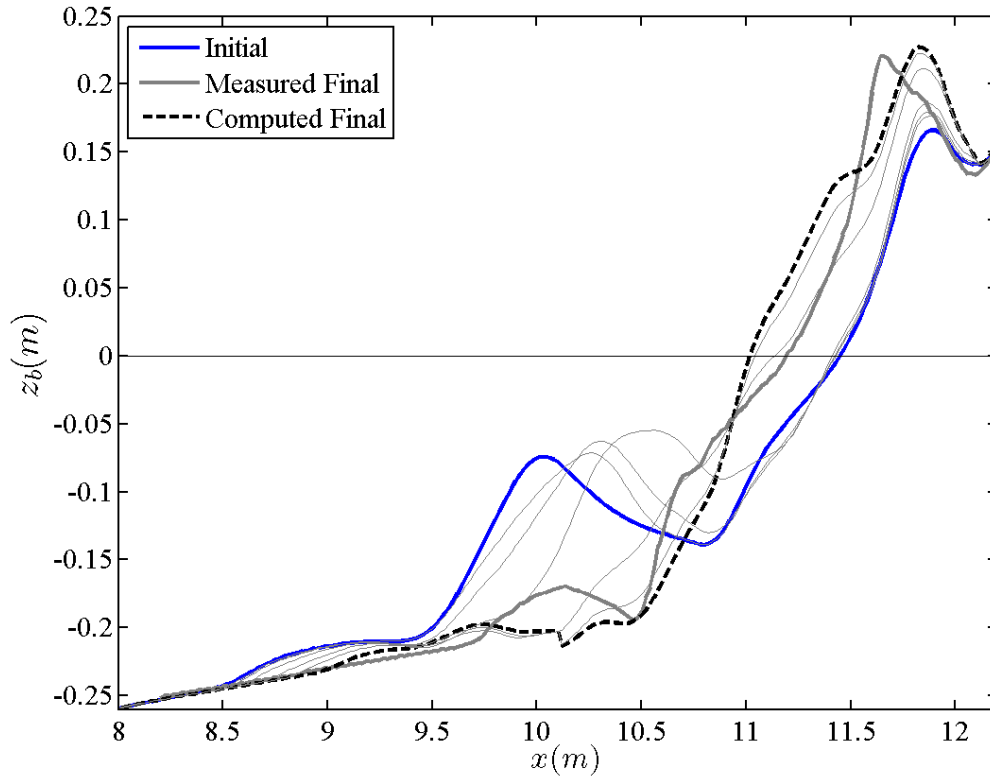


**Figure 5.10:** Computed profile evolution and measured and computed final profiles for the mild slope with a nearshore bar test MB

into four groups of nine bursts. Each figure also includes the measured statistics for each of the nine bursts displayed. The figures clearly show how the hydrodynamics changed throughout the test with the changing profile. Figure 5.12 showing bursts 1-9 clearly shows the influence of the bar as indicated by the stepped  $\sigma_\eta$  plot and the double peaked velocity plots. CSHORE also correctly captures the trends of the statistics, as shown by the increasing velocity predicted as the bar migrated onshore matching the trend in velocity statistics recorded by current meters EMCM5-6 in Figure 5.12. In Figure 5.13, displaying bursts 10 through 18, the decreasing effect of the bar is discernible as it approaches the beach face. The velocity statistics predicted for bursts 16-18 show only one peak in the velocity, reflecting the merger

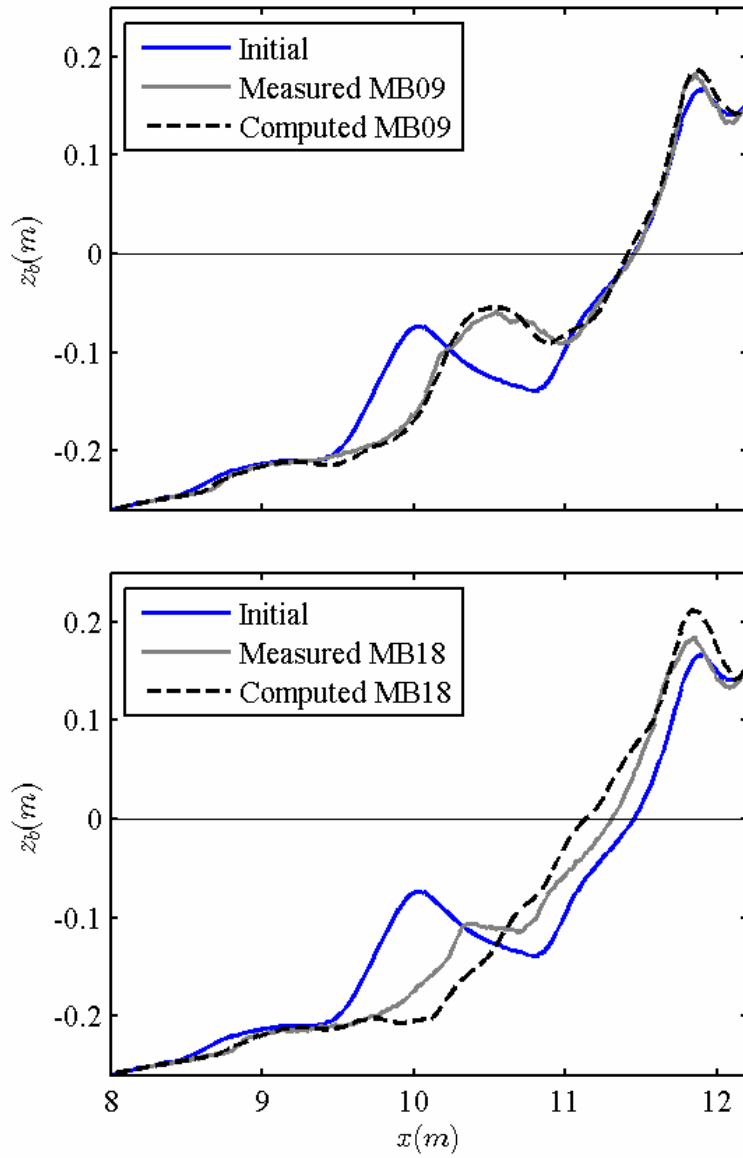


**Figure 5.11:** Comparison of measured and computed profiles after MB09 (top) and MB18 (bottom).

of the bar with the beach face. The final two hydrodynamic figures, 5.14 and 5.15 displaying bursts 19-27 and 28-36, more closely resemble the figures generated for the three previous tests because the nearshore bar was absent in these figures.

Test MB has the largest differences between measured and predicted hydrodynamic statistics. The larger differences are due to the larger changes in profile elevation and differences between the measured and computed profiles. Tests SL, SH, and MH experienced smaller changes and reached quasi-equilibrium conditions much more quickly than test MB. Consequently, the calibration of the buried wave gauges in test MB was less accurate than for tests SL, SH and MH. Discrepancy at gauge G8 can be further explained by the difference in measured and predicted bed elevation during later wave bursts. By the conclusion of test MB, there was a 6 *cm* difference between measured and predicted profiles at the location of gauge G8, which is clearly reflected in the  $\bar{\eta}$  and  $\sigma_{\eta}$  plots in Figures 5.14 and 5.15. The difference in bed elevation is also reflected in the wet probability  $P_w$  at gauge G8. CSHORE underpredicts the wet duration, which is expected due to the prediction of a higher bed elevation. The velocity predictions are more accurate, with differences staying within about 5 *cm/s* for both  $\bar{U}$  and  $\sigma_U$  because the velocity could be measured only in the wet zone with sufficient depth.

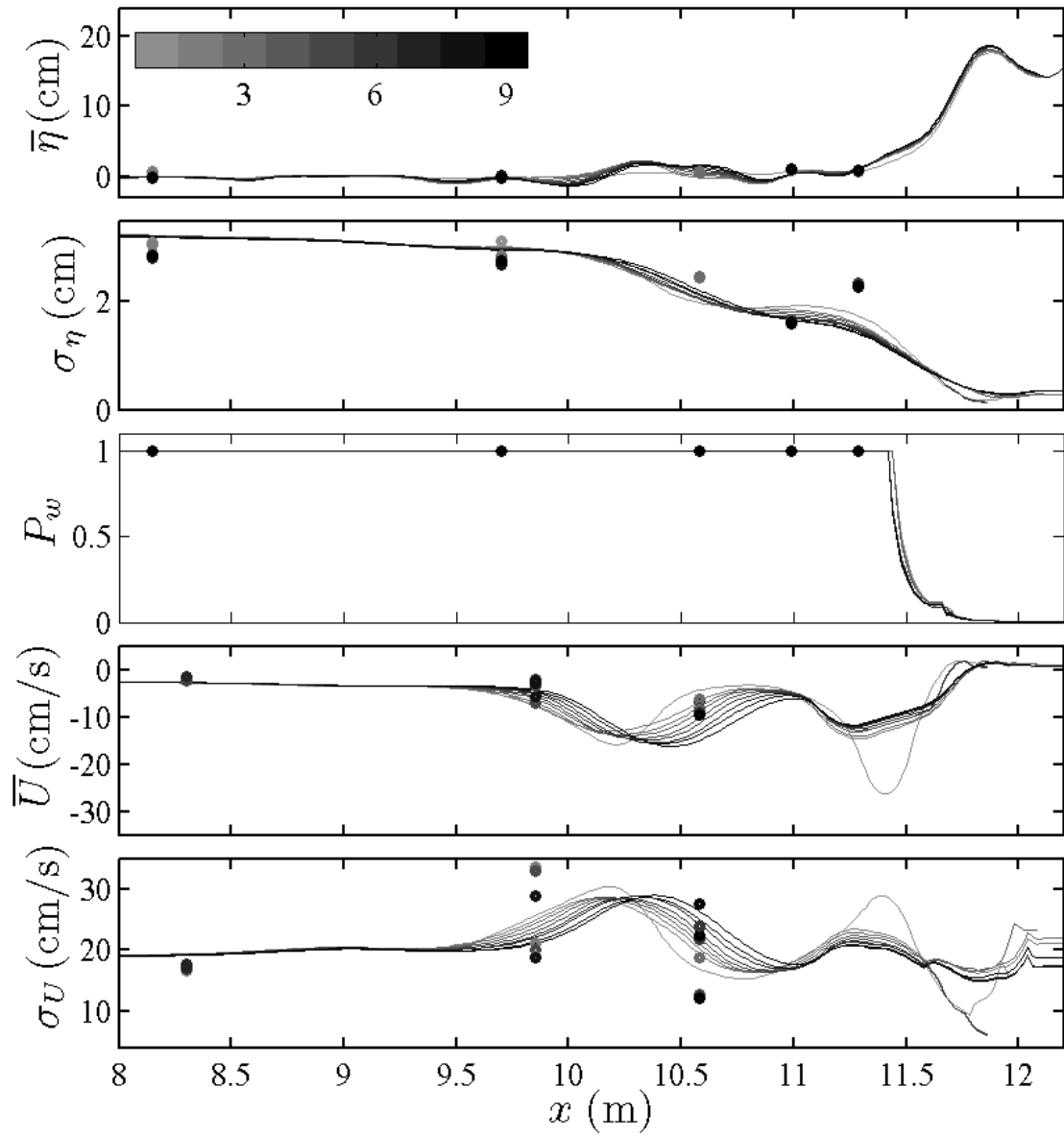


**Figure 5.12:** Comparison of measured free surface and fluid velocity statistics with numerical model predictions for test MB01-09

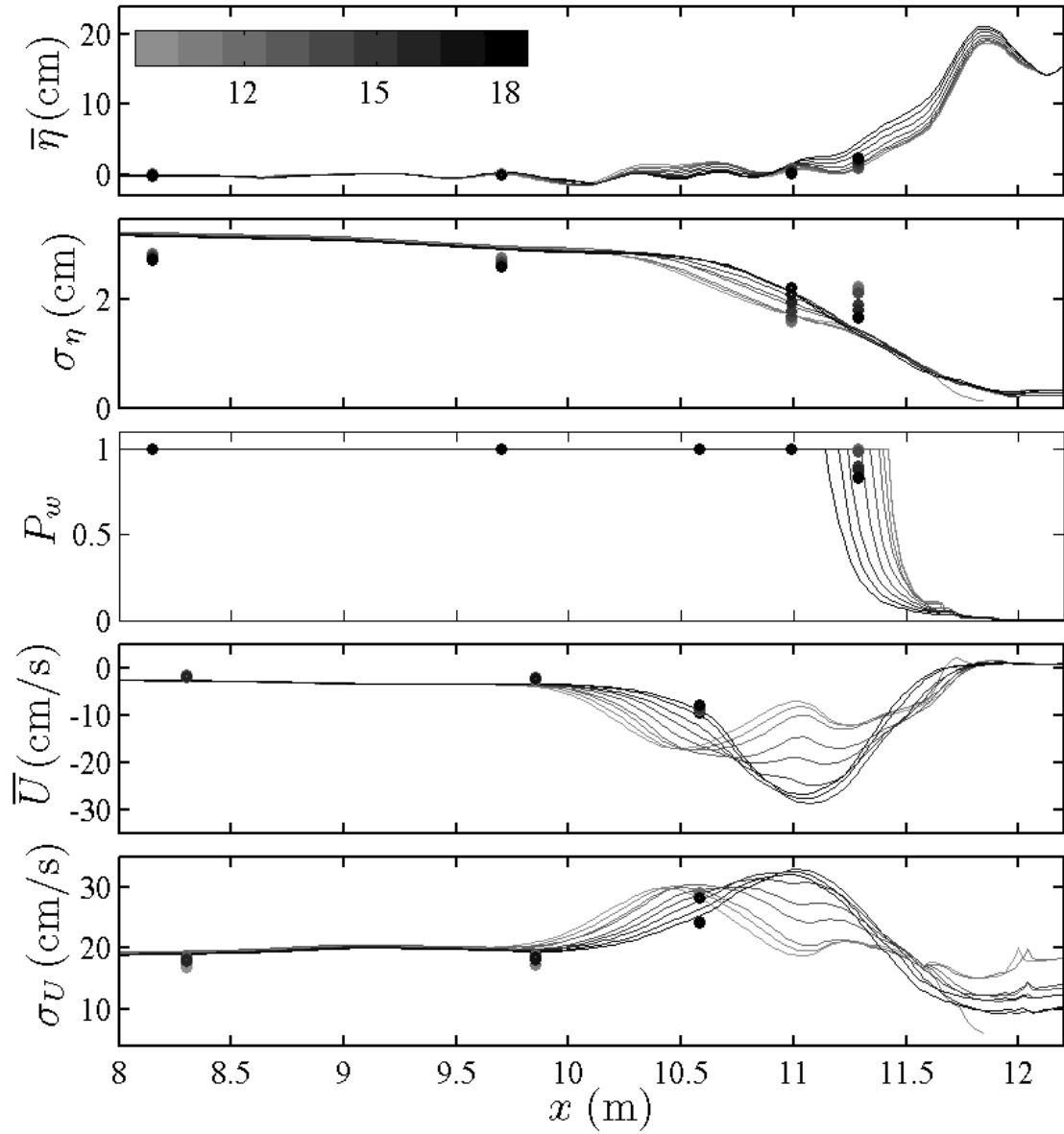


**Figure 5.13:** Comparison of measured free surface and fluid velocity statistics with numerical model predictions for test MB10-18

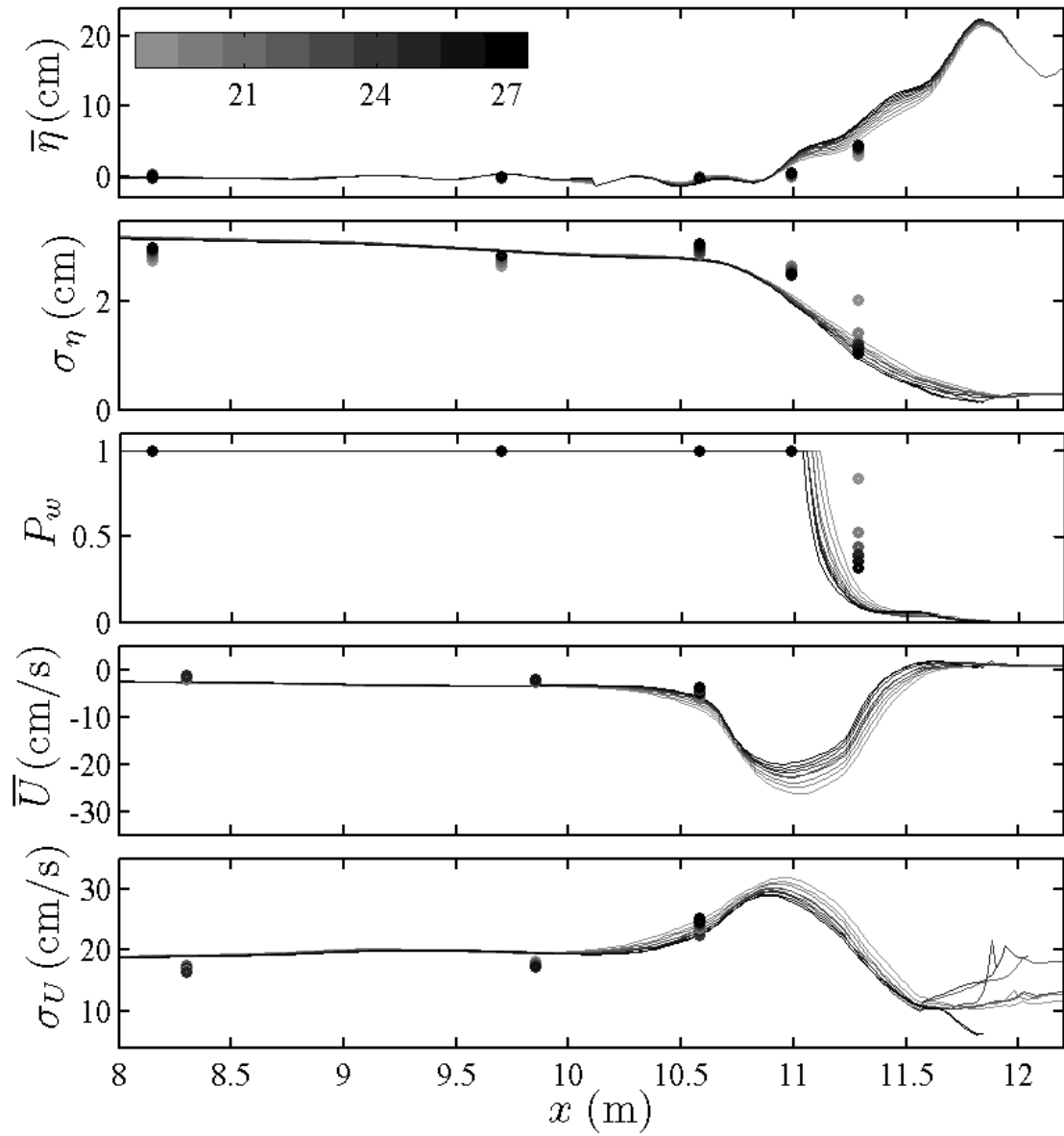


**Figure 5.14:** Comparison of measured free surface and fluid velocity statistics with numerical model predictions for test MB19-27

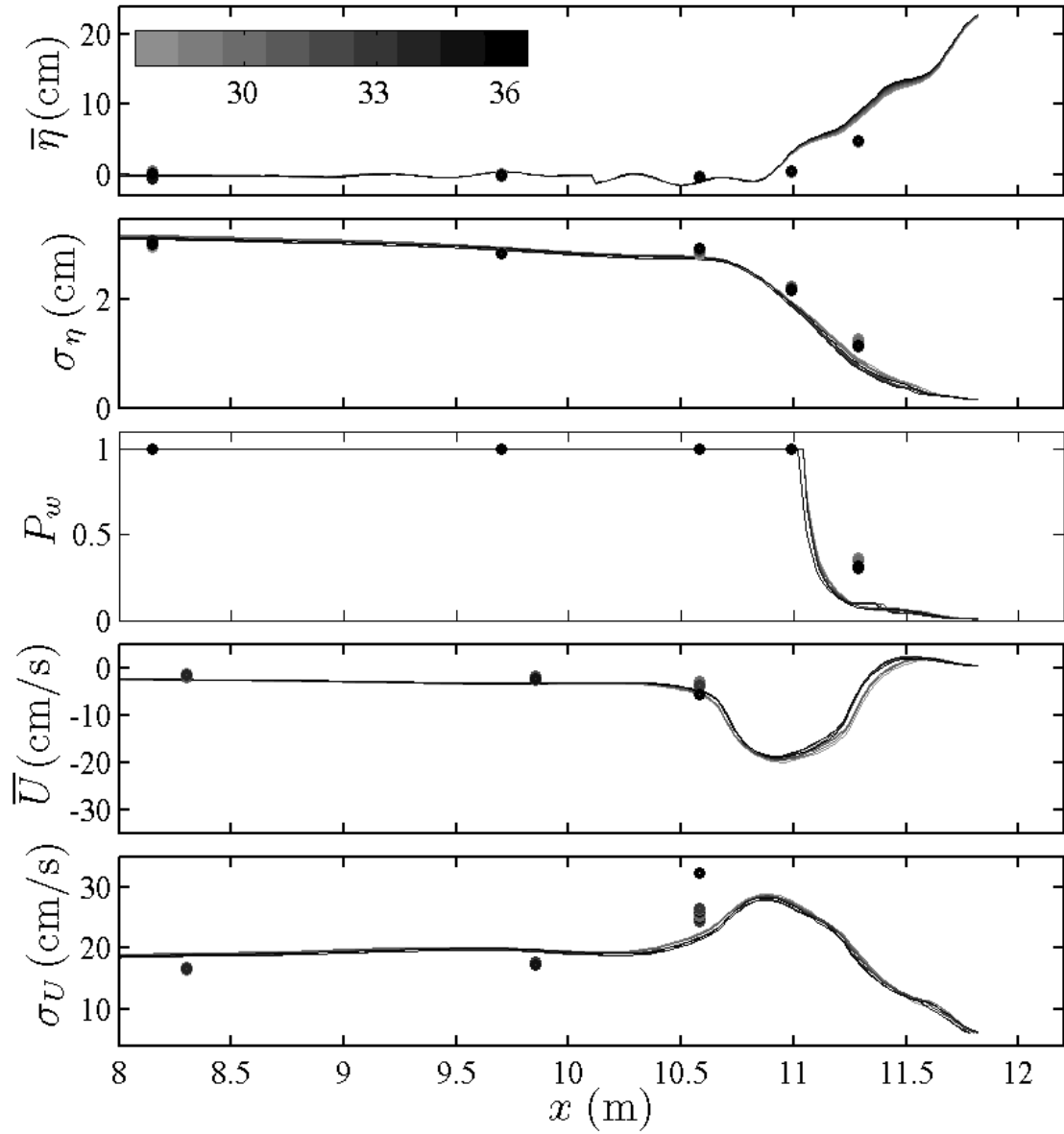


**Figure 5.15:** Comparison of measured free surface and fluid velocity statistics with numerical model predictions for test MB28-36

## 5.6 Gravel Edge Migration

As discussed in Table 3.2 in Chapter 3, the edge of gravel was observed to consistently migrate onshore, indicating net onshore transport across the 1/20 slope. This migration was most pronounced during the higher wave tests SH, MH and MB. The onshore progression of the gravel edge is summarized in Table 5.2 where migration is represented by the change in the cross-shore location of the gravel edge. CSHORE predicts no movement for test SL, which is consistent with the small measured onshore migration of 6 *cm*. As observed during the experiment, the larger wave height in tests SH, MH and MB increased onshore transport. Tests SH and MH were both accurately predicted with predictions staying within 4 *cm* of experimental results. The prediction for the final test MB, stayed consistent with measurements up to burst 18 after which the measured movement significantly accelerated. CSHORE does not predict this acceleration, largely underpredicting the gravel edge displacement at burst 27 and 36.

**Table 5.2:** Comparison of onshore movement of the seaward edge of the gravel layer on the impermeable slope of 1/34.2. The movement is presented as the change in cross-shore location relative to the initial gravel edge location.

Burst No.	Edge of gravel displacement (m)							
	SL		SH		MH		MB	
[-]	Meas.	Pred.	Meas.	Pred.	Meas.	Pred.	Meas.	Pred.
00	0.00	0.00	0.00	0.00	0.00	0.00	0.00	0.00
01	0.02	0.00	0.06	0.04	0.10	0.06	0.00	0.01
03	0.03	0.00	0.10	0.08	0.14	0.12	0.00	0.07
09	-	-	-	-	-	-	0.12	0.15
10	0.06	0.00	0.20	0.16	0.24	0.26	-	-
18	0.06	0.00	0.24	0.26	0.38	0.38	0.24	0.25
27	-	-	-	-	-	-	0.92	0.39
36	-	-	-	-	-	-	1.18	0.51



## Chapter 6

### CONCLUSIONS

A total of four tests were conducted in a laboratory wave flume to investigate cross-shore sediment transport on a gravel beach. The coarse grains having a fall velocity on the same order of magnitude as the wave-induced oscillatory velocity allowed for a close look at transport almost entirely restricted to bedload. Two tests (SL and SH) were performed on an initially steep slope of 1/2 with two different wave heights, both producing offshore transport conditions above the still water level (SWL). A third test examined accretional conditions on an initially milder slope of 1/5. The final test investigated the onshore migration of a nearshore gravel bar. Each test was observed to have rapid profile change and was carried out until quasi-equilibrium conditions were reached. The resulting profiles had similar shapes characterized by a beach terrace at the toe of the beach face and a prominent berm above the SWL which grew in size for the high wave tests, SH, MH and MB. A scour hole seaward of the beach terrace was observed for each test, believed to develop due to eddies generated by wave breaking on the terrace under the influence of backwash.

During each test, eight wave gauges were used to determine incident wave conditions, evaluate the reflection coefficient, and measure free surface elevation of the shoaling and breaking waves to generate time-averaged statistics. Data collected by three pairs of current meters was used to evaluate time-averaged velocity statistics. The free surface and velocity statistics were used in comparison with the hydrodynamic predictions generated by the time-averaged numerical model CSHORE. The

numerical model was successful in capturing the essential hydrodynamics of each of the four test conditions, including the rapidly changing hydrodynamics due to the onshore bar migration observed during test MB. The degree of agreement was found to be similar to those of previous studies by Figlus et al. (2009) and Kobayashi and Farhadzadeh (2008).

The bedload formula used for the prediction of damage progression of stone structures by Kobayashi et al. (2010) was found to successfully predict the profile evolution of the two steep slope tests, with the exception of minor profile features including the offshore erosion zone and the deposition above the still water level in test SH. The prediction of profile evolution for tests MH and MB required adjustments to the bedload transport equations including the increase of the bedload parameter  $b$  inside the surf zone for increased onshore transport. The adjusted sediment transport model successfully predicted the onshore transport within the wet zone, including both the rate of the onshore bar migration and the persistent onshore transport observed along the 1/20 submerged gravel slope. The model agreement was less satisfactory within the swash zone, CSHORE was unable to adequately predict the quasi-equilibrium profiles measured for the two accretional tests. The bottom slope function used in CSHORE to reduce bedload transport as the slope approaches a critical value may need to be improved in future studies of prediction of profile evolution.

## REFERENCES

- Ahrens, J.P., (1990). Dynamic Revetments. *Proc. 22nd Int. Conference on Coastal Engineering*, ASCE, Reston, Va., 1837-1850.
- Allan, J.C., and Komar, P.D., (2002). "A dynamic revement and artificial dune for shore protection." *Proc. 28th Int. Conference on Coastal Engineering*, World Scientific, Singapore, 2044-2056.
- Austin, M.J., and Masselink, G., (2006). "Observations of morphological change and sediment transport on a steep gravel beach." *Marine Geology*, 229, 59-77.
- Baldock, T.E., and Holmes, P., (1999). "Simulation and prediction of swash oscillations on a steep beach." *Coastal Engineering*, 36, 219-242.
- Battjes, J. and Stive, M. (1985). Calibration and verification of a dissipative model for random breaking waves. *Journal of Geophysical Research*, 90(C5):9159-9167.
- Blewett, J.C., Holmes, P., and Horn, D., (2000). "Swash hydrodynamics on sand and shingle beaches." *Proc. 27th Int. Conference on Coastal Engineering*, ASCE, Reston, Va., 597-609.
- Figlus, J., Kobayashi, N., Gralher, C., and Iranzo, V. (2009). "Experimental and numerical study on the transition from minor to major overwash of dunes." Research Report No. CACR-09-04, Center for Applied Coastal Research, University of Delaware, Newark, Delaware.
- Holland, K.T., Holman, R.A., and Sallenger, A.H., Jr. (1991). "Estimation of overwash bore velocities using video techniques." *Proc. Coastal Sediments '91*, ASCE, Reston, Va., 489-497.

- Kobayashi, N., (2009). "Documentation of cross-shore numerical model CSHORE 2009." Research Report No. CACR-09-06, Center for Applied Coastal Research, University of Delaware, Newark, Delaware.
- Kobayashi, N., Buck, M., Payo, A., and Johnson, B.D. (2009). "Berm and dune erosion during a storm." *Journal of Waterway, Port, Coastal, Ocean Engineering*, 135(1), 1-10.
- Kobayashi, N., and Farhadzadeh, A. (2008). "Cross-shore numerical model CSHORE for waves, currents, sediment transport and beach profile evolution." Research Report No. CACR-08-01, Center for Applied Coastal Research, University of Delaware, Newark, Delaware.
- Kobayashi, N., Farhadzadeh, A., Melby, J.A., Johnson, B., and Gravens, M. (2010). "Wave overtopping of levees and overwash of dunes." *Journal of Coastal Research* (in press).
- Kobayashi, N., Herrman, M.N., Johnson, B.D., and Orzech, M.D. (1998). "Probability distribution of surface elevation in surf and swash zones." *Journal of Waterway, Port, Coastal, Ocean Engineering*, 124(3), 99-107.
- Kobayashi, N., Meigs, L.E., Ota, T., and Melby, J.A. (2007). "Irregular breaking wave transmission over submerged porous breakwaters." *Journal of Waterway, Port, Coastal, Ocean Engineering*, 133(2), 104-116.
- Mei, C.C. (1989). *The Applied Dynamics of Ocean Surface Waves*. Advanced Series on Ocean Engineering. World Scientific, Singapore.
- Melby, J.A., and Kobayashi, N. (1998). "Progression and variability of damage on rubble mound breakwaters." *Journal of Waterway, Port, Coastal, Ocean Engineering*, 124(6), 286-294.
- Pedrozo-Acuña, A., Simmonds, D., Otta, A.K., and Chadwick, A.J. (2006). "On the cross-shore profile change of gravel beaches." *Coastal Engineering*, 53, 335-347.
- Pilarczyk, K.W., and den Boer, K., "Stability and profile development of coarse materials and their application in coastal engineering." *roc. Int. Conference on Coastal and Port Engineering in Developing Countries*, Comobo, Sri Lanka, Mar 1983.

- Wurjanto, A., and Kobayashi, N. (1993). "Irregular wave reflection and runup on permeable slopes." *Journal of Waterway, Port, Coastal, Ocean Engineering*, 119(5), 537-557.
- van der Meer, J.W., and Pilarczyk, K.W. (1986). "Dynamic stability of rock slopes and gravel beaches." *Proc. 20th Int. Coastal Engineering Conf.*, ASCE, Reston, Va., 1713-1726.
- van Gent, M.R.A. (1995). "Porous flow through rubble-mound material." *Journal of Waterway, Port, Coastal, Ocean Engineering*, 121(3), 176-181.
- van Hyum, E., and Pilarczyk, K.W., (1982). "Gravel beaches, equilibrium profile and longshore transport of coarse material under regular and irregular wave attack." Delft Hydraulics Laboratory, Publication No. 274.



## Appendix A

### WAVE GAUGE AND VELOCITY DATA

#### A.1 Offshore Incident Wave Conditions

**Table A.1:** Offshore wave conditions obtained from gauges G1-G3 for the steep slope, low wave height (SL) test.

Test No.	$H_{mo}$	$H_{rms}$	$H_s$	$T_p$	$T_s$	$R$
[-]	[cm]	[cm]	[cm]	[sec]	[sec]	[-]
SL01	-	-	-	-	-	-
SL02	5.71	4.04	5.52	1.94	1.84	0.34
SL03	5.68	4.01	5.44	1.92	1.84	0.34
SL04	5.70	4.03	5.42	1.94	1.84	0.34
SL05	5.71	4.03	5.45	1.94	1.81	0.35
SL06	5.68	4.02	5.43	2.00	1.80	0.35
SL07	5.66	4.00	5.41	1.94	1.82	0.35
SL08	5.66	4.00	5.41	1.94	1.81	0.35
SL09	5.65	4.00	5.41	2.00	1.80	0.35
SL10	5.66	4.00	5.32	1.93	1.81	0.35
SL11	5.63	3.98	5.30	1.93	1.81	0.36
SL12	-	-	-	-	-	-
SL13	5.63	3.98	5.30	1.92	1.78	0.35
SL14	5.62	3.97	5.31	1.94	1.79	0.36
SL15	5.60	3.96	5.29	1.94	1.79	0.36
SL16	5.47	3.87	5.13	1.94	1.80	0.36
SL17	5.61	3.97	5.32	1.94	1.80	0.36
SL18	5.61	3.97	5.42	1.93	1.81	0.35
mean	5.64	3.99	5.37	1.94	1.81	0.35

**Table A.2:** Offshore wave conditions obtained from gauges G1-G3 for the steep slope, high wave height (SH) test.

Test No.	$H_{mo}$	$H_{rms}$	$H_s$	$T_p$	$T_s$	$R$
[-]	[cm]	[cm]	[cm]	[sec]	[sec]	[-]
SH01	12.00	8.49	12.53	-	1.90	-
SH02	11.98	8.47	12.40	1.99	1.90	0.28
SH03	11.95	8.45	12.42	1.98	1.90	0.28
SH04	11.94	8.44	12.36	2.01	1.88	0.28
SH05	12.04	8.52	12.54	1.96	1.90	0.28
SH06	12.07	8.53	12.44	1.95	1.88	0.28
SH07	12.06	8.53	12.51	1.96	1.91	0.28
SH08	11.97	8.47	12.24	1.98	1.90	0.28
SH09	12.05	8.52	12.38	2.01	1.89	0.28
SH10	12.03	8.50	12.35	1.95	1.88	0.28
SH11	12.04	8.51	12.32	1.96	1.88	0.29
SH12	12.03	8.51	12.51	1.92	1.89	0.28
SH13	11.96	8.46	12.41	1.98	1.90	0.28
SH14	11.99	8.48	12.40	1.96	1.91	0.28
SH15	11.96	8.46	12.26	1.99	1.89	0.29
SH16	12.00	8.48	12.40	1.99	1.90	0.29
SH17	12.00	8.48	12.45	1.96	1.90	0.29
SH18	12.02	8.50	12.46	1.98	1.92	0.29
mean	12.01	8.49	12.41	1.97	1.90	0.28

**Table A.3:** Offshore wave conditions obtained from gauges G1-G3 for the mild slope, high wave height (MH) test.

Test No.	$H_{mo}$	$H_{rms}$	$H_s$	$T_p$	$T_s$	$R$
[-]	[cm]	[cm]	[cm]	[sec]	[sec]	[-]
MH01	12.35	8.73	12.86	1.95	1.89	0.23
MH02	12.43	8.79	12.91	1.98	1.90	0.25
MH03	12.46	8.81	12.92	2.01	1.89	0.25
MH04	12.35	8.73	12.75	2.01	1.91	0.25
MH05	12.39	8.76	12.66	2.01	1.91	0.25
MH06	12.36	8.74	12.80	2.01	1.91	0.25
MH07	12.34	8.73	12.36	2.01	1.92	0.26
MH08	12.36	8.74	12.78	1.96	1.91	0.26
MH09	12.32	8.71	12.74	1.95	1.90	0.26
MH10	12.38	8.75	12.76	1.98	1.91	0.26
MH11	12.34	8.72	12.78	1.98	1.89	0.26
MH12	12.32	8.71	12.43	1.95	1.92	0.26
MH13	12.34	8.72	12.34	2.01	1.94	0.26
MH14	12.28	8.68	12.27	1.92	1.93	0.27
MH15	-	-	-	-	-	-
MH16	12.36	8.74	12.38	1.96	1.93	0.27
MH17	12.35	8.73	12.39	1.95	1.92	0.27
MH18	12.30	8.69	12.31	1.98	1.93	0.28
mean	12.35	8.74	12.61	1.98	1.91	0.26

**Table A.4:** Offshore wave conditions obtained from gauges G1-G3 for the mild slope with a bar (MB) test.

Test No.	$H_{mo}$	$H_{rms}$	$H_s$	$T_p$	$T_s$	$R$
[-]	[cm]	[cm]	[cm]	[sec]	[sec]	[-]
MB01	12.41	8.78	12.92	1.96	1.90	0.23
MB02	12.38	8.75	12.93	1.96	1.90	0.23
MB03	12.46	8.81	13.08	1.98	1.90	0.24
mean	12.42	8.78	12.98	1.97	1.90	0.24
MB04	12.48	8.83	13.00	1.98	1.91	0.24
MB05	12.38	8.75	12.90	1.98	1.90	0.24
MB06	12.28	8.68	12.78	1.98	1.90	0.25
MB07	12.33	8.72	12.97	2.01	1.89	0.25
MB08	12.34	8.73	13.31	1.95	1.89	0.25
MB09	12.42	8.78	12.38	1.96	1.88	0.25
mean	12.37	8.75	12.89	1.98	1.89	0.25
MB10	12.45	8.80	13.03	2.01	1.91	0.25
MB11	12.46	8.81	13.48	1.98	1.89	0.25
MB12	12.41	8.78	12.77	1.96	1.92	0.25
MB13	12.36	8.74	12.99	2.09	1.90	0.25
MB14	12.34	8.72	12.97	1.99	1.89	0.25
MB15	12.34	8.73	12.97	1.98	1.90	0.26
MB16	12.27	8.67	13.00	2.01	1.88	0.26
MB17	12.20	8.63	12.28	1.99	1.93	0.27
MB18	12.24	8.65	12.25	1.96	1.91	0.29
mean	12.34	8.73	12.86	2.00	1.90	0.26
MB19	12.24	8.66	13.10	2.01	1.86	0.31
MB20	12.28	8.69	12.84	1.98	1.90	0.31
MB21	12.14	8.58	12.64	2.01	1.90	0.31
MB22	12.11	8.56	12.42	1.96	1.89	0.31
MB23	12.17	8.60	12.57	2.02	1.88	0.30
MB24	12.10	8.56	12.46	1.98	1.88	0.29
MB25	12.08	8.54	12.45	2.01	1.88	0.29
MB26	12.02	8.50	12.38	1.99	1.88	0.29
MB27	12.05	8.52	12.35	1.98	1.89	0.28
mean	12.13	8.58	12.58	1.99	1.89	0.30
MB28	12.05	8.52	12.56	2.01	1.89	0.28
MB29	12.17	8.60	12.73	1.96	1.90	0.28
MB30	12.21	8.63	12.72	2.01	1.90	0.28
MB31	12.09	8.55	12.55	2.01	1.89	0.28
MB32	11.98	8.47	12.42	1.99	1.90	0.28
MB33	11.99	8.48	12.42	1.98	1.90	0.28
MB34	11.95	8.45	12.35	1.92	1.90	0.28
MB35	11.98	8.47	12.36	1.92	1.90	0.28
MB36	11.93	8.44	12.39	2.01	1.90	0.28
mean	12.04	8.51	12.50	1.98	1.90	0.28

## A.2 Free Surface Data

**Table A.5:** Free surface statistics at Gauges G1-G5 for test SL.

Test No.	G1				G2		G3		G4		G5	
	$T_p$	$R$	$\bar{\eta}$	$\sigma_\eta$								
[-]	[sec]	[-]	[cm]	[cm]								
SL01	-	-	-	-	-	-	-	-	-	-	-	-
SL02	1.94	0.34	-0.04	1.43	-0.10	1.41	0.01	1.42	-0.03	1.41	-0.13	1.39
SL03	1.92	0.34	-0.01	1.42	-0.03	1.41	0.03	1.40	-0.02	1.40	-0.06	1.37
SL04	1.94	0.34	-0.01	1.43	-0.20	1.41	0.01	1.41	-0.02	1.41	-0.10	1.38
SL05	1.94	0.35	-0.02	1.43	-0.01	1.41	0.01	1.41	-0.03	1.40	-0.09	1.38
SL06	2.00	0.35	-0.01	1.42	-0.01	1.42	0.00	1.40	-0.03	1.40	-0.07	1.37
SL07	1.94	0.35	-0.03	1.41	-0.04	1.41	-0.02	1.40	-0.02	1.39	-0.06	1.37
SL08	1.94	0.35	-0.03	1.42	-0.01	1.41	-0.06	1.39	-0.05	1.40	-0.07	1.38
SL09	2.00	0.35	-0.04	1.41	-0.05	1.40	-0.01	1.39	-0.03	1.40	-0.06	1.38
SL10	1.93	0.35	-0.02	1.42	-0.02	1.41	-0.02	1.39	-0.04	1.40	-0.06	1.38
SL11	1.93	0.36	-0.01	1.41	-0.06	1.41	-0.02	1.39	-0.02	1.40	-0.07	1.38
SL12	-	-	-	-	-	-	-	-	-	-	-	-
SL13	1.92	0.35	-0.01	1.41	-0.00	1.40	-0.01	1.38	-0.06	1.40	-0.15	1.38
SL14	1.94	0.36	-0.02	1.40	0.02	1.41	-0.01	1.39	-0.03	1.40	-0.08	1.38
SL15	1.94	0.36	-0.01	1.40	-0.04	1.40	-0.01	1.38	-0.04	1.40	-0.08	1.38
SL16	1.94	0.36	-0.05	1.37	0.03	1.37	-0.01	1.36	-0.03	1.37	-0.10	1.35
SL17	1.94	0.36	-0.01	1.40	-0.03	1.41	-0.01	1.39	-0.04	1.39	-0.09	1.38
SL18	1.93	0.35	-0.02	1.40	-0.05	1.41	-0.02	1.38	-0.04	1.40	-0.09	1.37
mean	1.94	0.35	-0.02	1.41	-0.04	1.40	-0.01	1.39	-0.03	1.40	-0.08	1.38

**Table A.6:** Free surface statistics at Gauges G6-G8 for test SL.

Test No	G6		G7		G8			
	$\bar{\eta}$	$\sigma_{\eta}$	$\bar{\eta}$	$\sigma_{\eta}$	$P_w$	$\bar{h}$	$\bar{\eta}$	$\sigma_{\eta}$
[-]	[cm]	[cm]	[cm]	[cm]	[-]	[cm]	[cm]	[cm]
SL01	-	-	-	-	-	-	-	-
SL02	-0.06	1.34	-0.10	1.61	16.8%	1.06	4.76	0.82
SL03	0.08	1.34	-0.23	1.60	11.1%	0.71	4.41	0.53
SL04	-0.04	1.33	-0.05	1.58	16.6%	0.99	5.09	0.73
SL05	-0.05	1.31	-0.18	1.61	14.3%	0.90	5.00	0.65
SL06	-0.06	1.38	-0.17	1.66	14.8%	0.94	5.14	0.60
SL07	-0.07	1.28	-0.20	1.60	11.6%	0.89	5.09	0.57
SL08	-0.08	1.31	-0.21	1.62	9.7%	0.70	5.00	0.47
SL09	-0.08	1.31	-0.18	1.62	9.3%	0.70	5.00	0.47
SL10	-0.10	1.31	-0.19	1.61	9.8%	0.77	5.17	0.50
SL11	-0.09	1.34	-0.11	1.65	12.4%	0.97	5.37	0.64
SL12	-	-	-	-	-	-	-	-
SL13	-0.06	1.34	-0.20	1.63	11.5%	0.92	5.32	0.58
SL14	-0.07	1.34	-0.18	1.68	12.4%	0.92	5.32	0.52
SL15	-0.06	1.33	-0.18	1.64	10.8%	0.85	5.25	0.48
SL16	-0.04	1.31	-0.18	1.62	10.5%	0.80	5.20	0.52
SL17	-0.06	1.33	-0.17	1.61	11.0%	0.79	5.19	0.55
SL18	-0.08	1.32	-0.16	1.64	11.0%	0.82	5.22	0.55
mean	-0.06	1.33	-0.17	1.62	12.1%	0.86	5.10	0.57

Note: G7 was always submerged.

**Table A.7:** Free surface statistics at Gauges G1-G5 for test SH.

Test No	G1				G2		G3		G4		G5	
	$T_p$	$R$	$\bar{\eta}$	$\sigma_\eta$								
[-]	[sec]	[-]	[cm]	[cm]								
SH01	-	-	-0.09	3.00	-0.10	2.98	-0.13	3.08	-	2.95	-0.01	2.90
SH02	1.99	0.28	-0.12	3.00	-0.11	2.94	-0.06	3.05	-0.03	2.89	-	2.88
SH03	1.98	0.28	-0.14	2.99	-0.16	2.97	-0.13	3.05	-0.17	2.93	-0.15	2.90
SH04	2.01	0.28	-0.17	2.98	-0.11	2.94	-0.12	3.04	-	2.92	-0.19	2.90
SH05	1.96	0.28	-0.16	3.01	-0.11	2.97	-0.12	3.04	-0.20	2.92	-0.15	2.90
SH06	1.96	0.28	-0.16	3.02	-0.13	2.98	-0.12	3.04	-0.10	2.93	-0.12	2.94
SH07	1.96	0.28	-0.19	3.02	-0.11	2.98	-0.17	3.05	-0.18	2.95	-0.17	2.93
SH08	1.98	0.28	-0.17	2.99	-0.10	2.96	-0.13	3.04	-0.01	2.94	-0.18	2.92
SH09	2.01	0.28	-0.14	3.01	-0.11	2.99	-0.12	3.05	-0.24	2.95	-0.18	2.92
SH10	1.96	0.28	-0.18	3.01	-0.11	3.05	-0.11	3.05	-0.20	2.96	-0.17	2.96
SH11	1.96	0.28	-0.14	3.01	-0.07	2.99	-0.06	3.06	-	2.99	-0.09	2.94
SH12	1.92	0.28	-0.16	3.01	-0.12	2.98	-0.10	3.06	-0.10	2.98	-0.13	2.97
SH13	1.98	0.28	-0.15	2.99	-0.11	2.96	-0.11	3.06	0.03	2.98	-0.16	2.97
SH14	1.96	0.28	-0.15	3.00	-0.12	2.98	-0.11	3.06	-0.11	2.97	-0.15	2.96
SH15	1.99	0.29	-0.15	2.99	-0.11	2.97	-0.11	3.06	-0.17	2.99	-0.12	2.96
SH16	1.99	0.29	-0.14	3.00	-0.11	2.99	-0.06	3.06	-0.14	2.99	-0.15	2.97
SH17	1.96	0.29	-0.15	3.00	-0.11	3.00	-0.10	3.04	-0.17	3.02	-0.11	2.99
SH18	1.99	0.29	-0.14	3.00	-0.12	3.00	-0.09	3.04	-0.18	3.04	-0.16	3.00
mean	1.97	0.28	-0.15	3.00	-0.11	2.98	-0.11	3.05	-0.13	2.96	-0.15	2.94

**Table A.8:** Free surface statistics at Gauges G6-G8 for test SH.

Test No	G6		G7				G8			
	$\bar{\eta}$	$\sigma_{\eta}$	$P_w$	$\bar{h}$	$\bar{\eta}$	$\sigma_{\eta}$	$P_w$	$\bar{h}$	$\bar{\eta}$	$\sigma_{\eta}$
[-]	[cm]	[cm]	[-]	[cm]	[cm]	[cm]	[-]	[cm]	[cm]	[cm]
SH01	-	-	-	-	-	-	-	-	-	-
SH02	-0.39	2.36	97.2%	3.54	0.69	2.14	10.1%	0.92	5.22	0.81
SH03	-0.35	2.38	88.2%	3.53	0.83	1.96	9.2%	0.92	5.37	0.81
SH04	-0.36	2.40	95.9%	3.48	0.83	2.12	17.2%	1.46	6.16	1.12
SH05	-0.27	2.40	98.7%	3.48	0.73	2.17	14.2%	1.38	6.38	1.09
SH06	-0.31	2.42	99.4%	3.55	0.75	2.18	14.8%	1.39	6.39	1.06
SH07	-0.38	2.44	98.5%	3.45	0.75	2.17	15.3%	1.43	6.38	1.09
SH08	-0.35	2.44	97.5%	3.48	0.83	2.17	15.8%	1.44	6.39	1.08
SH09	-0.31	2.44	97.4%	3.45	0.80	2.16	15.9%	1.44	6.44	1.10
SH10	-0.34	2.42	98.5%	3.42	0.82	2.17	19.0%	1.56	6.31	1.44
SH11	-0.38	2.42	93.6%	3.39	0.79	2.05	22.7%	2.16	6.96	1.53
SH12	-0.35	2.47	98.8%	3.44	0.74	2.13	20.6%	2.00	7.10	1.48
SH13	-0.44	2.50	98.1%	3.50	0.85	2.16	20.1%	2.02	7.27	1.52
SH14	-0.41	2.50	97.6%	3.42	0.87	2.15	19.8%	2.01	7.36	1.50
SH15	-0.47	2.52	99.0%	3.42	0.82	2.19	20.2%	2.06	7.46	1.53
SH16	-0.50	2.54	100%	3.56	0.81	2.19	19.5%	2.08	7.63	1.50
SH17	-0.52	2.56	100%	3.66	0.86	2.21	20.5%	2.09	7.68	1.52
SH18	-0.50	2.57	99.9%	3.55	0.90	2.19	20.2%	2.14	7.79	1.57
mean	-0.39	2.46	97.5%	3.49	0.80	2.15	17.3%	1.68	6.72	1.28

**Table A.9:** Free surface statistics at Gauges G1-G5 for test MH.

Test No	G1				G2		G3		G4		G5	
	$T_p$	$R$	$\bar{\eta}$	$\sigma_\eta$								
[-]	[sec]	[-]	[cm]	[cm]								
MH01	1.95	0.23	-0.16	3.09	-0.12	3.00	-0.12	3.00	-0.09	2.89	-0.23	2.77
MH02	1.98	0.25	-0.14	3.11	-0.16	3.00	-0.09	3.03	-	2.90	-0.26	2.75
MH03	2.01	0.25	-0.14	3.11	-0.17	2.99	-0.12	3.04	-0.22	2.84	-0.28	2.74
MH04	2.01	0.25	-0.14	3.09	-0.17	3.00	-0.10	3.04	-	2.89	-0.23	2.74
MH05	2.01	0.25	-0.12	3.10	-0.07	3.01	-0.09	3.04	-0.17	2.86	-0.21	2.74
MH06	2.01	0.25	-0.10	3.09	-0.04	3.05	-0.07	3.04	-0.16	2.85	-0.23	2.73
MH07	2.01	0.26	-0.13	3.09	-0.11	2.99	-0.10	3.03	-0.21	2.85	-0.18	2.73
MH08	1.96	0.26	-0.10	3.09	-0.06	3.00	-0.10	3.03	0.07	2.81	-0.19	2.72
MH09	1.96	0.26	-0.12	3.08	-0.11	2.98	-0.09	3.03	-0.01	2.83	-0.20	2.72
MH10	1.98	0.26	-0.11	3.10	-0.08	3.00	-0.10	3.04	-0.21	2.82	-0.20	2.71
MH11	1.98	0.26	-0.07	3.08	-0.07	2.98	-0.06	3.04	-	2.84	-0.19	2.70
MH12	1.95	0.26	-0.12	3.08	-0.07	2.99	-0.11	3.04	-0.01	2.82	-0.20	2.70
MH13	2.01	0.26	0.13	3.09	-0.08	2.99	-0.12	3.05	-0.17	2.84	-0.20	2.69
MH14	1.92	0.27	-0.12	3.07	-0.08	2.97	-0.11	3.06	-0.19	2.84	-0.20	2.69
MH15	-	-	-	-	-	-	-	-	-	-	-	-
MH16	1.96	0.27	-0.11	3.09	-0.11	2.98	-0.13	3.06	-0.10	2.79	-0.18	2.70
MH17	1.95	0.28	-0.10	3.09	-0.08	2.96	-0.12	3.06	0.04	2.80	-0.10	2.69
MH18	1.98	0.28	-0.10	3.07	-0.10	2.95	-0.12	3.07	-	2.81	-0.17	2.70
mean	1.98	0.26	-0.10	3.09	-0.10	2.99	-0.10	3.04	-0.11	2.84	-0.20	2.72

**Table A.10:** Free surface statistics at Gauges G6-G8 for test MH.

Test No	G6		G7		G8	
	$\bar{\eta}$	$\sigma_{\eta}$	$\bar{\eta}$	$\sigma_{\eta}$	$\bar{\eta}$	$\sigma_{\eta}$
[-]	[cm]	[cm]	[cm]	[cm]	[cm]	[cm]
MH01	-	-	-	-	-	-
MH02	-0.25	2.95	-0.30	2.29	0.38	2.08
MH03	-0.21	2.98	-0.34	2.29	0.35	2.14
MH04	-	-	-0.25	2.28	0.42	2.09
MH05	-0.11	2.93	-0.32	2.29	0.45	2.08
MH06	-	-	-	-	-	-
MH07	-0.14	2.88	-0.33	2.30	0.42	2.11
MH08	-0.13	2.92	-0.32	2.31	0.43	2.11
MH09	-0.15	2.91	-0.42	2.31	0.43	2.12
MH10	-0.16	2.93	-0.32	2.30	0.45	2.11
MH11	-0.19	2.93	-0.31	2.29	0.51	2.09
MH12	-0.24	2.92	-0.36	2.32	0.51	2.07
MH13	-0.18	2.98	-0.37	2.29	0.55	2.09
MH14	-0.18	3.01	-0.36	2.31	0.55	2.11
MH15	-	-	-	-	-	-
MH16	-0.23	3.02	-0.38	2.34	0.57	2.12
MH17	-0.21	3.01	-0.41	2.33	0.62	2.12
MH18	-0.26	2.97	-0.38	2.36	0.70	2.11
mean	-0.19	2.95	-0.35	2.31	0.49	2.10

Note: Gauges G7 and G8 were always submerged.

**Table A.11:** Free surface statistics at Gauges G1-G5 for test MB.

Test No	G1				G2		G3		G4		G5	
	$T_p$	$R$	$\bar{\eta}$	$\sigma_\eta$								
[-]	[sec]	[-]	[cm]	[cm]								
MB01	1.96	0.23	-0.08	3.10	-0.01	3.02	-0.09	3.10	-	3.10	-0.12	3.12
MB02	1.96	0.23	-0.08	3.10	-0.15	2.98	-0.10	3.03	-	3.04	0.08	2.84
MB03	1.99	0.24	-0.10	3.12	-0.20	2.99	-0.10	3.03	-0.17	2.87	-0.23	2.82
mean	1.97	0.24	-0.09	3.10	-0.18	2.98	-0.10	3.03	-0.17	2.96	-0.07	2.83
MB04	1.98	0.24	-0.09	3.12	-0.02	3.04	-0.09	3.04	-0.07	2.86	-0.20	2.73
MB05	1.98	0.24	-0.12	3.09	-0.10	3.02	-0.10	3.03	-0.17	2.84	-0.21	2.69
MB06	1.98	0.25	-0.10	3.07	-0.04	2.98	-0.11	3.01	-0.09	2.82	-0.19	2.68
MB07	2.01	0.25	-0.12	3.08	-0.14	2.94	-0.11	3.03	-0.17	2.83	-0.19	2.68
MB08	1.95	0.25	-0.06	3.09	0.04	2.98	-0.11	3.00	-0.20	2.83	0.01	2.70
MB09	1.96	0.25	-0.09	3.11	0.03	3.03	-0.09	3.01	-0.19	2.85	-0.20	2.75
mean	1.98	0.25	-0.09	3.09	-0.04	3.00	-0.10	3.02	-0.15	2.84	-0.16	2.71
MB10	2.01	0.25	-0.08	3.11	-0.22	2.96	-0.09	3.03	0.12	2.86	0.15	2.75
MB11	1.98	0.25	-0.12	3.12	-0.11	3.01	-0.09	3.03	0.17	2.86	-0.09	2.77
MB12	1.96	0.25	-0.13	3.10	-0.12	3.00	-0.10	3.03	-0.21	2.85	-0.03	2.77
MB13	2.09	0.25	-0.08	3.09	-0.06	2.98	-0.10	3.03	-0.24	2.82	-0.16	2.72
MB14	1.99	0.25	-0.08	3.08	-0.03	3.00	-0.10	3.04	-0.13	2.80	-0.09	2.69
MB15	1.99	0.26	-0.09	3.09	-0.04	3.01	-0.09	3.06	-0.21	2.78	-0.14	2.67
MB16	2.01	0.26	-0.11	3.07	-0.07	3.00	-0.11	3.07	-0.13	2.76	-0.17	2.61
MB17	1.99	0.27	-0.10	3.05	-0.01	2.96	-0.09	3.11	-0.25	2.75	-0.17	2.61
MB18	1.96	0.29	-0.13	3.06	-0.09	2.98	-0.11	3.14	-0.13	2.73	-0.18	2.62
mean	2.00	0.26	-0.10	3.09	-0.08	2.99	-0.10	3.06	-0.11	2.80	-0.10	2.69
MB19	2.02	0.30	-0.13	3.06	-0.23	2.97	-0.12	3.17	-0.18	2.75	-0.01	2.67
MB20	1.98	0.31	-0.14	3.07	-0.16	2.99	-0.12	3.17	-0.07	2.83	-0.22	2.74
MB21	2.01	0.31	-0.12	3.04	-0.09	2.97	-0.12	3.16	0.26	2.85	-0.17	2.76
MB22	1.96	0.31	-0.11	3.03	-0.16	2.95	-0.12	3.14	-0.29	2.90	-0.19	2.82
MB23	2.02	0.30	-0.11	3.04	-0.01	3.00	-0.22	3.14	-0.20	2.92	-0.16	2.86
MB24	1.98	0.29	-0.14	3.02	-0.16	2.94	-0.12	3.12	-0.25	2.98	-0.19	2.86
MB25	2.01	0.29	-0.13	3.02	-0.17	2.94	-0.12	3.12	-0.16	2.96	-0.17	2.86
MB26	1.99	0.29	-0.11	3.01	-0.17	2.92	-0.12	3.10	-0.23	2.98	-0.17	2.87
MB27	1.98	0.28	-0.14	3.01	-0.11	2.96	-0.12	3.10	0.10	2.99	-0.18	2.85
mean	1.99	0.30	-0.12	3.03	-0.14	2.96	-0.13	3.14	-0.11	2.91	-0.16	2.81
MB28	2.01	0.28	-0.14	3.01	-0.11	2.96	-0.12	3.11	-0.18	2.98	-0.18	2.88
MB29	1.96	0.28	-0.15	3.04	-0.19	2.94	-0.11	3.12	0.24	3.02	0.05	2.88
MB30	2.02	0.28	-0.10	3.05	-0.18	2.96	-0.12	3.13	0.40	3.08	-0.14	2.88
MB31	2.01	0.28	-0.11	3.02	-0.19	2.92	-0.12	3.11	-0.14	3.05	-0.17	2.87
MB32	1.99	0.28	-0.11	2.99	-0.19	2.90	-0.11	3.10	-0.42	3.07	-0.16	2.86
MB33	1.98	0.28	-0.13	3.00	-0.21	2.92	-0.12	3.10	-0.16	3.06	-0.19	2.86
MB34	1.92	0.28	-0.11	2.99	0.01	2.95	-0.11	3.09	-0.17	3.05	-0.17	2.87
MB35	1.92	0.28	-0.11	3.00	-0.17	2.91	-0.12	3.11	-0.65	3.10	-0.17	2.86
MB36	2.01	0.28	-0.14	2.98	-0.19	2.93	-0.12	3.11	0.01	3.03	-0.16	2.86
mean	1.98	0.28	-0.12	3.01	-0.16	2.93	-0.12	3.11	-0.12	3.05	-0.14	2.87

**Table A.12:** Free surface statistics at Gauges G6-G8 for test MB.

Test No	G6		G7		G8			
	$\bar{\eta}$	$\sigma_{\eta}$	$\bar{\eta}$	$\sigma_{\eta}$	$P_w$	$\bar{h}$	$\bar{\eta}$	$\sigma_{\eta}$
[-]	[cm]	[cm]	[cm]	[cm]	[-]	[cm]	[cm]	[cm]
MB01	-	-	-	-	-	-	-	-
MB02	0.71	2.44	0.77	1.68	100%	3.88	0.69	2.34
MB03	0.51	2.47	0.78	1.60	100%	3.97	0.72	2.34
mean	0.61	2.46	0.78	1.64	100%	3.93	0.71	2.34
MB04	-	-	0.95	1.66	100%	4.06	0.74	2.35
MB05	-	-	0.87	1.63	100%	4.11	0.72	2.33
MB06	-	-	0.95	1.63	100%	4.11	0.76	2.31
MB07	-	-	0.96	1.63	100%	4.10	0.77	2.29
MB08	-	-	1.00	1.60	100%	4.52	0.79	2.30
MB09	-	-	0.97	1.61	100%	4.81	0.83	2.28
mean	-	-	0.95	1.63	100%	4.29	0.77	2.31
MB10	-	-	0.90	1.59	100%	4.55	0.85	2.25
MB11	-	-	0.77	1.61	100%	4.15	0.87	2.23
MB12	-	-	0.80	1.63	100%	3.67	0.94	2.20
MB13	-	-	-	-	-	-	-	-
MB14	-	-	0.58	1.69	98.3%	3.35	1.10	2.12
MB15	-	-	0.44	1.80	89.8%	2.97	1.57	1.92
MB16	-	-	0.21	1.96	87.2%	2.67	1.97	1.82
MB17	-	-	0.05	2.11	83.3%	2.32	2.22	1.69
MB18	-	-	0.01	2.21	82.9%	2.04	2.39	1.66
mean	-	-	0.42	1.62	82.4%	2.86	1.32	1.76
MB19	-0.25	2.99	0.08	2.56	83.4%	2.39	2.89	2.03
MB20	-0.20	2.94	-0.09	2.66	52.7%	2.33	3.48	1.43
MB21	-0.28	2.89	0.03	2.63	44.1%	2.09	3.79	1.25
MB22	-0.18	2.90	0.15	2.59	44.1%	1.98	3.83	1.21
MB23	-0.22	2.94	0.21	2.56	38.4%	1.86	3.91	1.14
MB24	-0.25	2.95	0.31	2.54	39.4%	1.93	3.98	1.18
MB25	-0.28	3.01	0.40	2.51	39.4%	1.95	3.95	1.20
MB26	-0.27	3.04	0.39	2.50	35.4%	1.74	4.14	1.13
MB27	-0.32	3.07	0.44	2.51	31.5%	1.58	4.33	1.04
mean	-0.25	2.97	0.21	2.56	45.4%	1.98	3.81	1.29
MB28	-0.30	2.82	0.42	2.26	35.9%	2.04	4.64	1.28
MB29	-0.23	2.88	0.42	2.24	36.6%	2.05	4.60	1.28
MB30	-0.34	2.89	0.36	2.24	34.5%	1.94	4.74	1.23
MB31	-0.34	2.91	0.41	2.24	32.0%	1.78	4.78	1.15
MB32	-0.35	2.92	0.44	2.21	30.8%	1.68	4.73	1.13
MB33	-0.35	2.95	0.45	2.20	30.4%	1.70	4.75	1.13
MB34	-0.38	2.96	0.46	2.20	30.4%	1.74	4.74	1.16
MB35	-0.40	2.95	0.48	2.20	31.4%	1.82	4.82	1.16
MB36	-0.38	2.96	0.47	2.18	31.0%	1.67	4.87	1.16
mean	-0.34	2.92	0.44	2.22	32.5%	1.82	4.74	1.19

Note: Gauge G7 was always submerged.

### A.3 Velocity Data

**Table A.13:** Velocity statistics for test SL. Note: EMCM3-4 and EMCM5-6 were moved to different cross-shore locations after test SL due to the amount of air exposure EMCM5-6 experienced during test SL. Consequently, no data from EMCM5-6 was used in the data analysis of test SL

Test No	EMCM1		EMCM2		EMCM3		EMCM4	
	$\bar{U}$	$\sigma_U$	$\bar{U}$	$\sigma_U$	$\bar{U}$	$\sigma_U$	$\bar{U}$	$\sigma_U$
[-]	[cm/s]		[cm/s]		[cm/s]		[cm/s]	
SL01	-	-	-	-	-	-	-	-
SL02	-0.55	9.04	-0.59	8.76	-1.93	11.02	-2.09	11.95
SL03	-0.44	8.69	-0.39	8.65	-1.24	10.86	-1.44	11.63
SL04	0.01	8.58	-0.04	8.66	-1.55	10.61	-1.82	11.50
SL05	-0.50	8.52	-0.33	9.38	-2.11	10.56	-1.82	11.46
SL06	-0.43	9.24	-0.41	8.68	-1.54	11.27	-1.78	12.11
SL07	-0.11	9.41	-0.02	8.73	-1.21	10.31	-1.85	11.16
SL08	-0.03	8.83	0.03	8.72	-1.77	10.62	-2.29	11.45
SL09	0.19	8.69	-0.01	8.66	-1.84	10.63	-2.19	11.31
SL10	0.39	8.57	0.01	8.45	-1.40	10.60	-1.68	11.32
SL11	0.02	8.43	-0.19	8.29	-1.56	10.55	-2.12	11.32
SL12	-	-	-	-	-	-	-	-
SL13	0.18	8.24	-0.15	8.29	-1.34	10.13	-1.52	11.14
SL14	-0.17	8.07	-0.52	8.23	-1.23	10.10	-2.05	11.16
SL15	0.41	8.00	-0.35	8.08	-1.13	10.16	-1.75	11.17
SL16	0.25	7.61	-0.36	7.82	-1.29	9.78	-1.92	10.89
SL17	0.20	8.65	-0.51	8.63	-1.44	10.35	-1.76	11.23
SL18	0.14	8.50	-0.47	8.46	-1.46	10.48	-1.82	11.40
mean	-0.03	8.57	-0.27	8.53	-1.50	10.50	-1.87	11.39

**Table A.14:** Velocity statistics for test SH.

Test No	EMCM1		EMCM2		EMCM3		EMCM4		EMCM5		EMCM6	
	$\bar{U}$	$\sigma_U$										
[-]	[cm/s]											
SH01	-	-	-	-	-	-	-	-	-	-	-	-
SH02	-2.09	17.16	-1.74	16.64	-3.36	16.29	-1.47	18.20	-5.72	24.10	-2.83	22.06
SH03	-1.96	17.18	-1.70	16.53	-3.45	16.38	-1.48	18.37	-5.41	24.62	-2.17	22.59
SH04	-2.02	17.34	-1.80	16.50	-3.44	16.90	-1.73	18.71	-6.52	25.38	-2.51	23.29
SH05	-2.38	16.94	-2.08	16.25	-3.78	16.74	-1.67	18.69	-6.46	25.71	-2.30	23.38
SH06	-2.23	16.70	-1.96	16.04	-3.75	16.93	-1.76	18.75	-6.35	26.37	-2.48	23.67
SH07	-1.99	17.36	-1.84	16.22	-3.14	16.99	-1.37	18.74	-5.91	26.44	-2.62	23.94
SH08	-1.86	16.82	-1.86	16.00	-3.43	16.93	-1.35	18.94	-6.28	26.65	-2.27	23.76
SH09	-1.97	17.23	-1.73	16.11	-3.71	16.99	-1.47	18.85	-6.58	26.75	-2.23	23.71
SH10	-2.23	18.90	-2.18	16.54	-3.83	17.74	-1.71	18.89	-6.65	26.89	-2.94	24.12
SH11	-2.54	21.16	-1.96	16.48	-4.23	18.07	-1.90	18.57	-6.06	25.94	-2.66	23.42
SH12	-1.84	16.67	-1.57	15.82	-3.38	16.65	-1.36	18.46	-5.41	27.07	-1.55	23.25
SH13	-1.58	16.74	-1.52	15.91	-3.51	16.92	-1.62	18.61	-6.39	27.43	-1.59	24.26
SH14	-1.72	16.84	-1.65	15.93	-3.39	16.96	-1.69	18.65	-6.11	28.10	-1.28	24.47
SH15	-1.51	20.51	-1.82	16.53	-4.06	18.23	-2.11	18.54	-6.40	28.32	-1.68	24.58
SH16	-2.10	17.53	-1.97	16.09	-4.22	16.99	-1.92	18.37	-7.08	29.50	-0.91	24.24
SH17	-1.71	17.10	-1.73	15.89	-3.36	16.76	-1.72	18.18	-7.03	30.11	-0.92	24.96
SH18	-1.81	17.46	-1.67	16.00	-3.14	16.79	-1.56	17.95	-6.84	30.46	-0.72	24.67
mean	-1.97	17.63	-1.81	16.21	-3.60	17.02	-1.64	18.56	-6.31	27.05	-1.98	23.79

**Table A.15:** Velocity statistics for test MH.

Test No	EMCM1		EMCM2		EMCM3		EMCM4		EMCM5		EMCM6	
	$\bar{U}$	$\sigma_U$										
[-]	[cm/s]											
MH01	-1.75	17.83	-1.84	17.07	-3.27	19.57	-2.37	20.12	-7.74	16.85	-5.91	16.97
MH02	-2.05	18.96	-1.98	17.63	-3.32	19.81	-2.47	21.00	-7.61	17.42	-6.56	17.26
MH03	-1.79	18.11	-1.77	17.42	-3.12	19.42	-3.06	20.69	-7.55	17.17	-6.46	17.12
MH04	-1.92	18.12	-2.10	17.23	-3.32	19.73	-2.58	21.11	-7.45	17.03	-5.94	16.95
MH05	-1.84	18.53	-1.54	17.31	-2.62	20.06	-2.03	21.08	-6.72	17.11	-5.42	17.11
MH06	-	-	-	-	-	-	-	-	-	-	-	-
MH07	-1.60	17.60	-1.41	17.04	-3.03	17.67	-2.56	19.77	-7.08	17.81	-4.75	18.14
MH08	-1.94	17.37	-1.67	16.94	-3.45	17.33	-2.74	19.58	-7.38	18.13	-5.11	18.83
MH09	-1.25	17.73	-1.52	17.14	-3.15	17.27	-2.76	19.58	-7.03	18.30	-4.96	19.06
MH10	-1.35	16.11	-1.13	15.66	-2.81	16.00	-2.17	18.05	-6.82	17.34	-3.86	17.88
MH11	-2.32	17.63	-2.12	17.20	-3.32	17.22	-2.98	19.48	-7.41	19.22	-5.76	19.51
MH12	-2.26	17.82	-2.05	17.28	-2.91	17.02	-2.41	19.35	-7.34	19.20	-5.31	20.13
MH13	-2.33	17.70	-2.20	17.31	-3.58	18.00	-3.21	19.78	-7.19	19.38	-5.82	20.33
MH14	-1.45	17.92	-1.68	17.26	-3.21	17.57	-2.72	19.37	-7.05	19.26	-5.54	19.50
MH15	-	-	-	-	-	-	-	-	-	-	-	-
MH16	-1.85	17.79	-1.89	17.31	-3.36	17.35	-2.90	19.38	-7.38	19.44	-6.11	19.63
MH17	-1.87	18.08	-1.87	17.34	-3.24	16.85	-2.94	19.08	-7.43	19.40	-6.11	19.45
MH18	-2.39	17.72	-1.84	17.28	-3.33	17.36	-3.13	19.43	-6.84	19.34	-5.51	19.18
mean	-1.87	17.81	-1.79	17.15	-3.19	18.01	-2.69	19.80	-7.25	18.28	-5.57	18.57

**Table A.16:** Velocity statistics for test MB.

Test No	EMCM1		EMCM2		EMCM3		EMCM4		EMCM5		EMCM6	
	$\bar{U}$	$\sigma_U$										
[-]	[cm/s]											
MB01	-1.95	17.00	-1.63	16.16	-	-	-5.84	33.66	-6.51	12.63	-6.42	12.65
MB02	-2.36	17.09	-2.19	16.43	-	-	-6.97	33.05	-6.35	12.68	-7.12	12.53
MB03	-2.26	18.43	-1.83	16.86	-	-	-5.64	28.91	-5.49	13.97	-7.29	10.07
mean	-2.19	17.51	-1.88	16.48	-	-	-6.15	31.87	-6.12	13.09	-6.94	11.75
MB04	-1.65	17.46	-1.62	16.65	-3.95	20.74	-3.11	21.56	-5.88	19.46	-6.77	18.17
MB05	-2.09	17.46	-1.80	16.77	-3.84	19.46	-2.90	20.45	-	-	-8.07	21.75
MB06	-2.28	17.43	-1.94	16.83	-3.12	18.47	-2.51	19.54	-	-	-8.90	22.35
MB07	-1.66	17.94	-1.41	17.07	-2.47	18.41	-2.12	19.70	-	-	-8.50	24.02
MB08	-2.03	17.79	-1.55	17.05	-2.25	18.21	-1.67	19.42	-	-	-8.90	23.95
MB09	-1.76	17.85	-1.52	16.97	-2.68	18.16	-2.18	19.37	-	-	-9.56	27.52
mean	-1.91	17.65	-1.64	16.89	-3.05	18.91	-2.42	20.01	-5.88	19.46	-8.45	22.96
MB10	-1.65	17.99	-1.41	17.11	-2.72	18.08	-1.98	19.25	-	-	-8.54	24.33
MB11	-2.22	18.01	-1.81	17.28	-2.83	17.52	-2.20	18.95	-	-	-9.47	24.34
MB12	-1.56	18.46	-1.49	17.17	-2.16	17.55	-1.92	18.68	-	-	-9.64	24.19
MB13	-1.38	17.28	-1.54	16.13	-2.55	16.91	-1.79	17.60	-	-	-8.87	29.02
MB14	-1.96	19.53	-1.32	17.38	-2.28	18.84	-2.07	18.94	-	-	-8.53	35.98
MB15	-1.94	18.42	-1.70	17.42	-2.96	17.56	-2.44	18.76	-	-	-9.58	39.42
MB16	-1.76	19.07	-1.54	17.69	-2.74	18.22	-2.30	19.09	-	-	-9.07	44.95
MB17	-1.78	19.08	-1.76	17.80	-2.62	18.09	-2.33	19.05	-	-	-8.77	50.20
MB18	-1.80	18.55	-1.89	17.61	-2.31	17.99	-2.25	18.89	-	-	-8.05	28.24
mean	-1.78	18.49	-1.61	17.29	-2.58	17.86	-2.14	18.80	-	-	-8.94	33.41
MB19	-1.49	17.67	-1.53	17.22	-2.87	17.47	-1.79	18.62	-6.20	25.31	-5.68	24.34
MB20	-1.65	17.69	-1.36	17.07	-2.52	17.10	-1.41	18.31	-5.14	25.08	-5.39	24.15
MB21	-1.10	17.34	-1.37	16.74	-2.95	16.72	-1.43	18.01	-4.76	25.60	-4.98	24.68
MB22	-1.93	17.17	-1.83	16.50	-2.97	16.67	-1.83	17.92	-4.76	23.29	-4.46	22.07
MB23	-2.10	17.38	-1.92	16.43	-3.23	17.21	-1.68	18.11	-4.76	23.32	-3.03	21.58
MB24	-1.76	17.11	-1.78	16.34	-3.14	16.86	-1.95	17.81	-5.66	24.39	-3.40	22.03
MB25	-1.77	17.08	-1.58	16.25	-2.95	17.07	-1.55	17.73	-5.15	24.81	-2.53	22.20
MB26	-1.54	16.69	-1.76	16.15	-3.28	16.90	-1.90	17.95	-5.68	25.85	-2.87	22.58
MB27	-1.59	16.59	-1.58	16.16	-2.54	16.61	-1.49	17.82	-5.36	26.05	-2.22	22.92
mean	-1.66	17.19	-1.63	16.54	-2.94	16.96	-1.67	18.03	-5.27	24.85	-3.84	22.95
MB28	-1.18	16.83	-1.48	16.16	-2.95	16.75	-1.74	17.99	-5.68	26.76	-2.31	23.49
MB29	-2.21	17.07	-1.95	16.17	-2.94	17.09	-1.70	18.01	-5.12	26.11	-2.15	22.76
MB30	-1.70	17.16	-1.37	16.21	-2.52	16.65	-1.13	17.82	-5.32	26.84	-1.99	23.34
MB31	-1.57	17.36	-1.39	16.19	-2.98	17.20	-1.37	18.01	-4.99	26.98	-1.61	23.34
MB32	-1.72	17.14	-1.39	16.15	-2.34	16.93	-1.35	17.92	-4.82	27.80	-1.52	23.69
MB33	-1.90	17.23	-1.93	16.12	-3.02	17.35	-1.88	18.10	-5.41	27.88	-1.89	24.12
MB34	-1.77	16.83	-1.62	16.04	-3.05	16.95	-1.67	18.01	-4.86	28.28	-0.82	24.15
MB35	-1.98	17.35	-1.83	16.15	-3.18	17.11	-2.03	17.83	-5.59	28.48	-1.78	24.68
MB36	-1.68	16.96	-1.61	16.13	-2.87	16.59	-1.62	17.69	-7.10	32.34	-4.36	32.21
mean	-1.74	17.10	-1.62	16.15	-2.87	16.96	-1.61	17.93	-5.43	27.94	-2.05	24.64

Note: If current meters were exposed to air during a burst, that data was unreliable and omitted.

## Appendix B

### NUMERICAL PREDICTIONS OF CROSS-SHORE SEDIMENT TRANSPORT

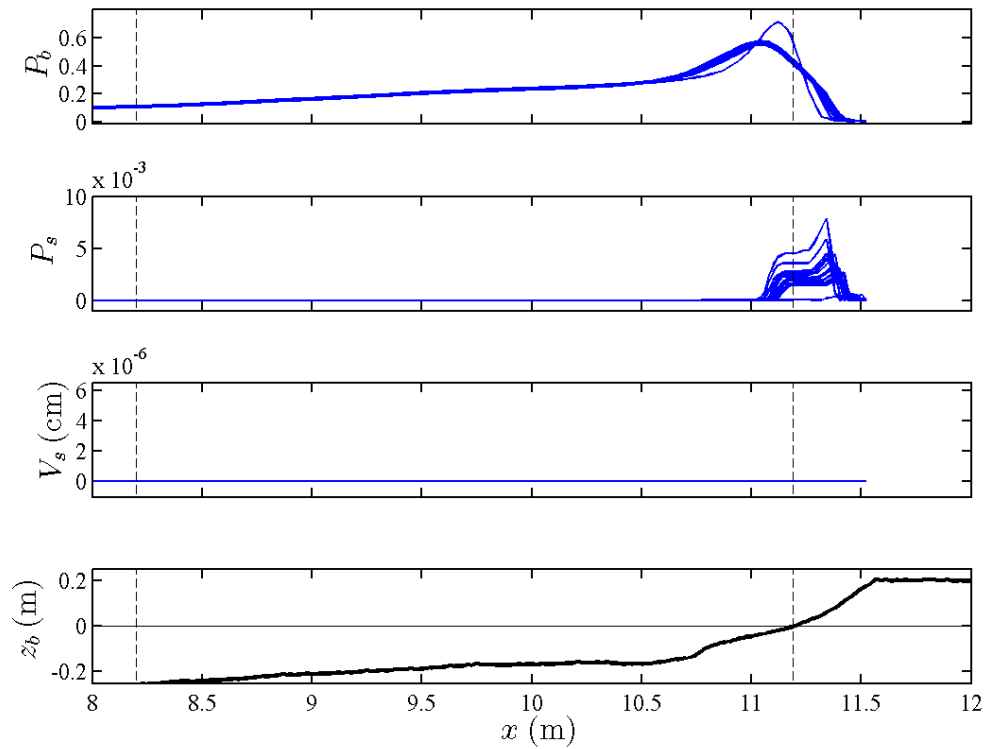


**Figure B.1:** CSHORE predictions of the probability of sediment movement (top), probability of sediment suspension (second from top), volume of suspended sediment (third from top), and the measured final profile (bottom) for reference from the steep slope, low wave height test SL.

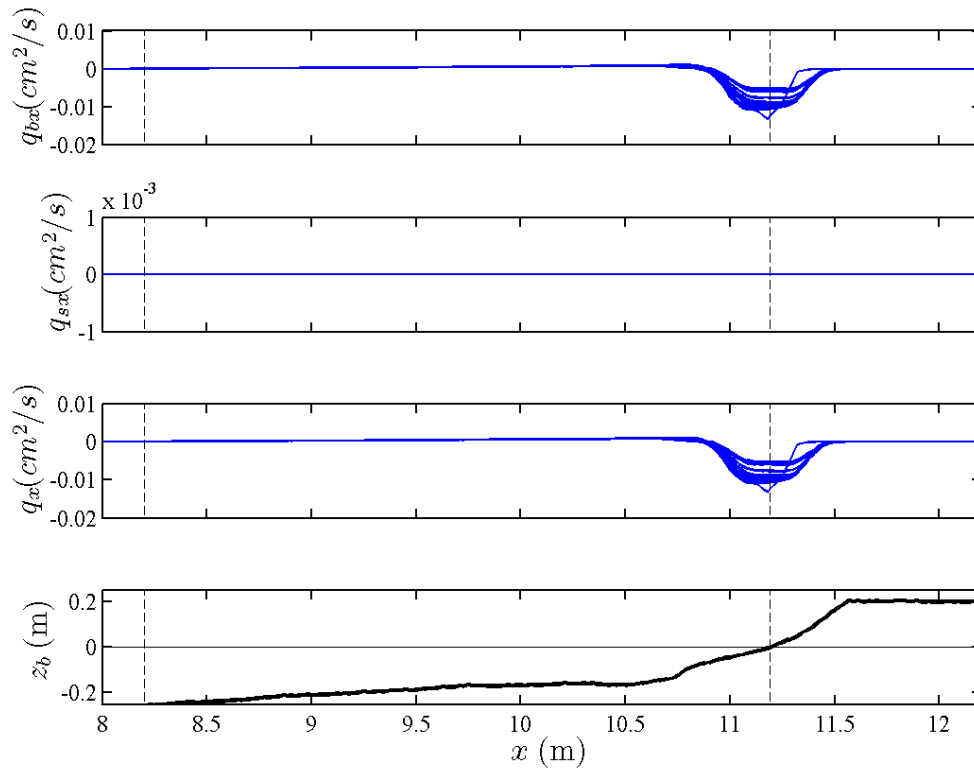


**Figure B.2:** CSHORE predictions of the bedload transport rate (top), suspended load transport rate (second from top), total sediment transport rate (third from top), and the measured final profile (bottom) for reference from the steep slope, low wave height test SL.

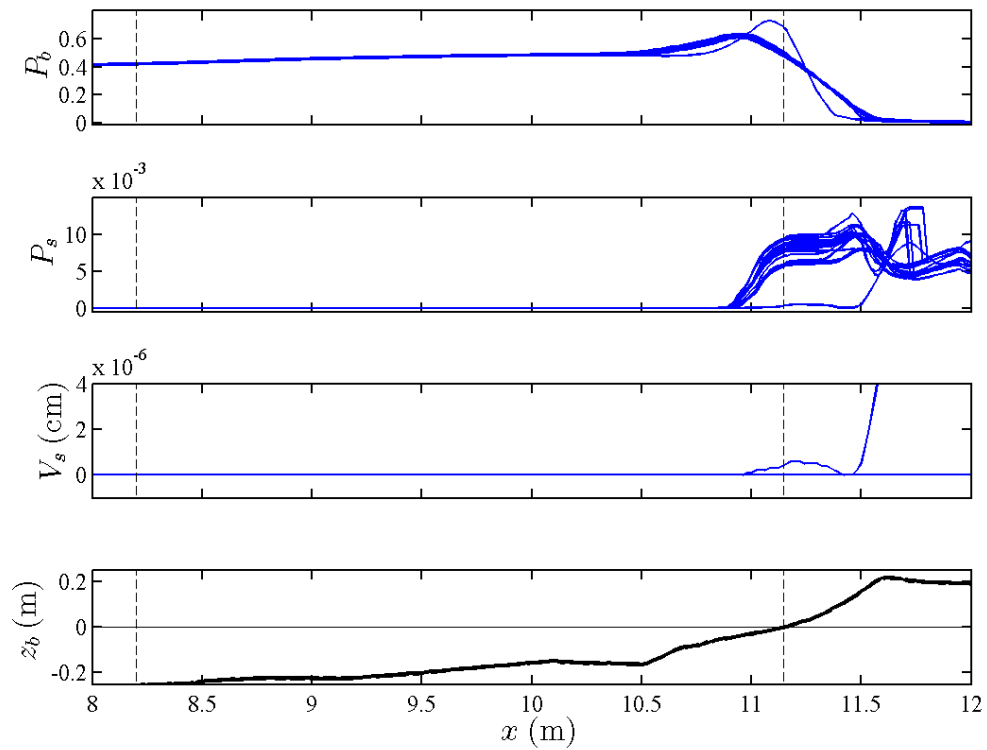


**Figure B.3:** CSHORE predictions of the probability of sediment movement (top), probability of sediment suspension (second from top), volume of suspended sediment (third from top), and the measured final profile (bottom) for reference from the steep slope, high wave height test SL.

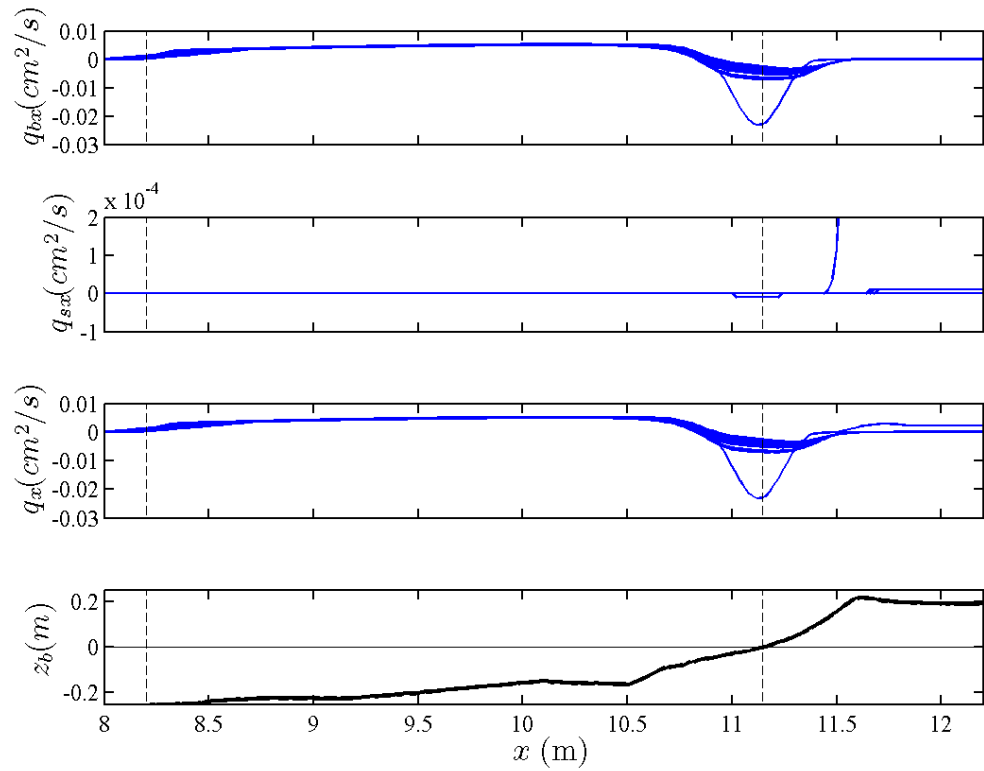


**Figure B.4:** CSHORE predictions of the bedload transport rate (top), suspended load transport rate (second from top), total sediment transport rate (third from top), and the measured final profile (bottom) for reference from the steep slope, high wave height test SH.

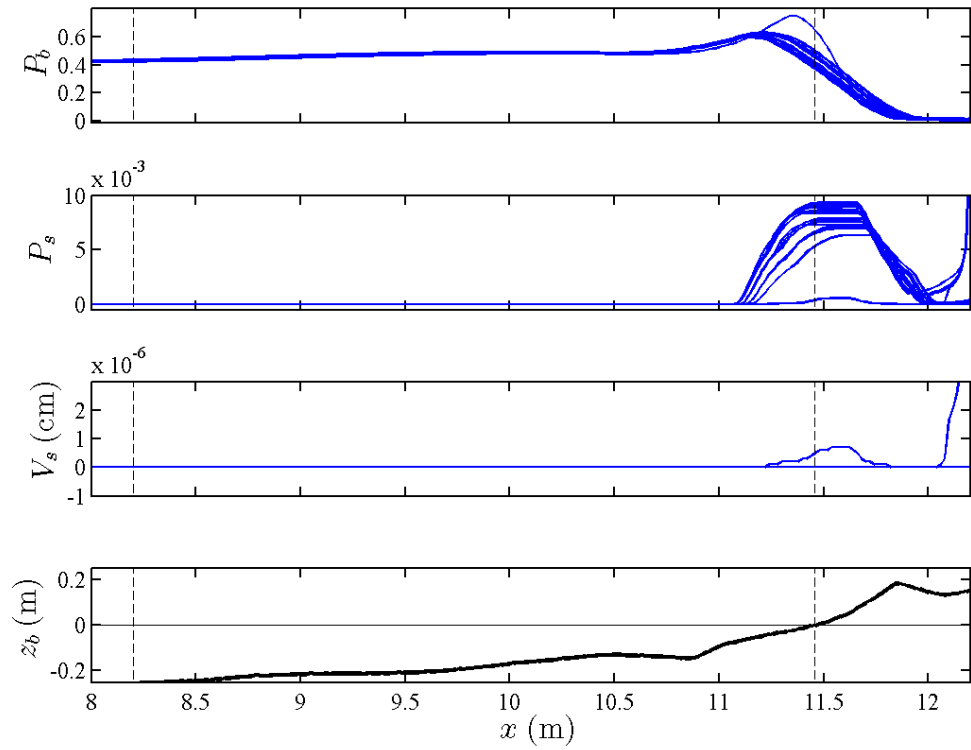


**Figure B.5:** CSHORE predictions of the probability of sediment movement (top), probability of sediment suspension (second from top), volume of suspended sediment (third from top), and the measured final profile (bottom) for reference from the mild slope, high wave height test MH.

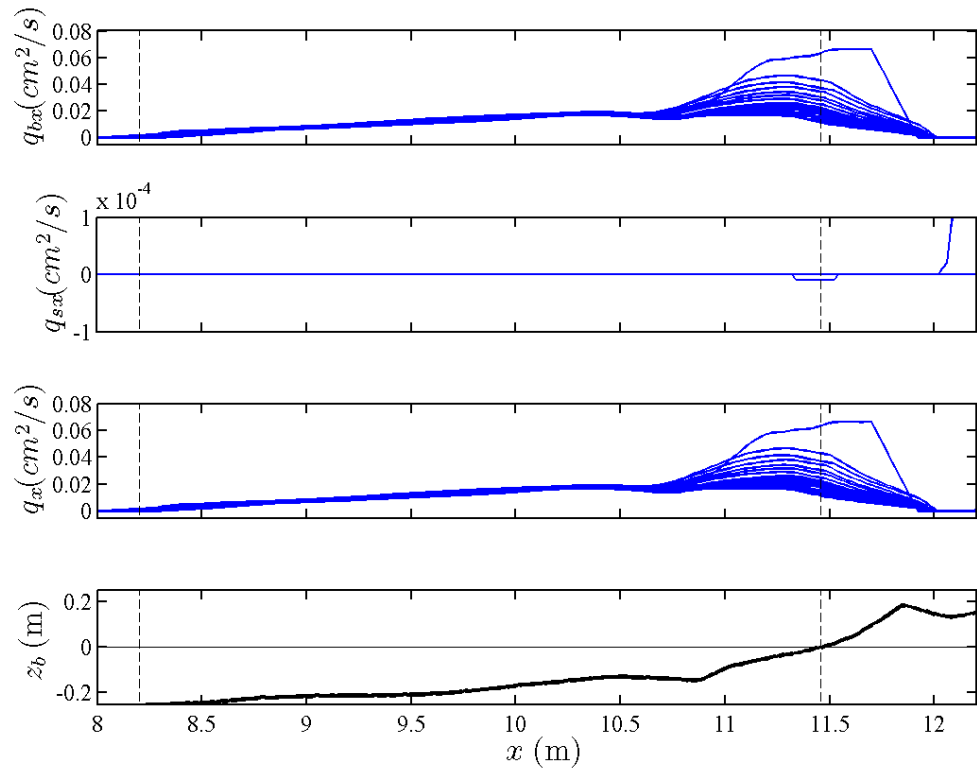


**Figure B.6:** CSHORE predictions of the bedload transport rate (top), suspended load transport rate (second from top), total sediment transport rate (third from top), and the measured final profile (bottom) for reference from the mild slope, high wave height test MH.

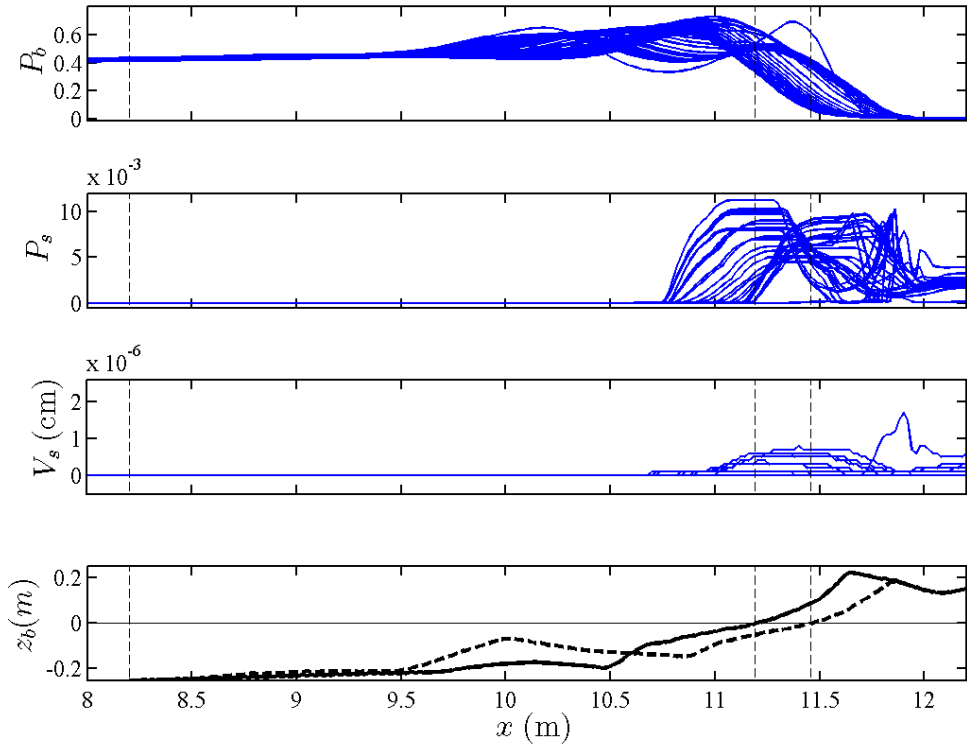


**Figure B.7:** CSHORE predictions of the probability of sediment movement (top), probability of sediment suspension (second from top), volume of suspended sediment (third from top), and the measured initial (dashed) and final profiles (bottom) for reference from the mild slope with a nearshore bar test MB.

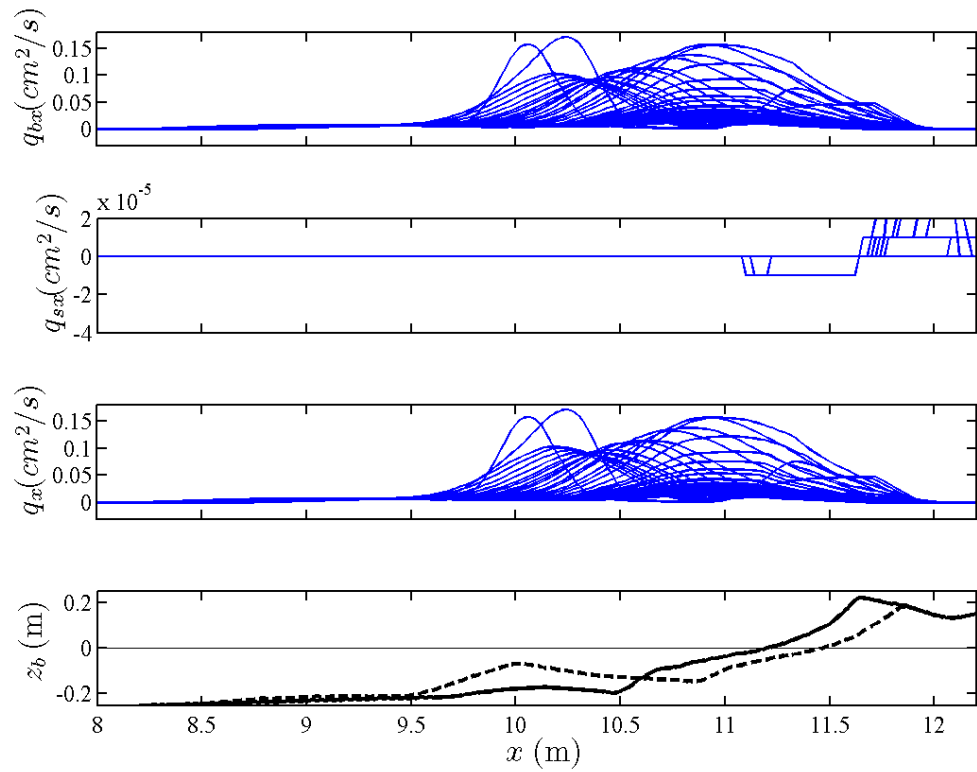


**Figure B.8:** CSHORE predictions of the bedload transport rate (top), suspended load transport rate (second from top), total sediment transport rate (third from top), and the measured initial (dashed) and final profiles (bottom) for reference from the mild slope with a nearshore bar test MB.